U.PORTO
FEUP FACULDADE DE ENGENHARIA
UNIVERSIDADE DO PORTO

Departamento de Engenharia Mecânica

Testing of Low-Loss Polymer Gears

André Falcão Lourenço

Porto, June of 2015

Testing of Low-Loss Polymer Gears

André Falcão Lourenço

Master thesis submited to:

Faculdade de Engenharia da Universidade do Porto
Mestrado Integrado em Engenharia Mecânica

Supervisors:

Prof. Jorge H. O. Seabra
Dr. Luís M.L. Magalhães
Dr. Carlos M. C. G. Fernandes

Departamento de Engenharia Mecânica
Faculdade de Engenharia da Unviersidade do Porto

Acknowledgements

I would like to thank to Professor Jorge Seabra and Professor Ramiro Martins for the opportunity and support given, specially in the most important decisions made during this work.

My sincere thanks to Professor Luís Magalhães for all the interest, support and friendship given during this past five months. He was very important in the way I conducted this work with the given ideas that made things go forward, always with joy and a good mood.

I would like to express my gratitude to Carlos Fernandes for his patient guidance and full time availability to teach, help, advise and guide during all this work.

I would also like to acknowledge the people I knew in CETRIB for their sympathy and help: Beatriz Graça, Pedro Marques, David Gonçalves, André Gama, Anvar Maxkamov. Even without a direct function on this work, it was very important to hear from them all that "free" information and opinions.

A special acknowledgement to my colleges in CETRIB that were also finishing their MSC thesis: David Costa, Pedro Aires, Cláudio Pinto, José Sarilho and António Coimbra. They were important to discuss some ideas of the moment, and helped me a lot in the most various areas, even if these areas were not particularly necessary for their works. With no doubt that this past five months would not have been the same without them.

A big thanks to my father, Sílvio Lourenço, my mother, Lúcia Lourenço and my sister, Sara Neves, for the full time support, understanding and patience during the last five years, that converged in this work. They were family and teachers although none of them is an engineer.

Abstract

In a time when the sustainable management of energy resources has become increasingly important, efforts have been made so that the transmission systems can exhibit the highest efficiency possible in the most various systems.
The energy costs cover not only the expenditure on operation, but the whole process from the assembly, disassembly or transport. Thus, the use of lighter equipment benefits the environment.
In 2007, the emergence of the concept of "Low loss gears" led to the creation of new tooth geometries which can be up to three times more efficient than the ones of ordinary gears. It is believed that the possibility of making lighter or even more efficient gears can also be achieved through the use of other materials.
During this work, tests to thermal and load capacities were performed on type C14 POM gears under oil bath lubrication in an FZG test rig. After the first idea about the material behaviour under this type of conditions was obtained, tests under controlled temperature at constant speed and load were performed in order to evaluate the material resistance. Finally, tests of POM low-loss gears were performed under controlled temperature and load in order to evaluate the allowed life time extension.

Sumário

Numa época em que as gestão sustentável de recursos energéticos é cada vez mais importante, o esforço para que os sistemas de transmissão apresentem o mais alto rendimento possível nos mais variados sistemas ganha uma importância relevante.
Os custos energéticos cobrem não só o gasto em funcionamento, mas todo o processo desde a montagem, desmontagem ou o transporte. Deste modo, o uso de equipamentos mais leves, resultará em equipamentos mais amigos do ambiente.
Em 2007 o surgimento do conceito "Low loss gears" (em português, engrenagens de alto rendimento), levou à criação de geometrias de dentes para engrenagens até três vezes mais eficientes que as geometrias de engrenagens comuns. Pensa-se que possibilidade de tornar estas engrenagens mais leves, ou eventualmente ainda mais eficientes poderá ser atingida através do uso de outros materiais.
Neste trabalho, testes à capacidade de carga e térmica de engrenagens de plástico (POM) do tipo C14 lubricadas em banho de óleo foram feitos numa máquina FZG. Depois de obtida uma primeira ideia do comportamento do material nestes ensaios, foram feitos testes a temperatura e velocidade constantes, de forma a avaliar a resistência do material à pressão superficial. Para finalizar, ensaios a temperatura controlada com engrenagens de plástico "low-loss" foram feitos para avaliar a eventual extensão do seu tempo de vida.

Keywords

Plastic Gears
Polymers
Low loss
Power loss
FZG
POM
VDI 2736

Palavras chave

Engrenagens de Plástico
Polímeros
Alto rendimento
Perda de potência
FZG
POM
VDI 2736

Contents

Acknowledgements i
Abstract iii
Sumário v
Keywords vii
Contents ix
List of Figures xiii
List of Tables xvii
Symbols and Abbreviations xix

1 Introduction **1**
1.1 Thesis purpose 1
1.2 Thesis outline 1

2 Polymer Materials in Gear Industry **3**
2.1 Contextualizing plastic gears 3
2.1.1 Advantages and disadvantages of plastic gears 3
2.1.2 Distinguishing engineering plastics 4
2.1.3 Some polymer gear properties 4
2.1.4 Manufacturing processes 5
2.2 Failure modes and causes for a plastic gear 6
2.2.1 Tooth temperature 6
2.2.2 Tooth deflection 10
2.2.3 Wear on plastic gears 11
2.2.4 Chemical incompatibility 11
2.3 Failure modes and life-time for a plastic gear 13
2.3.1 Failure modes for a plastic gear 13
2.3.2 Increasing plastic gears life-time 13
2.4 Lubrication on plastic gears 17
2.4.1 Distinguishing lubrication types 17
2.4.2 Fillers 17
2.4.3 Greases 19
2.4.4 Oils 19
2.5 Elastohydrodynamic Lubrication for Polymer Gears 21
2.5.1 Lubrication Regimes 21
2.5.2 Comparing steel with plastic gears 24

3 Experimental devices for plastic gears **27**
3.1 Test rigs for plastic gears 27
3.1.1 Non-mechanically strained test rig 27

3.1.2 Mechanically strained test . . . 29
3.1.3 Pulse test . . . 29
3.2 FZG test rig . . . 30

4 Load-carrying capacity and tooth geometry of plastic gears 33
4.1 Low-loss tooth geometry . . . 33
4.1.1 Power losses in a gearbox . . . 33
4.2 Influence of gear tooth geometry on power losses . . . 34
4.3 Geometry optimization for power savings . . . 35
4.4 Load-carrying capacity . . . 37
4.4.1 Material meshing simulations . . . 37
4.4.2 Performance comparison - K1 . . . 39
4.4.3 Performance comparison - K2 . . . 40
4.4.4 Performance comparison - K3 . . . 41
4.4.5 Wear, Deformation and Temperatures . . . 42
4.4.6 Life-time and Failure Causes . . . 44
4.4.7 Conclusions . . . 45

5 Experimental Procedures, Operating Conditions and Results 47
5.1 Materials and methods . . . 47
5.1.1 Test rig, measuring equipment and lubricant . . . 48
5.1.2 Gears Material . . . 52
5.1.3 Gears . . . 52
5.1.4 Wear measurement . . . 56
5.2 Preliminary Tests . . . 58
5.2.1 Operating Conditions and Results . . . 58
5.2.2 Specific Film Thickness Calculation . . . 64
5.2.3 Wear . . . 67
5.2.4 Discussion . . . 69
5.3 S-N tests . . . 73
5.3.1 Operating Conditions and Results . . . 73
5.3.2 Results . . . 74
5.3.3 Specific Film Thickness Calculation . . . 82
5.3.4 Wear . . . 83
5.3.5 Discussion . . . 85
5.3.6 S-N curve . . . 94

6 Conclusions and Future Work 95
6.1 Conclusions . . . 95
6.1.1 Materials and Methods . . . 95
6.1.2 Preliminary Tests . . . 95
6.1.3 S-N Tests . . . 96
6.1.4 General Conclusions . . . 96
6.2 Future Works . . . 97
6.2.1 Polymer gears . . . 97
6.2.2 Low-Loss Polymer gears . . . 97

A VDI 2736 - Calculation procedure 103

B Standard calculation methods for plastic gears **117**

C Oil Datasheet - BP Energol GR-XP 150 **124**

D POM (homopolymer) - Material Properties **127**

E Test Datasheets - FZG and Roughness Tests **134**

List of Figures

2.1 Stress-strain curve fo PA66. 5
2.2 Flank (σ_{HlimN}) and root (σ_{FlimN})strength for PA 66. 6
2.3 Elasticity modulus for PA 66. 7
2.4 Temperature distribution in a plastic gear tooth. 8
2.5 Influence of hysteresis and friction on tooth heating. 8
2.6 Influence of water absorption rate on volume increasing. 8
2.7 Temperature effect on logarithmic decrement. 9
2.8 Effect of temperature on POM thermal expansion coefficient. 9
2.9 Tooth deflection. 10
2.10 Hysteresis loop of plastics. 10
2.11 Wear on plastic gears (at 1000 rpm). 11
2.12 Auto-cooling method. 14
2.13 Sliding speed direction on driven and driver gears. 15
2.14 Resulting wear on driven and driver gears. 15
2.16 Influence of changing the pair drive/driven gear materials 15
2.17 Effect of PTFE lubrication on various resins. 18
2.18 Effect of lubrication on wear and tooth temperature 20
2.19 Effect of lubrication on oil temperature. 20
2.20 Different solutions from different authors and their application regions on the map of Johnson. 22
2.21 Different lubrication regimes distinguished by Johnson. 23
2.22 Comparison between Myers and Dowson solution for the film thickness along the meshing line while increasing load (μm) 26
2.23 Comparison between Myers and Dowson solution for the film thickness along the meshing line while increasing speed (μm). 26

3.1 Block diagram for a non-mechanically strained test rig. 28
3.2 Test rigs for plastic gears. 28
3.3 Schematic representation of JIS B 1759 test rig. 28
3.4 Block diagram for a mechanically strained test rig. 29
3.5 Block diagram for a pulse test rig. 29
3.6 Schematic view of the FGZ test rig. 30

4.1 Power loss contributions. 34
4.2 Influence of speed on power losses components in a gearbox. 34
4.3 Influence of geometric parameters on local gear loss factor H_{VL} 36
4.4 S_F and S_H for the cases "POM as pinion" and "POM as wheel". 38
4.5 Simulations performed for K1 load stage with an n_1 of 750 rpm. 40
4.6 Simulations performed at K2 load stage, n_1 = 750, 1500 and 3000 rpm. 40

4.7 Simulations performed at K3 load stage, $n_1 = 750$ rpm. 41
4.8 S_{W_m} - Wear safety factor for 10^7 and 10^8 cycles with $n_1 = 750$ rpm. . . 42
4.9 S_λ - Tooth deformation safety factor for with $n_1 = 750$ rpm. 43
4.10 Increase of the tooth temperatures with the applied load (K1, K2 and K3) for gears C14, H501 and H951 at 750 rpm on the pinion. 44

5.1 Experiment for thermographic camera calibration and resulting temperatures. 49
5.2 Schematic view of FGZ test rig 50
5.3 Schematic view of the FGZ test rig with the torque measuring transducer [1]. 50
5.4 Type K thermocouples locations. 50
5.5 Kinematic viscosity and thermoviscosity variation with temperature. . . 51
5.6 POM monomer. 52
5.7 Roughness measuring positions. 53
5.8 Roughness profiles from the POM *pinions 1, 2 and 3* in unused condition. 53
5.9 Roughness profiles from the POM *pinions 1, 2 and 3* after failure. . . . 54
5.10 Roughness profiles from the pinions 4, 5 and 6 in unused condition. . . 54
5.11 Roughness profiles of pinions 4, 5 and 6. 54
5.12 FTIR comparison between the experimental results and the results found in [2]. 55
5.13 Weight of POM pinion. 56
5.14 Distance $\overline{w}$ [μm] measured to evaluate wear. 57
5.15 Tooth flank breakage fail of *pinion 1*. 59
5.16 Tooth temperature after *pinion 1* failure. 59
5.17 Oil and ambient stabilization temperatures with *pinion 1*. 60
5.18 Total power loss during tests performed with *pinion 1*. 60
5.19 *Pinion 2* aspect after the test. 61
5.20 Thermographic photo after failure of *pinion 2*. 61
5.21 Stabilization temperatures on tests performed with *pinion 2*. 61
5.22 Total power loss on tests performed with *pinion 2*. 62
5.23 Tooth flank breakage fail of *pinion 3* and grown crack. 62
5.24 Tooth temperature after *pinion 3* failure. 62
5.25 Oil bath, room, and FZG base temperatures during pinion 3 tests. . . . 63
5.26 Total power loss during pinion 3 tests. 63
5.27 Calculated specific film thickness Λ for the preliminary tests. 64
5.28 Flow chart of the *pinion 1* tests procedure. 65
5.29 Flow chart of test procedure made with *pinion 2* and *pinion 3*. 66
5.30 Tooth profile of a new C14 pinion. 67
5.31 Tooth profile of *pinion 1* after tests. 67
5.32 Tooth shape of *pinion 2* after tests. 68
5.33 Tooth (next to broke tooth) profile of *pinion 2* after tests. 68
5.34 Tooth profile of *pinion 3* after tests. 68
5.35 Specific speed for C14 pinion (max/min=-3.5865/0.6801) and wheel (max/min=-2.1259/0.7820) at K2 load stage. [3]. 70
5.36 Broken tooth - failure mode (*pinion 2*). 70
5.37 Crack found on *pinion 2*. 70

5.38 Average power loss in 10 minutes periods during the last half hour of the test and during the "after failure" test performed with *pinion 2* (4500 rpm, K3 load stage). 72
5.39 Oil temperature before and after failure on *pinion 2*. 72
5.40 Damage found after the "after failure" test performed with *pinion 2*. . 72
5.41 An example of an S-N curve. 73
5.42 Flow chart of S-N tests. 74
5.43 Thermographic photo at the end of K2 load stage S-N test. 74
5.44 Top view of the right crack (Figure 5.46) found on *pinion 5*. 75
5.45 Topography of a crack found at the end of K3 load stage S-N test (*pinion 5*). 76
5.46 Two cracks found at the end of K3 load stage S-N test (*pinion 5*). . . . 76
5.47 Thermographic photo at the end of K3 load stage S-N test (*pinion 5*). . 76
5.48 Roughness profiles of a crack found at the end of K3 load stage S-N test (*pinion 5*). 77
5.49 Plastic chips removed from the oil after the test. 78
5.50 Various cracks found at the end of K4 load stage S-N test. 78
5.51 Thermographic photo at the end of K3 load stage S-N test. 78
5.52 Black spots found on unloaded flanks. 79
5.53 Damage at the end of the tests performed with *pinion 7*. 80
5.54 Tooth breakage on *pinion 7*. 80
5.55 Tooth temperature at *pinion 7* after the test. 80
5.56 Damage found on *pinion 8*. 81
5.57 Tooth temperature at the end of the test of *pinion 8*. 81
5.58 Calculated specific film thickness Λ for the S-N tests (n_1=1500 rpm; C14 POM pinions; $\vartheta_o il$=50°C). 82
5.59 Tooth shape of *pinion 4* after the test. 83
5.60 Tooth shape of *pinion 5* after the test. 83
5.61 Tooth shape of *pinion 6* after the test. 84
5.62 Tooth shape of a new H501 pinion. 84
5.63 Tooth shape of *pinion 7* after run in. 84
5.64 Tooth shape of *pinion 8* after run in on the tooth immediately after the broken teeth. 85
5.65 Tooth shape of *pinion 8* after run in a tooth far from the broken teeth. 85
5.66 Mass loss during S-N tests with C14 gears (n_1=1500 rpm;$\vartheta_o il$ = 50 °C). 86
5.67 Tooth temperature measured at the test (n_1=1500 rpm). 86
5.68 Oil temperature at the last hour of C14 S-N tests. 87
5.69 Total power loss on of C14 S-N tests. 87
5.70 Wear rate for S-N tests. 88
5.71 Transmission error and the inverse of the system stiffness for a POM/Steel gear pair with $T_d = 0.034N \cdot m$ (Results obtained with: *KISSsoft*®). . . 90
5.72 Displacement on the base circle at K4 load stage (Results obtained with: *KISSsoft*®). 90
5.73 Normal force along the meshing line at K4 load stage ($\mu = 0$; Results obtained with: *KISSsoft*®). 91
5.74 Specific sliding at K4 load stage (Results obtained with: *KISSsoft*®). . 91
5.75 Specific sliding for the pinion of a C14 POM/Steel gear pair (Results obtained with: *KISSsoft*®). 92

5.76 Tooth cut performed on *pinion 6* (C14). 93
5.77 Huge spall at the on the tests made with *pinion 7*. 93
5.78 S-N curve: experimental and theoretical comparison. 94

A.1 Flow chart for cylindrical plastic gears calculation. 104
A.2 Y_{Fa} values for reference profiles as per DIN 867. 109
A.3 Y_{Sa} values for reference profiles as per DIN 867. 109
A.4 Suggested values of Z_H for $\alpha_n = 20°$ (DIN 3990). 111
A.5 Suggested values of Z_ε for $\alpha_n = 20°$ (DIN 3990). 111
A.6 Suggested values of σ_{FlimN} for POM for different tooth root operating temperatures and number of cycles. 111
A.7 Suggested values of σ_{HlimN} for PA 66 for different tooth flank operating temperatures and number of cycles, under oil lubrication. 111
A.8 Elasticity modulus for POM in function of tooth root temperature. . . 112

B.1 Notch effect meshing moment (high stress concentrations). 121

List of Tables

2.1 Advantages and disadvantages of the use of polymers on gears. 4
2.2 Examples of some polymer properties on typical gear running conditions. 5
2.3 Water absoportion @24 hours for POM (homopolymer) and PA 66. . . 8
2.4 Chemical resistance for some polymers. 12
2.5 Failure types and main causes. 16
2.6 Fillers for internal lubrication and their effects. 18
2.7 Lubricant selection according to the service temperature 19
2.8 Dielectric constant for some oils and polymers. 20
2.9 Obtained values for h_0 [μm] and Λ for a plastic/steel gear pair using different authors solutions while increasing load at 1000 rpm. 25
2.10 Obtained values for h_0 [μm] and Λ for a plastic/steel gear pair using different authors solutions while increasing speed (rpm) at K4 load stage. 25

3.1 FZG standard load stages. 32

4.1 Geometric parameters of gears C14, 501, 701 and H951. 37
4.2 Material meshing cases. 38
4.3 Temperatures for the cases "POM as pinion" and "POM as wheel". . . 39
4.4 Tooth root ($\vartheta_{Fu\beta}$) and flank (ϑ_{Fla}) temperatures, deformation and wear safety factors for K1 simulations at 750 rpm on the pinion. 39
4.5 Tooth root ($\vartheta_{Fu\beta}$) and flank (ϑ_{Fla}) temperatures, deformation and wear safety factors for K2 simulations at 750 rpm on the pinion. 41
4.6 Tooth root ($\vartheta_{Fu\beta}$) and flank (ϑ_{Fla}) temperatures, deformation and wear safety factors for K3 simulations at 750 rpm on the pinion. 41
4.7 Failure causes and life-time for different tooth geometries at K1, K2 and K3 load stages, at 750 rpm on the pinion. 44

5.1 Gears and tests. 47
5.2 Technical specifications of the torque measuring. 48
5.3 BP Energol GR-XP 150 oil properties (according to the manufacturer). 51
5.4 Roughness and weight data of POM *pinions 1, 2 and 3*. 53
5.5 Roughness and weight data from POM *pinions 4, 5, 6, 7 and 8*. 54
5.6 Specific sliding for C14 POM pinion at different load stages. 89

A.1 Coefficient of friction μ. 105
A.2 Values calculated of H_V, for C14, 501 and 951 gears. 106
A.3 Heat transfer coefficients $k_{\vartheta,Fu\beta}$ and $k_{\vartheta,Fla}$ of the plastic gear in $K \cdot (m/s)^{0,75} \cdot mm^{1,75}/W$. 106
A.4 Heat transfer resistance of the mechanism housing in $K \cdot m^2/W$. 106

A.5 Application factor possibilities. 108
A.6 Wear coefficients for different cases in $10^{-6}mm^3/(N \cdot m)$. 113
A.7 Coefficients/parameters used or calculated. 115

B.1 σ_{FlimN} for POM given by VDI 2545 (MPa). 119
B.2 σ_{FlimN} for POM given by VDI 2736 (MPa). 120
B.3 σ_{HlimN} for PA-66 oil lubricated given in VDI 2545 (MPa). 122
B.4 σ_{HlimN} for PA-66 oil lubricated given by VDI 2736 (MPa). 122
B.5 Correction factors for different standard calculation methods. 123

Symbols and Abbreviations

Abbrv.	**Description**
E.P.	General-purpose engineering plastics
PA	Polyamide/Nylon
PE-UHMW	Polyethylene - Ultra high molecular weight
PET	Polyethylene terephthalate
POM	Polyoxymethylene/Polyacetal/Acetal/polyformaldehyde
Q.S.P.	Quasi-super-engineering plastics
S.P.	Super-engineering plastics

Symbol	**Description**	**Units**
A_G	Area of the housing	m^2
b	Face width	mm
d	Pitch diameter	mm
d'	Working pitch circle diameter	mm
d_a	Tip diameter	mm
d_b	Base diameter	mm
d_f	Root diameter	mm
m_n	Normal module	mm
E	Elasticity modulus	Mpa
$F_N(x, y)$	Local force per width unity	N/m
F_t	Nominal tangential force on teeth (reference circle)	N
F_{tb}	Nominal tangential force on teeth (reference circle)	N
g	Path of the contact	mm
g_1	Viscosity parameter	-
g_3	Elasticity parameter	-
g_4	System character parameter	-
i	Gear ratio	-
k	Tip diameter modification coefficient	mm
$\overline{h}$	Film thickness parameter	-
h_0	Film thickness	μm
H_v	Degree of tooth loss	-
H_{VL}	Local gear loss factor using rigid load distribution	-
k_2	Material combination factor (VDI 2545)	-
k_3	Housing conditions factor (VDI 2545)	-
K_A	Application factor	-
K_F	Tooth root load factor	-
$K_{F\alpha}$	Face factor	-
$K_{F\beta}$	Width factor	-

Symbol	Description	Units
K_H	Tooth flank loading factor	-
K_v	Dynamic factor	-
$k_{\vartheta,Fu\beta}$	Heat transfer coefficient of plastic gear - root	$K \cdot (m/s)^{0,75}.mm^{1,75}/W$
$k_{\vartheta,Fla}$	Heat transfer coefficient of plastic gear - flank	$K \cdot (m/s)^{0,75}.mm^{1,75}/W$
m_n	Normal module	mm
P	Transmitted power	W
P_{IN}	Input power	W
P_{VZP}	Meshing gears power losses	W
$R_{\lambda,G}$	Heat transfer resistance of the mechanism housing	$K \cdot m^2/W$
r_b	Radius of the base circle	mm
S_F	Tooth root safety factor	-
S_H	Tooth flank safety factor	-
S_S	Tooth scuffing safety factor	-
S_{W_m}	Tooth wear safety factor	-
S_λ	Tooth deformation safety factor	-
u	Transmission ratio	-
v	Circumferential speed at the reference circle	m/s
v_g	Mean sliding speed	m/s
$v_g(x,y)$	Local sliding speed	m/s
v_{ga}	Maximum sliding speed	m/s
v_{tb}	Circumferential speed at the base circle	m/s
$\overline{w}$	Wear depth	μm
x	Addendum modification coefficient	-
Y_B	Rim thickness factor	-
Y_f	Fillet factor	-
Y_{Fa}	Form factor	-
Y_{Sa}	Stress correction factor	-
Y_β	Helix angle factor	-
Y_ε	Contact ratio factor	-
$z_{1,2}$	Teeth number: pinion, wheel	-
Z_E	Material factor	-
Z_H	Zone factor	-
Z_ε	Overlap factor	-
Z_β	Spiral angle factor	-
α_{Therm}	Thermal expansion coefficient	$\mu m/(m \cdot K)$
α_{wt}	Operating pressure angle in the transverse section	$^\circ$
α_n	Pressure angle in the normal section	$^\circ$
β_b	Helix angle at the base circle	$^\circ$
$\Delta\overline{w}$	Wear depth rate	μm /hour
ε_1, ε_2	Partial contact ratios	-

Symbol	**Description**	**Units**
ε_r	Dielectric constant	-
ε_s	Yield strain	%
ε_α	Transverse contact ratio	-
ε_β	Overlap contact ratio	-
ε_γ	Total contact ratio	-
ϑ_0	Ambient temperature	°C
$\vartheta_{1,2}$	Body temperature of gears 1 and 2 (VDI 2545)	°C
$\vartheta_{Fla_{1,2}}$	Tooth flank temperature of gears 1 and 2 (VDI 2736)	°C
$\vartheta_{Fu\beta_{1,2}}$	Tooth root temperature of gears 1 and 2 (VDI 2736)	°C
ϑ_{pm}	Peak temperature of melting range	°C
$\vartheta_{service}$	Service temperature	°C
$\vartheta_{zul,dauemd}$	Permissible temperature for continuous operation	°C
Λ	Logarithmic decrement (Figure 2.7)	-
Λ	Specific film thickness	-
μ	Coefficient of friction on meshing gears	-
ρ	Density	g/cm^3
σ_F	Tooth root stress	MPa
σ_{FlimN}	Fatigue strength under pulsating stress (tooth root)	MPa
σ_H	Tooth flank pressure (Hertzian pressure)	MPa
σ_{HlimN}	Rolling contact fatigue strength (tooth flank)	MPa
σ_s	Yield stress	MPa

Chapter 1

Introduction

1.1 Thesis purpose

The power losses for a gear transmission occur due to different ways of energy dissipation, in different gearbox parts (bearings, gears, seals). Low loss gear geometries proved their importance in reducing power losses [4, 5]. Besides geometry modifications, the influence of the use of different materials on gears needs to be clarified.

The use of polymers on gear transmissions have been increasing. With much lower mechanical resistance than steel, some advantages such as dry running possibility or good vibrations absorption make polymers suitable for some applications. As polymers are mainly manufactured by injection processes, the low price is also a very important factor.

New low-loss gears were already tested in some materials such as carburized steel and austempered ductile iron (ADI) [6], but not in plastic.

Besides the lower power loss promoted, low loss geometries operating temperatures match with one of the polymer gears main failure cause, the decrease of the mechanical resistance with the increase of the temperature.

Due to the importance of polymers in gear industry, combining low-loss geometry with plastic could be an important achievement.

1.2 Thesis outline

On Chapter 2, plastic gears are contextualized: manufacturing processes are described, followed by tooth failure modes and causes. Chapter 2 ends up with a section about lubrication of plastic gears.

On Chapter 3 the different types of experimental devices used to test plastic gears are described and characterized. Some examples of test rigs are given. This chapter finishes with a description of the standard FZG test rig.

On Chapter 4 after a description and explanation about the low loss gear geometries

used, some calculations on load carrying capacity and life-time are performed for a comparison between three different gear tooth geometries, the standard C-type and two low loss helical gears.

On Chapter 5 the test procedures, are described as all the equipment used on them. The obtained results are shown and discussed for two different types of tests made: load/thermal capacity of plastic gears and material testing (S-N curve).

Chapter 6 the conclusions made after this work are listed, followed by the possible future works.

Chapter 2

Polymer Materials in Gear Industry

Polymers are divided in two subgroups, plastics and elastomers. The first subgroup, plastics, is divided in another two subgroups: thermoplastics (materials that become pliable or moldable above a specific temperature) and thermosets (materials that irreversibly cure generally induced by heat, a chemical reaction or irradiation). In this section the terms plastic or polymer will be used to refer polymers that are commonly used on the industry of gears: thermoplastics. Weak and strong points of polymer gears are pointed and described. Some properties are given as example, followed by some possible failure causes and modes. At the end of this chapter, lubrication types and modes are described.

2.1 Contextualizing plastic gears

Since long ago (1950s) that plastic gears have been in use [7]. In the last decade, the popularity of plastic gears increased due to manufacturing processes like injection moulding, and the improvement of plastic materials properties. With the improvement made on polymers industry, the application of plastic gears in several different areas such as automotive industry, office machines, food industry, textile industry and medicine became possible. [7, 8].

2.1.1 Advantages and disadvantages of plastic gears

Gear design can be limited by different parameters. If the main objective is tooth bending resistance, polymers are not, in general, a good solution, but if the objective is to run an equipment without lubricant, with less noise, working on a corrosive environment, plastic gears may be a good solution [7, 9, 10].

Some advantages and disadvantages mentioned in literature are summarized on Table 2.1.

Table 2.1: Advantages and disadvantages of the use of polymers on gears [7, 9, 10].

Advantages	**Disadvantages**
Dry run possibility	Low tooth bending resistance
Silent running and good vibration absorption	Low wear resistance
High corrosion resistance	Low heat resistance
Light weight	High higroscopicity
Cheap manufacturing process	High hysteresis during tooth deformations

2.1.2 Distinguishing engineering plastics

A lot of plastics have been studied. However, the number of plastics beeing sold in large quantities is about forty [11].

Plastics having a minimum heat-resistance of 100 °C, tensile strength of at least 49 MPa, and yield modulus of at least 2.4 GPa are called "general purpose engineering plastics" or simply "E.P.". In addition to the "E.P.", it is possible to distinguish plastics that can work in a specific engineering application over 150 °C, this plastics are called "super-engineering plastics" or simply "S.P.". The plastics with characteristics intermediate between E.P. and S.P. are called "quasi-super-engineering plastics", "Q.S.P." [11].

There are two types of E.P.: the thermosetting resins and the thermoplastic resins. Since the first studies made with polymer gears that two thermoplastic resins had some highlight: polyamide (or PA) and acetal (or POM).

2.1.3 Some polymer gear properties

Changing from steel to thermoplastic materials on gear applications is not an easy task.

Temperature dramatically changes elasticity modulus, tensile strength, or water absorption rate. The fact of a polymer part being wet, moist, or dry also has influence on yield modulus and yield strength[1] (check Figure 2.1). With new properties that go beyond the fact of plastics having lower mechanical resistance, the gear designer must be warned for these aspects.

Some properties are listed on Table 2.2 , some of them with a range of value taking into account the normal service conditions. The properties listed are the density (ρ), the peak temperature of melting range (ϑ_{pm}), permissible temperature for continuous running conditions ($\vartheta_{zul,dauemd}$), yield stress (σ_s), yield strain (ε_s) and elasticity modulus (E).

Water absorption and vibration damping will be analysed, as the temperature influence on these factors. Detailed information about tooth and flank resistance for gear meshing will also be given also as a function of temperature.

[1] The properties marked with an asterisk "$*$" in Table 2.2, are given for three distinct situations: wet, moist and dry.

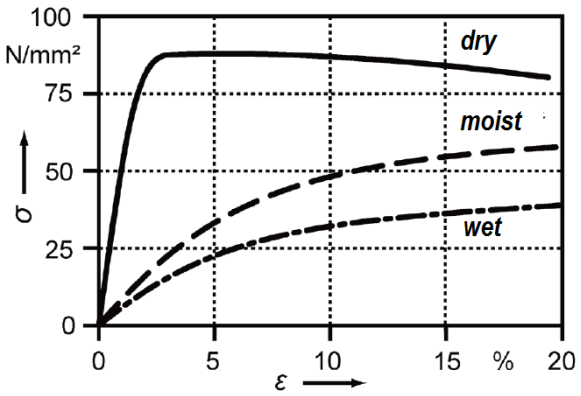

Figure 2.1: Stress-strain curve fo PA66 [12].

Table 2.2: Examples of some polymer properties on typical gear running conditions [12].

Polymer	ρ $[g/cm^3]$	ϑ_{pm} [°C]	$\vartheta_{zul,dauemd}$ [°C]	σ_s [MPa]	ε_s [%]	E [MPa]
PA 66	1,13...1,16	225...265	80...100	85/60/-*	5/20/-*	3000/1600/800*
PET	1,38...1,40	250...260	100	55...80	4...7	2100...3100
POM	1,39...1,43	164...175	90...100	60..75	15...>50	2600...3200
PBT	1,30...1,32	220...230	~100	50...60	3,5...7	2500...2800
PPS	~1,34	275	200...240	~88	~3	4000

2.1.4 Manufacturing processes

The most used manufacturing process is injection moulding. However, casting and machining may also be used. The chosen method usually depends on the gear material, the desired quantity, size and geometry. [12]

Injection moulding

Injection moulding is usually the right choice if the production volumes are large. Sometimes, when the quality requirements are too high, a finishing process using machining auxiliary processes may be necessary. One of the limitations of the process, is the wall thickness. In a moulding process, the shrinkage of a semi-crystalline plastic depends on the wall thickness. Generally, larger wall thicknesses require a longer heating cycle and tend to have more defects. Nowadays, it is common to use injection moulding up to 10 mm of wall thickness. Injection moulding requires an high control of the temperatures in all the volume. The injection point on the part and the injection speed are also very important parameters to take into account [12].

Casting

Casting process is suitable for gears with large dimensions, weighing about 1 kg. For this method only cast polyamides such as PA 6-G, PA 12-G and polyurethane elastomers can be currently be processed. It is also common to have a finishing cutting work due to the low accuracy of this method [12].

Machining

Machining is advantageous for small and medium series since the tool costs are lower when comparing to injection moulding. The methods used to machine plastic gears are the same ones used to metal gears [12]: gear forming (by milling or broaching) and gear generation processes (i.e. hobbing) are some possibilities.

2.2 Failure modes and causes for a plastic gear

2.2.1 Tooth temperature

Tooth temperature is a very important parameter for plastic gears. It is used as an indicator to evaluate power losses and is a crucial factor affecting the service life-time.

One of the main problems of increasing the temperature is the stiffness reduction and the tooth root and flank load capacities (check Figures 2.2 2.3) [12]. Another fact of plastics is that the low thermal conductivity makes this problem even worse, since it is harder to evacuate the heat: as an example POM has a thermal conductivity approximately between 0.22 and 0.35 $W/m{\cdot}°C$, while a stainless steel has a value between 12 and 24 in the same measure units.

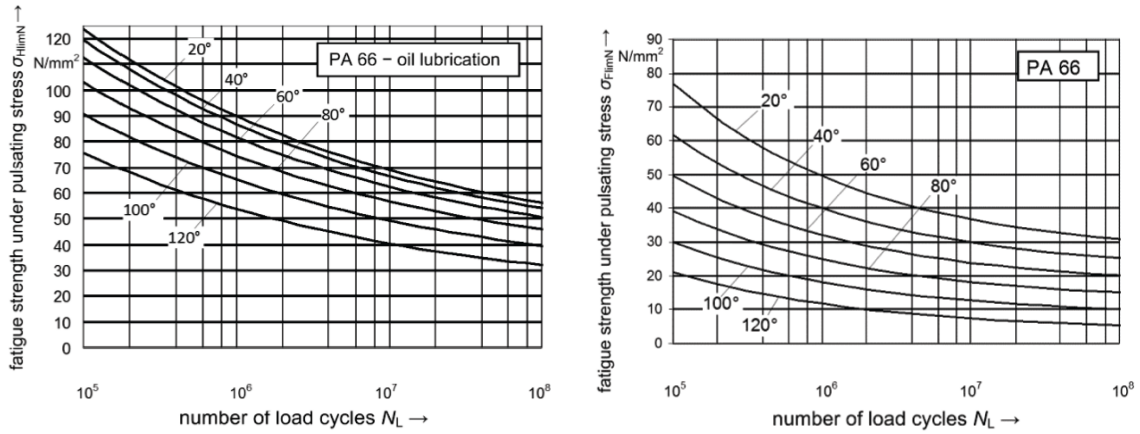

(a) Permissible rolling contact fatigue strength σ_{HlimN}.

(b) Permissible fatigue strength under pulsating stress σ_{FlimN}.

Figure 2.2: Flank (σ_{HlimN}) and root (σ_{FlimN})strength for PA 66 [13].

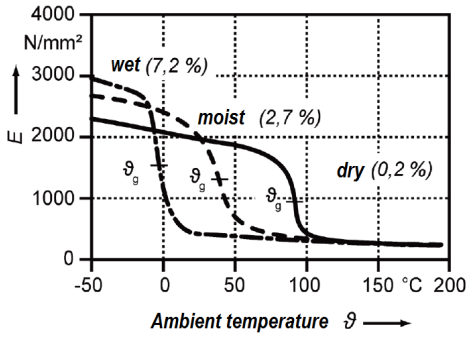

Figure 2.3: Elasticity modulus for PA 66 [12].

Temperature distribution

For a plastic gear, temperature tends to be higher near the pitch point, which makes this zone a typical failure zone. When tooth break occurs without a large increase of temperature, it is probably the result of an overload and the failure occurs on the tooth root. However, differently from steel gears, if temperatures raise up to a critical level, the critical section tends to be near the pitch point, where mechanical resistance is substantially reduced due to the temperature increase. The breakage position at the tooth is usually decided in a balance between the zones with higher stresses and the zones with higher temperatures (less mechanical resistance) [14].

In Figure 2.4, an approach for temperature distribution in a plastic gear tooth was made. It shows that temperatures are higher near the pitch point (where rolling contact occurs) than near tooth tip and root (where sliding occur). This temperature distribution is explained by the ease with which each zone is able to release the heat generated due to tooth deformation hysteresis (explained ahead on Section 2.2.2). The heat is released faster at the tip and at the root because the radiation cooling is easier in that areas [11]. The influence of hysteresis and friction on tooth heating is shown as a function of the distance to the pitch point on Figure 2.5 [11]. Tooth deflection hysteresis will be discussed on Section 2.2.2.

Influence of Temperature on Hygroscopy

Hygroscopy is the capacity of a substance to attract and hold water (absorption) and is a very common problem on plastics. The water absorption results in the reduction of mechanical resistance, and volume increasing. Dimension changing is a an important problem specially in gears with tight tolerances.

Hygroscopy intensity increases with the increase of the temperature, which, for applications under external lubrication, makes this an important aspect to take into account [12].

Hygroscopy influence on volume increasing is given in percentage relatively to the plastic body in analysis on Figure 2.6. Comparing nylon (PA) with polyacetal (POM), it is clear in Figure 2.6 that PA has a lower dimension change rate, although it is highly hygroscopic. Notice that the material dimension change rate is not directly related with the quantity (in weight) of absorbed moisture.

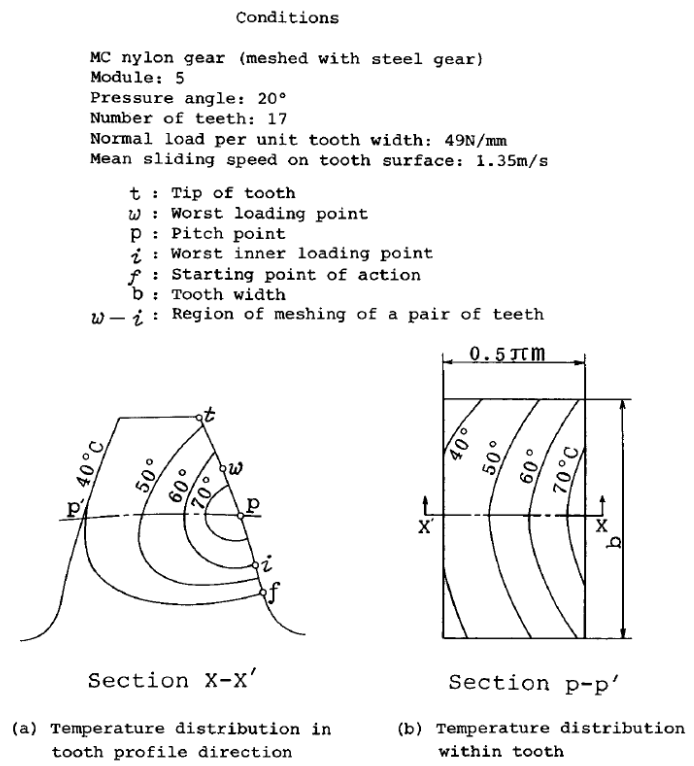

Figure 2.4: Temperature distribution in a plastic gear tooth (*steel/nylon* gear meshing; $m_n = 5$ mm; z=17; $F_n = 49N/mm$; $v_g = 1,35m/s$) [11].

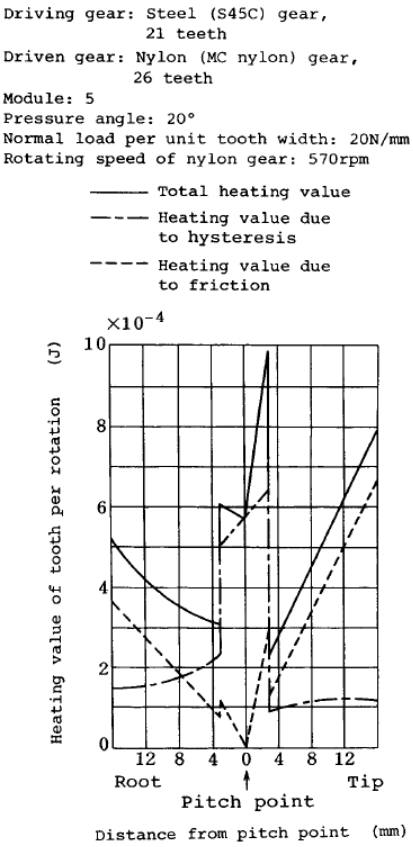

Figure 2.5: Influence of hysteresis and friction on tooth heating [11].

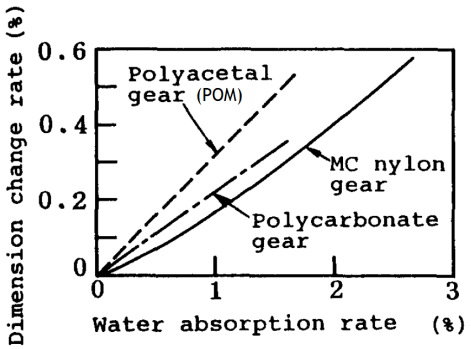

Figure 2.6: Influence of water absorption rate on volume increasing [11].

Table 2.3: Water absoportion @24 hours for POM (homopolymer) and PA 66 [15].

Material	Water absorption @24 hours
POM	0,2 - 0,22
PA 66	0,62 - 1,00

Although POM dimension change rate is higher than PA, due to its less hygroscopy, it is a suitable material for gears running, for example, underwater. [11].

ISO 62 defines the test procedure for weigh gain after 24 hours immersed in distilled water at 23 °C [15]. Properties for POM and PA are shown on Table 2.3.

Influence of Temperature on Vibrations Damping

Besides all the negative effects of heating on plastic gears, there is a positive one: the increasing of vibrations absorption capacity. Figure 2.7 shows that the range where the logarithmic decrement is higher, for almost all the materials shown, somehow coincides with typical working temperatures for a gear transmission system.

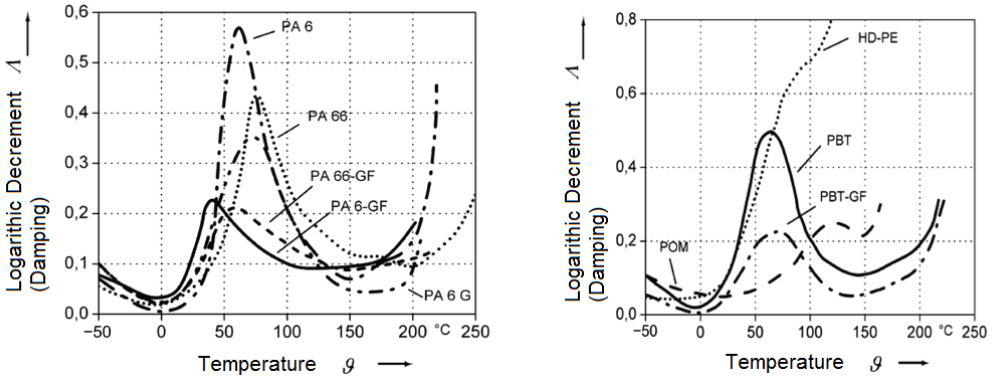

Figure 2.7: Temperature effect on logarithmic decrement [12].

Thermal expansion

Finally, temperature increasing, as generally in all materials, dilates original solid form increasing the volume. It is an expected aspect, but more important in plastics since this effect is added to hygroscopy. An example is shown on Figure 2.8.

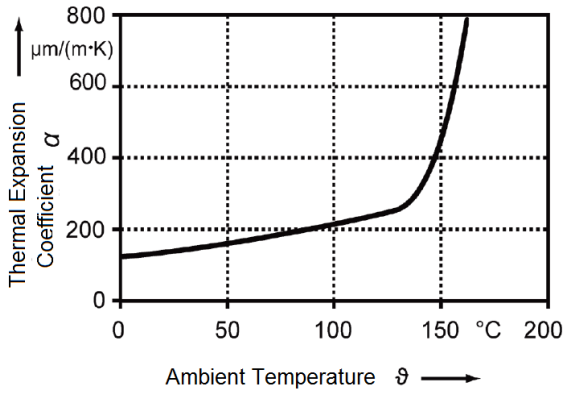

Figure 2.8: Effect of temperature on POM thermal expansion coefficient [12].

2.2.2 Tooth deflection

As the stiffness of plastics is much lower when comparing to steel (i.e. E for POM is a value between 2,6 and 3,2 GPa, and E for steel is a value around 210 GPa), the tooth deflection must be considered. Figure 2.9 shows an example of the tooth deflection for a specific case.

Tooth deflection in plastics depends on the in-load time: if a static load is applied continuously, the deflection tends to increase with time. To exemplify, in Figure 2.9, the initial deflection is 30 μm , however, after 4 minutes, the deflection is close to 40 μm .

The problem gets worse if the static load is applied for a long period: permanent deformation occurs, and the deflection does not reach the value 0 when no-load state is returned [11].

Hysteresis

Figure 2.9, also shows that POM has higher deformations than PA since POM has a lower stiffness. However, due to the possession of a lower viscosity, POM recovers faster the original shape. Plastics are visco-elastic, which means that they need some time to recover their original no-loaded shape after being loaded for a time period (short or not). This behaviour results in a tooth deformation hysteresis loop as shown on Figure 2.10 [11].

For high rotational speeds, tooth pairs may enter in contact while deformations are still present, changing engagement geometry, increasing sliding speed, and, consequently, increasing power loss and wear (specially near the tooth root). [11].

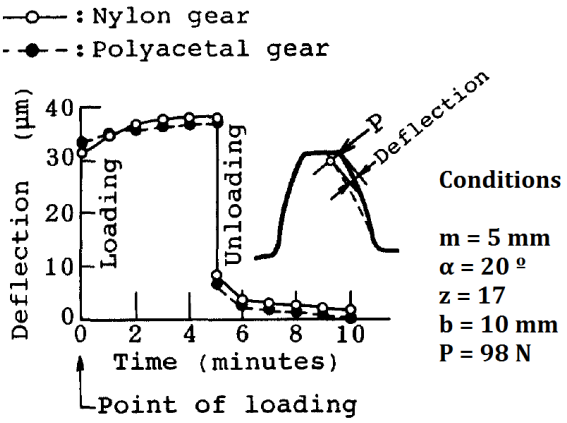

Figure 2.9: Tooth deflection [11].

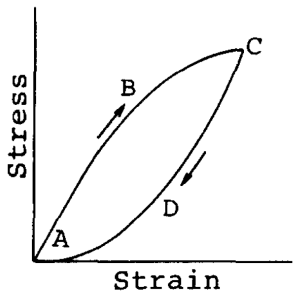

Figure 2.10: Hysteresis loop of plastics [11].

2.2.3 Wear on plastic gears

In this section wear on POM and PA gears is analysed. Tests made by Mao *et all.* [9] with POM, PA and steel gears seem to prove that the wear behaviour depends a lot on the material used and the drive/driven material combination [9].

For POM-POM and PA-PA cases, wear can be divided into three phases: the "initial running in", a "nearly linear" and a "final fracture" phases. The running in period is short, but the wear that happens on this period is considerable. A nearly linear period takes place increasing the wear progressively until it reaches a critical value. After reached the critical value, wear rate increases dramatically leading to failure. The results from the tests made by Mao *et all.* [9] are shown in Figure 2.11.

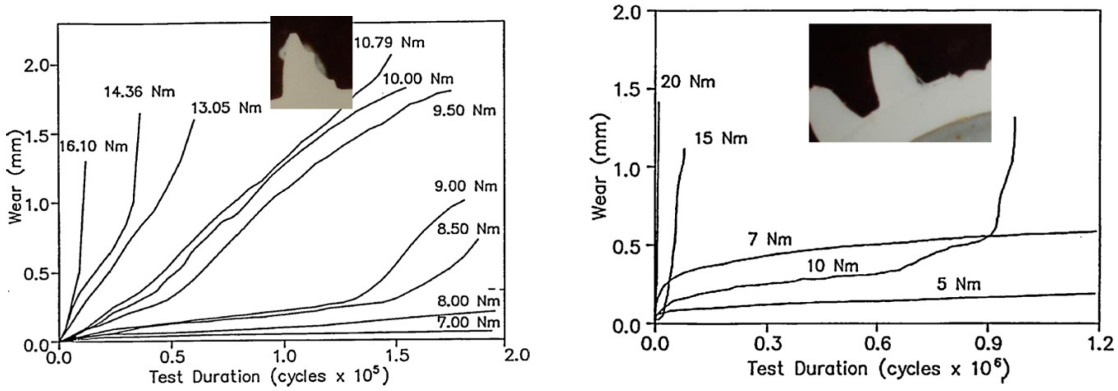

(a) Wear for acetal against acetal.

(b) Wear for nylon against nylon.

Figure 2.11: Wear on plastic gears (at 1000 rpm) [9].

The number of cycles achieved have an high dependence on the load. For low torques, it seems that wear does not lead to fracture, and high cycles number is achieved ($> 10^7$ cycles). However, for less than 10^6 cycles, the life time period depends mainly on applied load, and tooth fracture occurs near the pitch point at the driving gear teeth [9].

For dissimilar material combinations results are quite different. The combination N/A (nylon as the driving gear and acetal as the driven gear) resulted in similar results comparing to A/A combination, however A/N combination resulted in a big increasing of life time [9]. This topic will be discussed in Section 2.3.2.

2.2.4 Chemical incompatibility

Plastics compatibility with other substances is relevant since it can lead to fast wear and failure. Washing products, fuels, and other substances that are suitable to enter in contact with a plastic gear are listed in Table 2.4.

Table 2.4: Chemical resistance for some polymers [12].
Note: + resistant;± limited resistance; − unstable.

Chemical		POM	PA 66	PA 46	PPA	PET	PBT	PEEK	PPS	PF
Alcohols	Methanol	+	±	+	+	+	+	+	+	+
	Ethanol	+	±	+	+	+	+	+		+
	Propanol	+	±	+	+	+	+	+		
Water	Cold	+	+	+	+	+	+	+	+	+
	Hot	±	±	±		−	−	+	±±	±
Fats, Oils	Check lubrication Section on 2.4									
Fuels	Gasoline	+	+	+	+	+	+	+	+	±
	Diesel	+	+	+	+	+	+	+	+	
Acids	Hydrochloric acid	−	−	−	−	−	±	±		
	Sulfuric acid	−	−	−	−	−	−	−		
	Acetic acid	−	−	−	−	−	−	+		
	Strong	−	−		−	±	−	±		−
	Weak	±	−		−	+	±	+		±
Alkalis	Potassium hydroxide	+	+			−	−	+		
	Sodium hydroxide	+	+				−	+		
	Ammonium hydroxide	+	±			±	±	+		
	Strong	+	±		+	−	+	+		−
	Weak	+	±		±	±	+	+		±

2.3 Failure modes and life-time for a plastic gear

Failure modes and life-time of a gear depend on many factors: gear geometry, gear materials, applied load, gear materials combination, load, speed, ambient chemistry, ambient temperature, manufacturing processes used to make the gears, lubrication etc [11, 12, 16].

Gear geometries may be designed to reduce sliding speed and, with it, reduce operating temperatures. The materials must be well chosen, as well as their combination and position (pinion material, wheel material, driving gear). Loads and speeds are crucial, and must take into account the properties of the material used and, very important, the operating temperatures. Manufacturing processes are determinant to the friction behaviour of a gear pair. Surface finishing may be a good way to reduce friction. Lubrication can be applied, since it decreases wear and friction dramatically, although hygroscopy problems may appear [11, 12, 16].

2.3.1 Failure modes for a plastic gear

Plastic gears life time and failure mode result from the combination of a lot of factors. Table 2.5 summarizes most of the failure modes and suggests some possible failure causes.

2.3.2 Increasing plastic gears life-time

Various methods have been studied in order to increase the life time of plastics. These methods may have different objectives: temperature reduction or wear reduction. In this section an auto-cooling method is introduced, and the best material combinations for the cases with dissimilar materials in therms of driver/driven and pinion/wheel are discussed.

Lubrication and tooth geometry modifications may also increase plastic gears life-time. Their effects are not described on this section. Lubrication on plastic gears is described in Section 2.4 and tooth profile modifications are described in Section 4.1.

Auto-cooling method

Specially in plastics, cooling may be very important. The normal gear movement helps to dissipate some of the heat generated on the gear meshing. However, normal auto-cooling may not be enough (specially for high loads and speeds when power losses are higher). A very interesting method to increase the auto-cooling effect for dry running is suggested by Tsukamoto.

This method consists on drilling small holes between the teeth, allowing the air to go inside the holes due to pressure gradient during rotation, and blow against the tooth flank. With this method, Tsukamoto increased the working number of cycles from $2 \sim 3 \cdot 10^6$ to more than 10^7 [16] (see Figure 2.12).

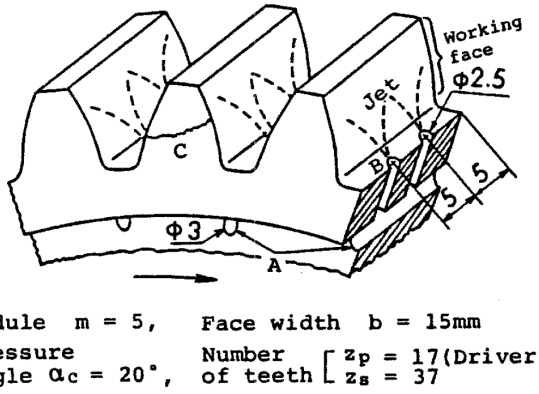

Figure 2.12: Auto-cooling method [16].

Plastic gear as wheel and steel gear as pinion

For dissimilar material gear meshing, the use of the plastic gear as wheel seems to result in higher life-time. Besides, the number of load cycles is lower on the wheel for the same running time, due to bigger number of teeth z_2, and cooling is also more effective.

The wheel teeth have more time to dissipate heat than the ones from the pinion which results in lower tooth temperatures. With this method, Tsukamoto shows an increase of the life-time higher than i (gear ratio) times more than while running with the plastic gear as pinion [16].

Plastic as driven gear and steel as driver gear

As the direction of the sliding speed is different on the driven and on the driving gear, the resulting damage will be different. In the driven gear, the direction of the tooth action is from the side of tip and the side of the root to the pitch circle, resulting that the hollow near the pitch circle (which may lead to tooth breakage) does not occur, unlike the opposite case. To better understand what happens, Figures 2.13 and 2.14 show the sliding speed direction, and the resulting wear.

If the gear material combination is plastic and steel, since plastic has lower wear resistance, then plastic should be used as driven gear.

The same analysis may be applied to a material combination of two plastics, when possible, the weakest plastic against wear should be used as driven gear.

Figure 2.16 shows some results found by Mao *et all.* in order to test this criterion revealing that it is possible to increase around 5 times a gear pair life-time.

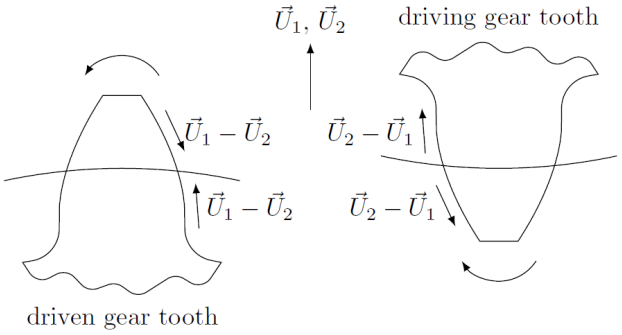

Figure 2.13: Sliding speed direction on driven and driver gears [17].

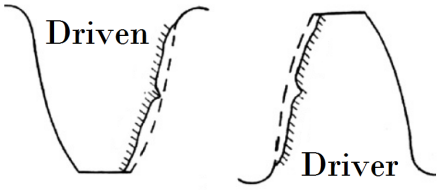

Figure 2.14: Resulting wear on driven and driver gears [9].

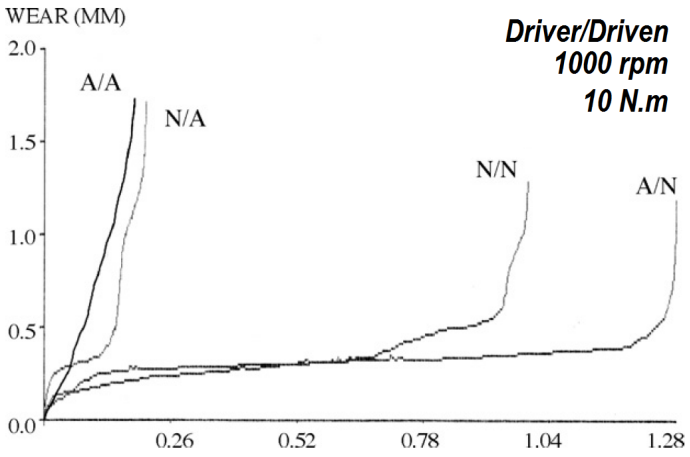

Module	2 mm
Teeth number	30, 30
Pressure angle	20 °
Face width	17 mm
Nominal backlash	0.18 mm
Tooth thickness	3.14 mm
Contact ratio	1.65

Figure 2.16: Influence of changing the pair drive/driven gear materials (number of cycles $\times 10^6$) [9].

Table 2.5: Failure types and main causes [12].

Damage	**Spur Gears**	**Helical gears**	**Main Cause**
Partial melting	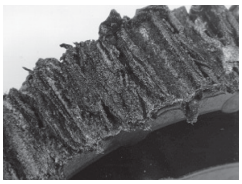	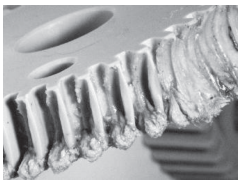	Excessive heating of the tooth flanks
Tooth root fracture	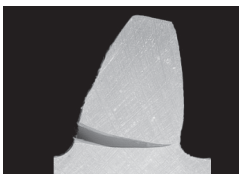	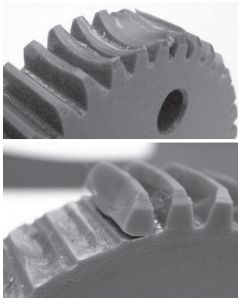	Too high stresses (left and bottom right - by bending stress; top right - by shear stress)
Tooth flank fracture (on the left) Dimples on the tooth flank (on the right)	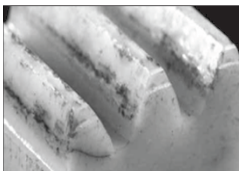		High hertzian pressures exposure of a small crack, combined with bending stresses, might critically grow the crack
Pitting	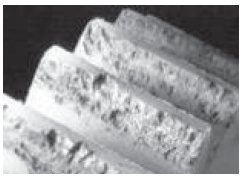	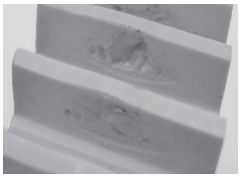	High hertzian pressures exposure
Tooth wear	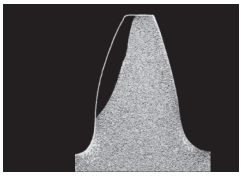	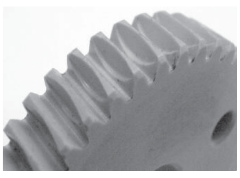	Low wear resistance
Tooth deformation	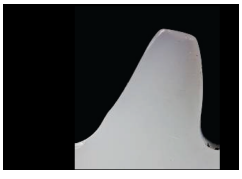	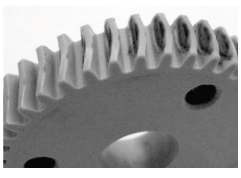	Excessive deformation due to high loads

2.4 Lubrication on plastic gears

Lubrication on plastic gears is not so well known as for steel gears. One of the best advantages of plastic gears is the possibility to operate without lubricant, which may be one of the main causes for this information absence.

In many plastic gears applications, it is common to operate without lubricant. However, when requirements for noise, wear, and extended life-time are necessary, lubrication may be used.

The most widely accepted standard for plastic gears calculation does not make any distinction between the different oil or grease types. Fillers (internal lubricants such as graphite) are not even considered, which leaves the experimental tests as the main option.

In this section lubrication types will be generally described.

2.4.1 Distinguishing lubrication types

For a polymer gear pair, the lubrication mode can be distinguished in two types:

- solid lubrication with internal fillers;
- external lubrication.

For the first case, with internal lubrication, it is important to define a good ratio for the between the base and the filler materials since some types of fillers may reduce mechanical properties.

For the second case, there are not unidirectional opinions and experiments should be made.

2.4.2 Fillers

In a similar way as fiber on composite materials (a matrix resin/polymer reinforced with fiber), fillers are added to the base polymer, although with an objective which may not be related to the increase of the mechanical resistance. Usually, fillers tend to decrease the mechanical resistance of the unfilled polymer, however, with the right filler portion, life-time may be increased. Some types of fillers and their effects are listed in Table 2.6. In figure 2.17 the effect of filling with PTFE on wear factor is shown.

For fillers use, the meshing quantities are a very important parameter, since a bad meshing may result in a worse situation.

Table 2.6: Fillers for internal lubrication and their effects [12].

Fillers	**Positive effects**	**Negative effects**
Glass, carbon and aramide fibers	Increases stiffness, tensile strength, bending resistance and heat resistance.	Reduces impact resistance
Polytetrafluorethylene (PTFE)	Reduces friction.	Reduces impact resistance, decreases bending capacity
Polyethylene (PE)	Reduces friction.	Reduces impact resistance
Graphite , Boron nitride	Reduces friction, increases thermal conductivity.	Reduces impact resistance
Silicone oil	Reduces friction, increases hardness.	
Mineral fillers	Increases thermal conductivity	

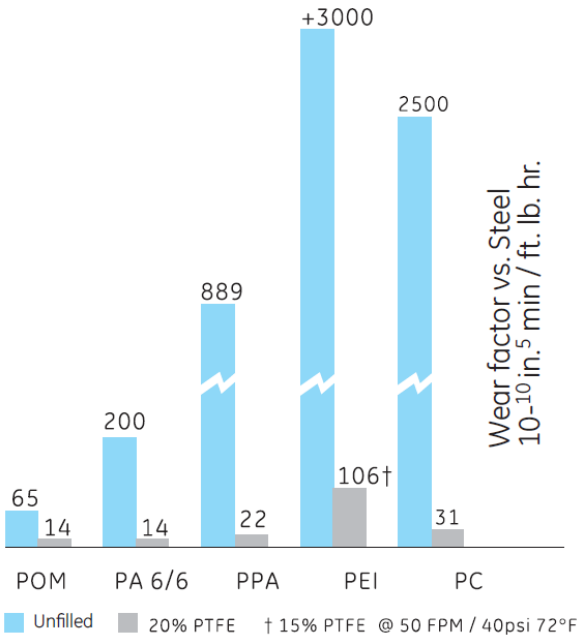

Figure 2.17: Effect of PTFE lubrication on various resins [18].

2.4.3 Greases

It is known that for synthetic greases, corrosion and volume increasing due to moisture absorption are not a big problem. Even the problem associated to the temperature increase does not negatively affect the lubrication parameters. The main warning is to guarantee that the lubricant used adheres firmly to the contacting surfaces. The peripherical speed is limited to a maximum of 5 m/s, so that the grease is not expelled due to centrifugal forces [12].

2.4.4 Oils

Based on experiments, it seems to be a good decision to select the lubricant according to the service temperature of the gears. Synthetic base oils are suitable for low service temperature. However, above 60 °C, only some synthetic oils should be used. The chosen oils/lubricants suggested by VDI 2736 based on service temperature are shown on Table 2.7.

Table 2.7: Lubricant selection according to service temperature [12].

$\vartheta_{service}$ [°C]	**Lubricants**
$[-80, 20]$	Synthetic base oils
$[20, 60]$	Mineral oils
$[60, 100]$	PAO, ester oils
$[100, 120]$	Ester oils, Silicone oil, PFPE

Polarity should be taken into account for the lubricant choice. Polar polymer gears should be lubricated with nonpolar base oils, and vice-versa. For PA and POM gears, as they are polar thermoplastics, the use of non-polar base oils is recommended [12]. For a specific material, the tendency to polarize is measured by the dielectric constant (relative permittivity, $\varepsilon_r = 1$ for vacuum). Polarization occurs when a material is placed inside an electric field, resulting in electric charges on the body surface. The dielectric constant (ε_r) for some lubricants and gear plastics is shown on Table 2.8 [15].

Additives and thickeners addition to oils may also affect plastics badly since they change oil chemical composition and properties such as polarity may be affected. Tests should be made, statical and dynamical, to accomplish this information [12].

To reduce hygroscopic behaviour, high viscosity oils should be used since they are less prone to penetrate on the polymer gear. The use of oils with an ISO VG 100 grade or more is recommended [19].

The impact of viscosity on tooth temperature is shown on Figure 2.19 for a specific case. High viscosity decreases tooth temperature (relatively to oil temperature), however it increases the oil temperature, as shown for the same case on Figure 2.18b. Less friction on meshing gears, and higher churning power losses may be a possible cause. The result on wear is shown on Figure 2.18a, and is not unidirectional. However, by Tsukamoto tests [22], the difference found on wear while changing viscosity does not seem to be great.

Table 2.8: Dielectric constant for some oils and polymers [15, 20, 21].

Base oils	ε_r	Polymers	ε_r
Hydrocarbon/Mineral	2.1-2.4	PPS	3-3.2
PAO	2.1-2.4	PBT	3.2-3.4
Diester	3.4-4.6	PET	3.5-3.7
Polyol Ester PAG	4.6-4.8	POM	3.6-3.8
Phosphate Ester	6.0-7.1	PA 66	6.8-9.6
PAG	6.6-7.3	Metal materials	∞

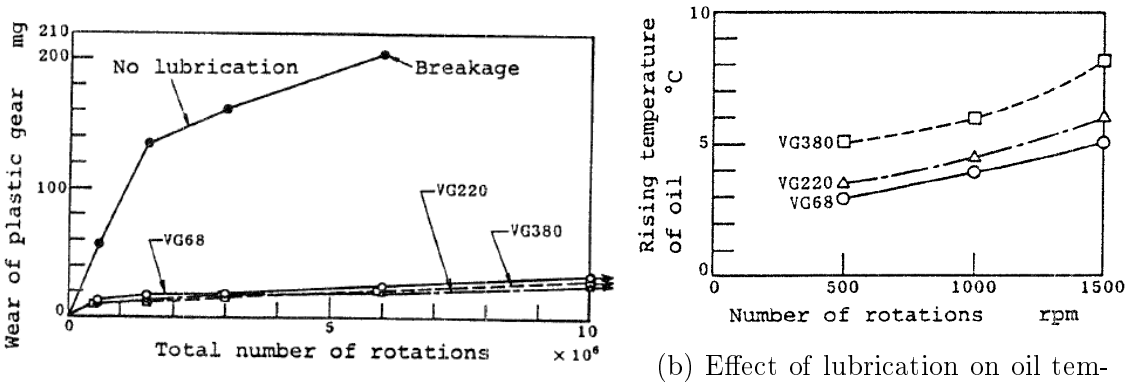

(a) Effect of lubrication on wear.

(b) Effect of lubrication on oil temperature.

Figure 2.18: Effect of lubrication on wear and tooth temperature [22].

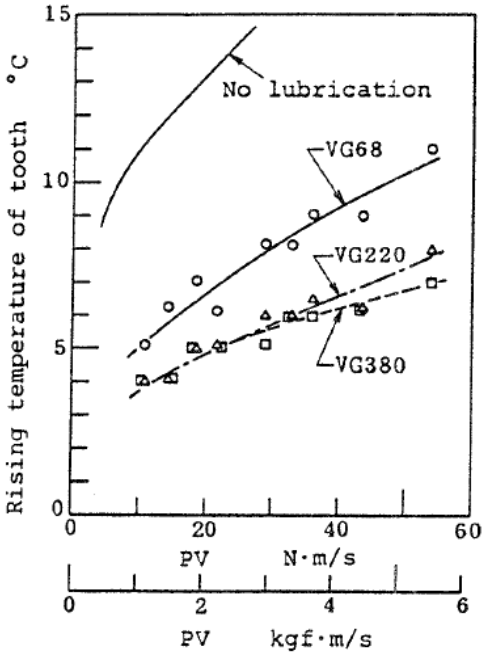

Figure 2.19: Effect of lubrication on oil temperature [22].

2.5 Elastohydrodynamic Lubrication for Polymer Spur Gears

Elastohydrodynamic (or EHD) describes contact and lubrication conditions of two surfaces in contact in a very small area, when loaded against each other [23].

During the contact, the elastic deformation of the bearing surfaces and the resulting pressures are determinant for the effectiveness of the lubricant [23, 24].

For highly loaded metal contacts lubricated by common oils, both of the effects are present. The same might not happen if the loads are sufficiently low and the speeds sufficiently high, since elastic deformations might not be considerable. For solids with low elasticity modulus changes in viscosity of the lubricant are usually small [24]

Due to all the possibilities, different regimes of elastohydrodynamic may occur.

2.5.1 Lubrication Regimes

Johnson [24] suggested a map based on two dimensionless parameters which he called g_1, the viscosity parameter, and g_3, the elasticity parameter (equations (2.1) and (2.3)). To create a map of the lubrication regimes, Johnson placed g_1 as y axis and g_3 as x axis as shown on Figure 2.20.

Based on different assumptions, different authors suggested different ways to calculate film thickness based on their own non-dimensional parameters. Johnson placed the names of the authors on the map according to the values of g_1 and g_3 where their parameters are valid. To make map areas more distinguishable, Johnson suggested another parameter (firstly used by Archard), g_4 which is called the system character parameter. It can be used to define regions (or boundaries) on the map since it depends on g_1 and g_3. By this way, g_4 (equation (2.4)) calculation is also another tool to identify the lubrication regime of a specific application on the map.

Film thickness (h_0) can then be calculated according to equation (2.5), after the calculation of the mean film thickness parameter ($\overline{h}$). The expression used to calculate the film thickness parameter depend on the author and their respective region on the map.

$$g_1 = \left(\frac{\alpha^2 w^3}{\eta_0 \overline{U} R^2}\right)^{1/2} \qquad (2.1)$$

$$g_2 = \left(\frac{\alpha^2 w E}{2\pi R}\right)^{1/2} \qquad (2.2)$$

$$g_3 = \left(\frac{w^2}{\eta_0 \overline{U} E R}\right)^{1/2} \qquad (2.3)$$

$$g_4 = \left(\frac{\alpha^4 E^3 \eta_0 \overline{U}}{R}\right)^{1/2} \qquad (2.4)$$

$$\overline{h} = \frac{h_0 w}{\eta_0 \overline{U} R} \qquad (2.5)$$

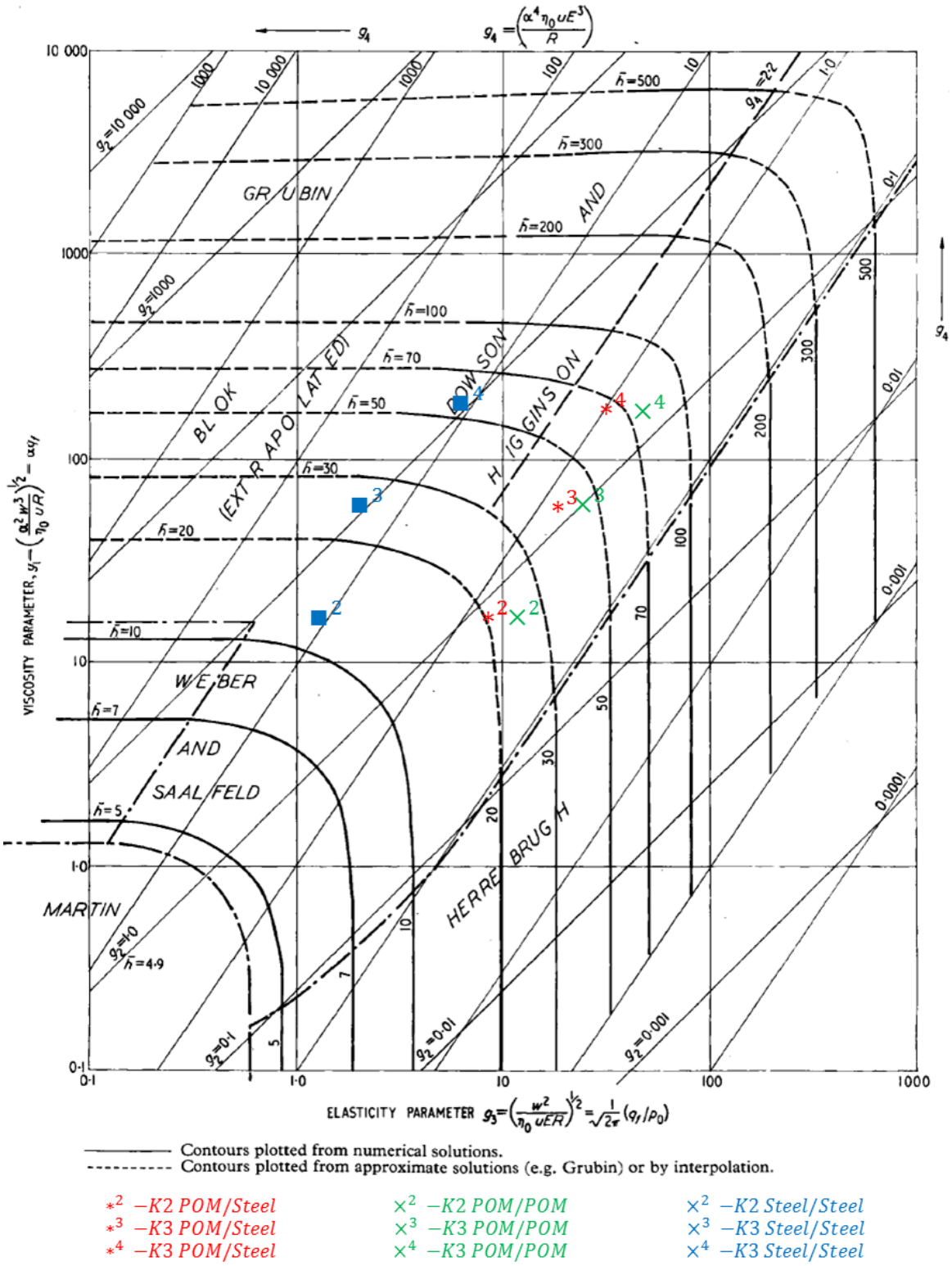

Figure 2.20: Different solutions from different authors and their application regions on the Johnsons' map [24].

The same map can be redrawn distinguishing the different EHD lubrication regimes as exemplified on Figure 2.21. For low values of g_1 and g_3 viscosity and elasticity variations can be neglected [24]. This region (bellow ACDBE on Figure 2.21) can be called rigid-isoviscous [23]. For low values of g_1 (until the boundary ML), while increasing g_3, Blok showed that there is a region where the viscosity variations can be neglected but the

elasticity ones cannot [24]. This region above the boundary AC and bellow ML can be called rigid-pieozoviscous [23]. Bellow the boundary BDE is the elastic-isoviscous region, and for values above the boundary MLCDFE, the EHD lubrication conditions are influenced by both the elasticity and viscosity variation effects. Solutions were earlier studied by Dowson and Higginson for values of g_4 bigger than 2.2. However, if g_4 is between 2.2 and 0.1, Johnson does not suggest a solution and says that this region applies to polymer materials lubricated with mineral oils.

This region was later studied by Myers *et all.* in [25]. In this region there is a rapid change due to the transition between elastic-piezoviscous and elastic-isoviscous behaviours [24].

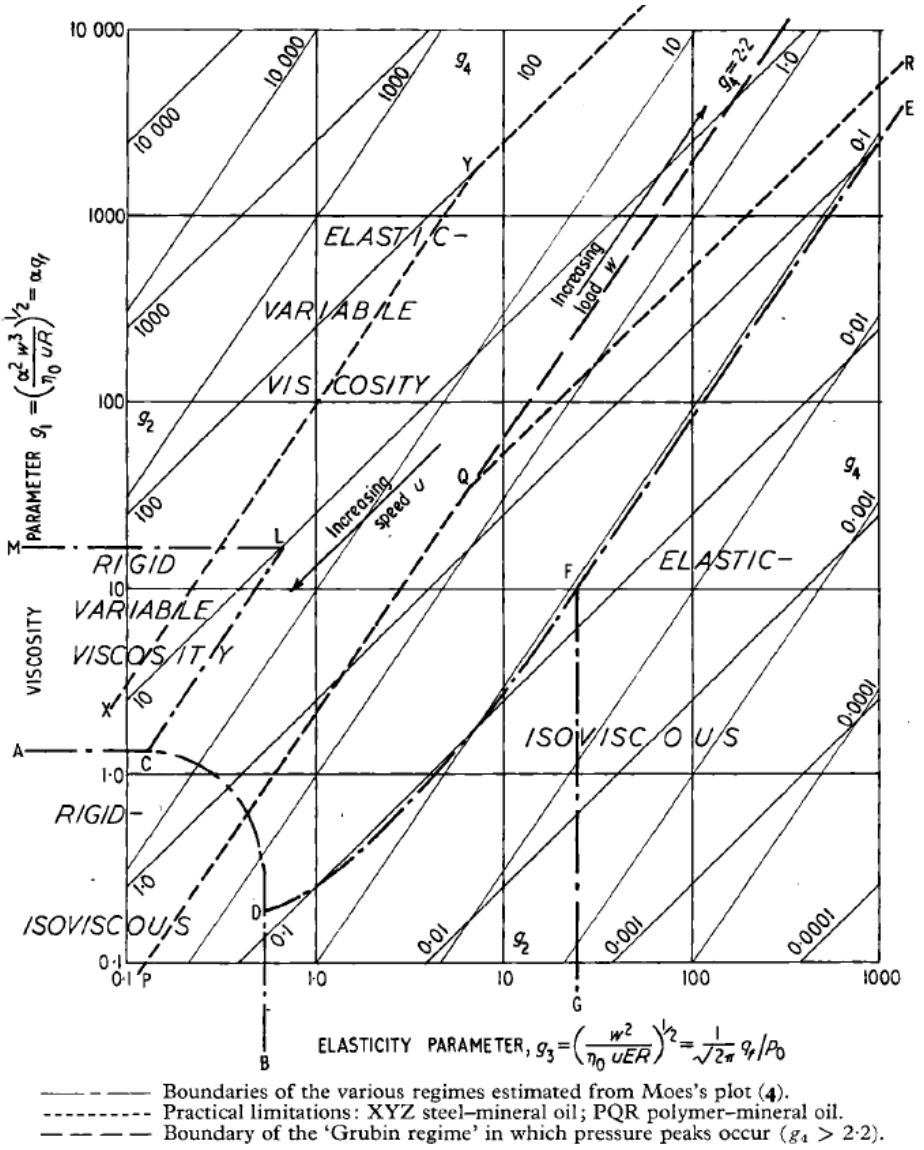

Figure 2.21: Different lubrication regimes distinguished by Johnson (*Contours of film-thickness parameter superimposed upon the map*) [24].

2.5.2 Comparing steel with plastic gears

As the present work has its main focus on plastic gears, some calculations were made in order to check the differences between the lubrication regimes of a plastic pinion running against a steel wheel, a plastic gear pair, and a steel gear pair under the same load and speed conditions (1000 rpm on the wheel, at K2, K3 (wear) and K4 FZG load stages[2]). The plastic considered was POM and the steel considered was 16MnCr5. The lubricant considered was a mineral oil, which data can be found in Appendix C, with an input temperature of 50 °C. The gear geometry considered was C14 type, which are described ahead on Section 4.3, and calculations were performed for the pitch circle contact (typically called point I) of a gear contact. The results found were plotted in the map of Johnson as shown on Figure 2.20.

By the calculations made, it is seen on Figure 2.20 that with the reduction of the stiffness of the gear pair, while maintaining all the other parameters, an horizontal displacement can be observed due to the increasing of the elasticity parameter. This displacement is sufficiently high to change the map region while changing from a steel/steel gear pair to a steel/plastic or a plastic/plastic gear pair.

The film thickness was then calculated to the steel/plastic gear pair in order to observe the differences between the obtained results following the different authors expressions (equations (2.6) - (2.9) [24] and equation (2.10) [23]) for the film thickness parameter $\overline{h}$. After calculation the equivalent surface roughness (R_{at}), replacing R_{a1} and R_{a2} by the RMS roughness measured values on tooth flanks, it is possible to obtain the specific film thickness λ as shown on equations (2.11) and (2.12) .

Calculations were made at constant speed (1000 rpm) while increasing load, and at constant load (K4 load stage) while increasing speed. For the first case, the results are shown on Table 2.9 and a comparison between Myers and Dowson solutions along the meshing line is shown on Figure 2.22. For the second case results are shown on Table 2.10 and the comparison between Myers and Dowson solutions is shown on Figure 2.23.

$$\overline{h}_{MARTIN} = 4.9 \qquad (2.6)$$

Rigid-Isoviscous Region

$$\overline{h}_{HERREBRUGH} = 3.10 \cdot g_3^{0.8} \qquad (2.8)$$

Elastic-Isoviscous Region

$$\overline{h}_{BLOK} = 1.66 \cdot g_1^{2/3} \qquad (2.7)$$

Rigid-Piezoviscous Region

$$\overline{h}_{DOWSON} = 2.65 \cdot g_1^{0.54} \cdot g_3^{0.06} \qquad (2.9)$$

Elastic-Piezoviscous Region

$$\overline{h}_{MYERS} = \begin{cases} 0.383 \cdot g_1 \cdot g_3^{-0.379} + 4.465 \cdot g_3^{0.667} & , \quad 1 < g_3 < 15 \\ 0.853 \cdot g_1 \cdot g_3^{-0.664} + 3.41 \cdot g_3^{0.77} & , \quad 1 < g_3 < 100 \end{cases} \qquad (2.10)$$

Transition between Elastic-Piezoviscous and Elastic-Isoviscous Regions

[2]FZG load stages are explained ahead on Section 3.2. K2, K3 (wear), and K4 correspond to an applied torque of 13.7, 28.8 and 60.8 N·m on the pinion.

$$R_{at} = \sqrt{R_{a1}^2 + R_{a2}^2} \qquad (2.11) \qquad\qquad \Lambda = \frac{h_0}{R_{at}} \qquad (2.12)$$

Table 2.9: Obtained values for h_0 [μm] and Λ for a plastic/steel gear pair using different authors solutions while increasing load at 1000 rpm.

	K2 - 13.7 N·m		K3 - 28.8 N·m		K4 - 60.8 N·m	
	h_0	Λ	h_0	Λ	h_0	Λ
Martin	0.2463	0.08370	0.1172	0.03982	0.0559	0.01898
Blok	0.7331	0.24911	0.7331	0.24911	0.7331	0.24911
Herrebrugh	0.9487	0.32237	0.8177	0.27785	0.7051	0.23960
Dowson	0.8868	0.30134	0.8051	0.27359	0.7312	0.24848
Myers	1.2250	0.4163	0.8220	0.2793	0.6933	0.2356

Table 2.10: Obtained values for h_0 [μm] and Λ for a plastic/steel gear pair using different authors solutions while increasing speed (rpm) at K4 load stage.

	1000 rpm		2000 rpm		3000 rpm	
	h_0	Λ	h_0	Λ	h_0	Λ
Martin	0.0559	0.01898	0.1117	0.03797	0.1676	0.05695
Blok	0.7331	0.24911	1.1637	0.39544	1.5249	0.51817
Herrebrugh	0.7051	0.23960	1.0687	0.36317	1.3631	0.46319
Dowson	0.7312	0.24848	1.1879	0.40366	1.5777	0.53614
Myers	0.6933	0.2356	1.0618	0.3608	1.3625	0.4630

With exception of the results found on K2 load stage, using Herrebrugh solution conducted to results that are similar to the ones found with Myers solution. Dowson solution got closer to Myers solution with load increasing, at low speeds. The results obtained from Martin and Blok solutions are slightly different while comparing with Myers, Dowson or Herrebrugh, which was expected since their regions on the map of Johnson are slightly far from the transitional region between Elastic-Piezoviscous and Elastic-Isoviscous regions.

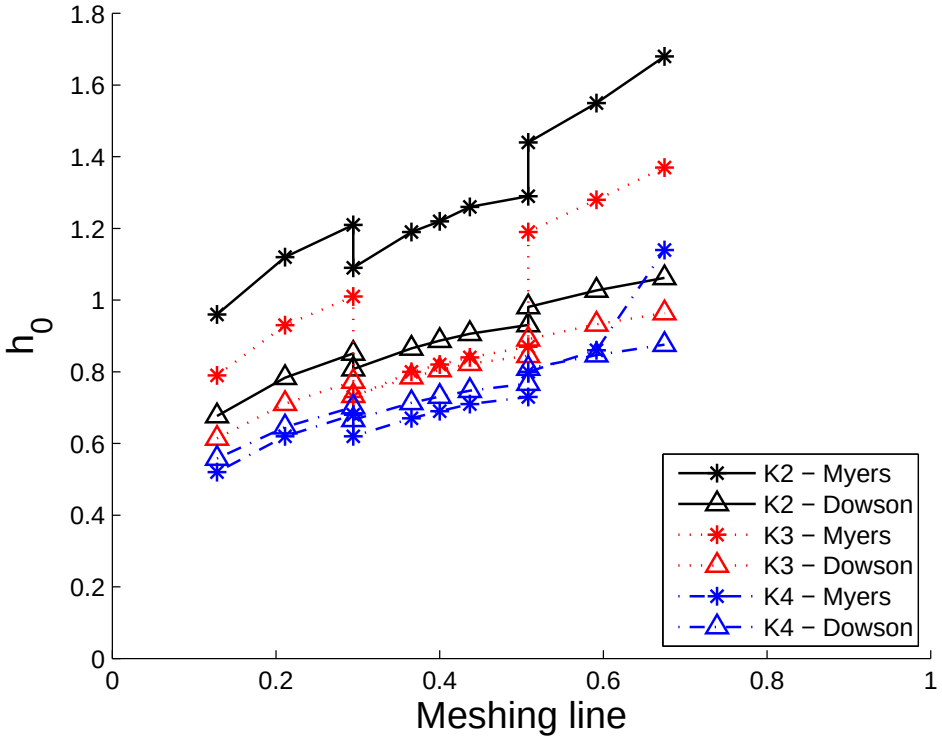

Figure 2.22: Comparison between Myers and Dowson solution for the film thickness along the meshing line while increasing load (μm) .

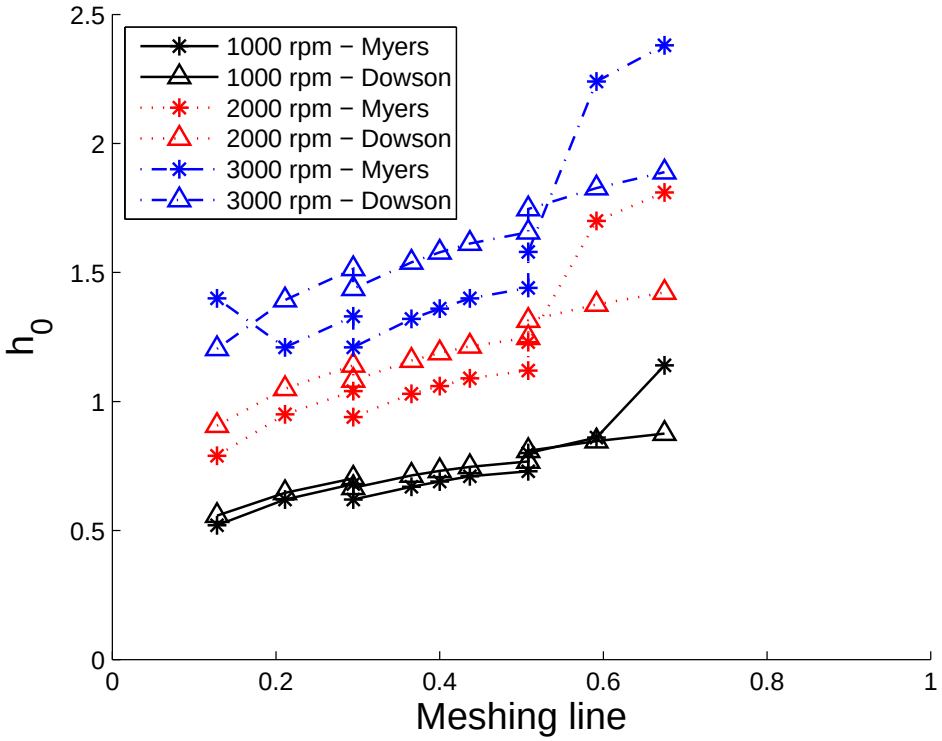

Figure 2.23: Comparison between Myers and Dowson solution for the film thickness along the meshing line while increasing speed (μm).

Chapter 3

Experimental devices for plastic gears

3.1 Test rigs for plastic gears

One of the biggest needs of plastic gears research is a standard test rig that may be used by all the researchers over the world in order to guarantee results that can be directly compared. It is common to see very different test rigs depending on the project, which slows the process of the plastic gears research.

VDI 2736 distinguishes three different arrangements of plastic gears tests: non- mechanically strained, mechanically strained and pulse ones. In this section some examples of test rigs are shown and explained.

3.1.1 Non-mechanically strained test rig

Also called power absorption type rigs, this type of test rig uses a brake to apply the torque and is not mechanically strained. Temperature measurement is done at the only existing gear pair, the one being tested, while tooth flank/root temperatures may need to be measured with a thermographic camera. Velocity and torque are measured at the input side (motor) and before the output (brake where load is applied). The use of a second electric motor as a brake is a possibility, as, for example, is done on the test rig used by the standard JIS B 1759 (Figure 3.3) [26, 27]. For better understanding, a block diagram is shown in Figure 3.1.

The test rig of Scholz GmbH & Co KG [28], Kronach, Germany, was designed in association with the University of Erlangen and is an example of a non mechanically strained test rig. The objective was to build a considerable number of these test rigs in order to make the measurement of several plastic materials possible with a good comparability of the obtained results. A picture of this test rig is shown on Figure 3.2a.

Another example of one existing test rig of this kind, is the one from Victrex Europe GmbH (which produces PEEK), made for their own tests (see Figure 3.2b).

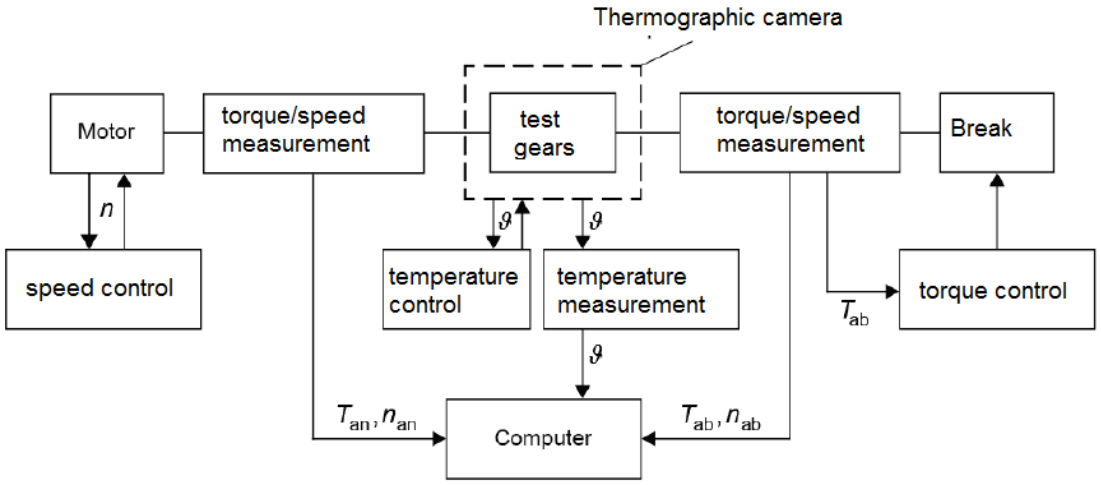

Figure 3.1: Block diagram for a non-mechanically strained test rig [26].

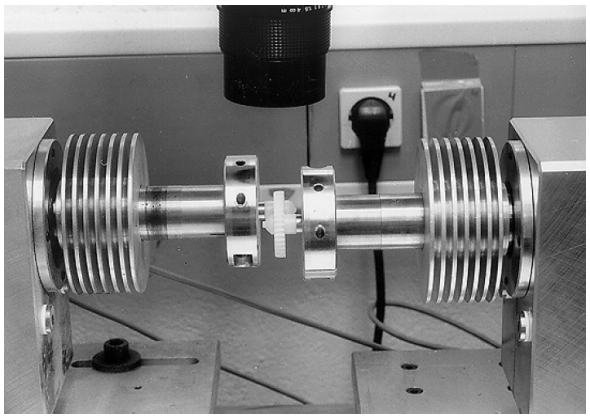

(a) Test rig of company Scholz GmbH & Co. KG .

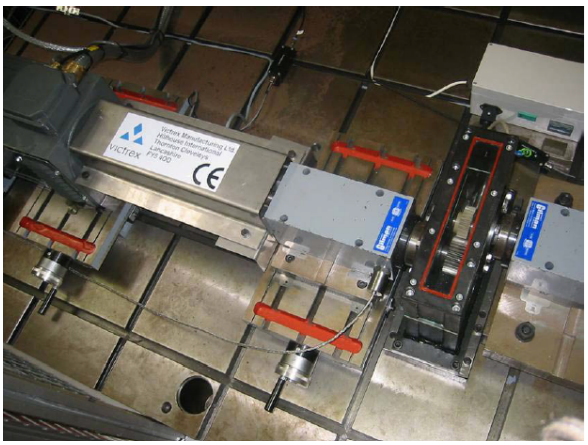

(b) Test rig of company Victrex GmbH.

Figure 3.2: Test rigs for plastic gears [28].

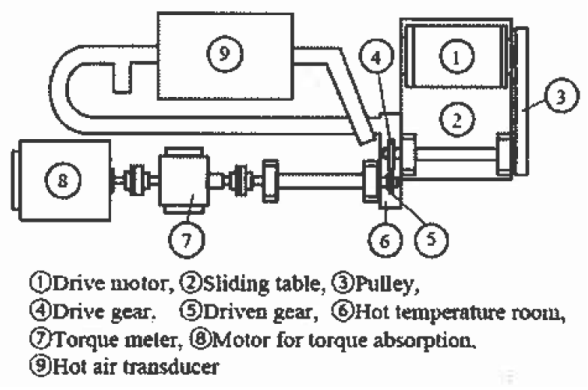

Figure 3.3: Schematic representation of JIS B 1759 test rig [27].

3.1.2 Mechanically strained test

In this type of test rigs, a power loop principle is implemented and the torque is statically applied in a load clutch. Because of the power loop principle, the torque and speed measured on the side of the motor determines the system power loss. FZG is a very well known machine used to test steel gears that is also based on this principle, as will be explained ahead on Section 3.2. This power loop principle is used in other test rigs, that are similar to FZG. Some examples can be found for example in [9] and in many works from Tsukamoto [10, 11, 14, 16, 22].

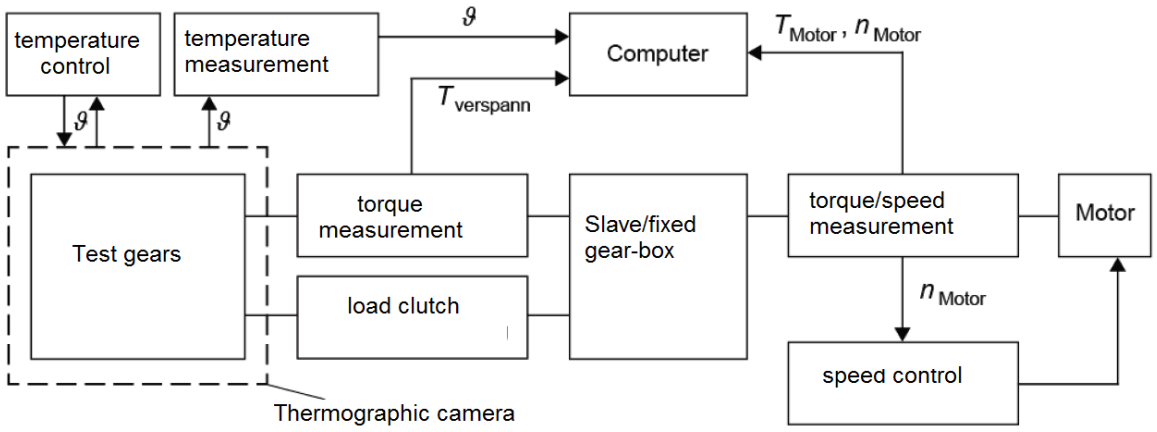

Figure 3.4: Block diagram for a mechanically strained test rig [26].

3.1.3 Pulse test

For tooth root strength a pulsator test rig is used (Figure 3.5). Temperature is controlled since it has a big influence on deformation and on tooth root fatigue strength under pulsating stress (σ_{FlimN}). Depending on the frequency and on the applied load, root resistance can be estimated in running tests. However, the tests made with a pulsator must always be confirmed with running experiments.

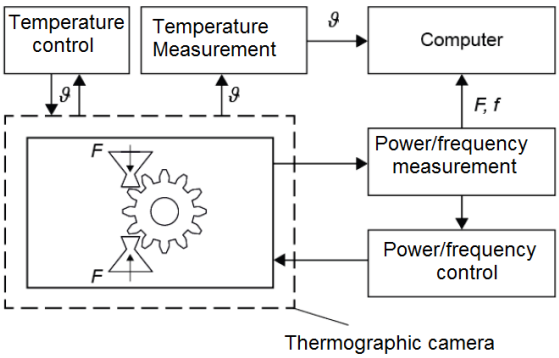

Figure 3.5: Block diagram for a pulse test rig [26].

3.2 FZG test rig

The first test method to determine the scoring and wear properties of gear oils on an FZG test rig was established more than 45 years ago, and then standardized on DIN 51 354. FZG (Forcshugstelle für Zahnräder und Getribebebau, in german, or Research Test Rig for Gears and Transmissions, in english) became one of the most important and widely used gear test rigs. Its versatility allows different tests to be performed on it [29]:

- scoring tests for gear oils;
- scoring and wear tests for greases;
- pitting tests for gear oils;
- shear stability tests for tractor hydraulic fluids;
- micro pitting tests for gear oils;
- efficiency test.

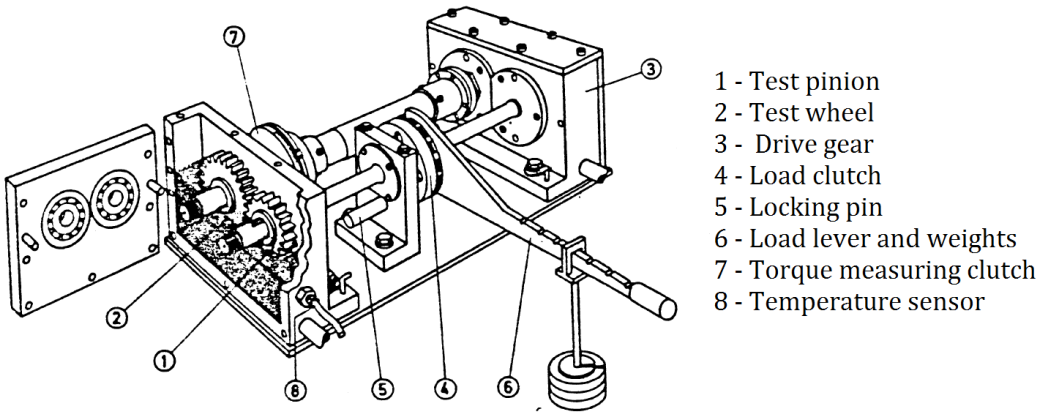

Figure 3.6: Schematic view of the FGZ test rig [29].

FZG test rig is based on a recirculating power loop principle with a fixed torque and rotational speed on the test gear pair. A schematic view of a FZG test rig is shown on Figure 3.6.

As seen on Figure 3.6, the FZG test rig has two gearboxes. The gearbox composed by the test gears is called test gearbox, the other gearbox is called the slave gearbox. The test pinion is connected to the slave pinion through the shaft passing by the load clutch, and the test wheel is connected to the slave wheel by the shaft passing by the torque measuring clutch.

The input power is supplied by an AC-motor with a maximum speed of 3000 rpm. The motor shaft is connected to the slave wheel, and power losses occurring on the power cycle slave wheel/test wheel/test pinion/test wheel/slave wheel (due to different power loss mechanisms) are compensated by the electric motor.

The shaft pinion connecting the two gearboxes is divided in two parts, making possible a relative rotation between them. That allows the load application. The torque measuring clutch (7) allows the measurement of the applied load.

For the load application, it is necessary to fix the half shaft connected to the test pinion with the locking pin so that the half shaft connected to the slave pinion can be twisted. To define the torque, a simple calculation must be made based on the load lever and weights (6) possibilities.

There are two load levers: the first one is the lightest one, it is only used to apply the lowest torque possible with an FZG test rig: 3.3 N·m on the test pinion. The second one is heavier and without any kind of weights (or weights support) allows the second lightest load on the test pinion: 13.7 N·m. To increase the load to highest levels, weights must be applied and the torque is calculated according to equation (3.1)

$$T_1 = T_H + (F_K + F_W) \cdot h \tag{3.1}$$

Where:

- T_1 is the torque applied on the pinion;
- T_H is the torque of the load lever (3.3 or 13.7 N·m);
- F_K is the weight of the load support rod which is 43.1 N·m;
- F_W is the weight of the loading weights;
- h is the length on the effort arm for F_K and F_W defined by the groove where the weights are supported.

As the FZG was originally made for steel gears, the load stages normally used may not be very well adapted for plastic ones. The torque increase of two consecutive load stages is very high thus only a few load stages are suitable for plastic gears testing. Some of the standard load stages are shown on Table 3.1. More intermediate load stages can be defined, in order to have more load test conditions.

Tests can be performed using dip lubrication or oil jet lubrication. While using dip lubrication, oil temperature may be set using the electrical heaters and the cooling coils mounted on the test gear box. Under oil JET lubrication conditions, the oil flow is guaranteed by an oil pump. The oil is pumped from a reservoir with heaters that can increase the temperature till a desired value. The reservoir includes a sensor so that the temperature can also be controlled.

Table 3.1: FZG standard load stages [N·m] (on the pinion) [30].

Load stage	Test type (steel gears)		
	Scoring Wear Shear Stability	Pitting	Micro - Pitting
K1	3.3	-	-
K2	13.7	-	-
K3	35.3	-	28.8
K4	60.8	-	-
K5	94.1	-	70.0
K6	135.3	135.3	98.9
K7	183.4	-	132.5
K8	239.3	239.3	171.6
K9	302.0	302.0	215.6
K10	372.6	-	265.1
K11	450.1	-	-
K12	534.5	-	-

Chapter 4

Load-carrying capacity and tooth geometry of plastic gears

In this chapter, VDI 2736 was used to compare the influence of tooth geometry on load carrying capacity and life-time of plastic gears.

The influence of the tooth geometry parameters on power loss is explained and some "low-loss" gear geometries are introduced. A comparison between the use of POM as pinion and the use of POM as wheel on a steel - POM gear pair is made, based on calculations performed.

This Chapter continues with some results for the FZG load levels K1(low load), K2 (medium load) and K3 (high load) at different speeds. The calculation method used on this chapter can be found on Appendix A.

4.1 Low-loss tooth geometry

In 2007, Höhn *et al.* [4] introduced a work entitled "Low Loss Gears" . The authors have shown that tooth geometry has a big influence on power loss. A new tooth geometry was purposed: it had lower module, higher number of teeth, higher pressure angle and larger width [1]. For better understanding how does geometry affect power losses, different power loss mechanisms are now described.

4.1.1 Power losses in a gearbox

In a gearbox, energy dissipation have origin in the different single elements such as bearings, seals and gears. The power losses can be divided into two types: load dependent, and load independent losses (Figure 4.1).

Load dependent losses occur only in elements that carry some of the input power (bearings and gears) [4]. If load is kept constant, they tend to increase linearly with speed and almost always represent the biggest portion of power losses (except for high speeds).

Load independent losses can be understood as the energy dissipation that happens when a gear-box is running in unloaded state. They are dependent on speed, input power, lubricant characteristics, and gearbox design [31]. They tend to increase progressively with speed [4]. The behaviour "speed against power losses" is shown on figure 4.2 [4].

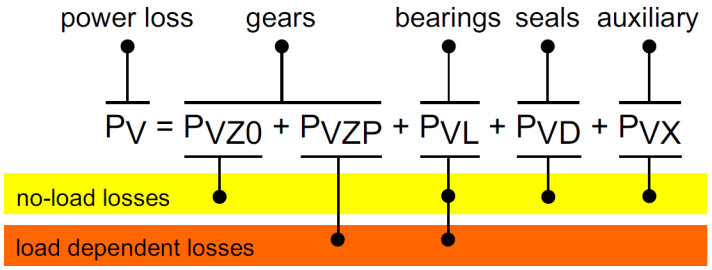

Figure 4.1: Power loss contributions [31].

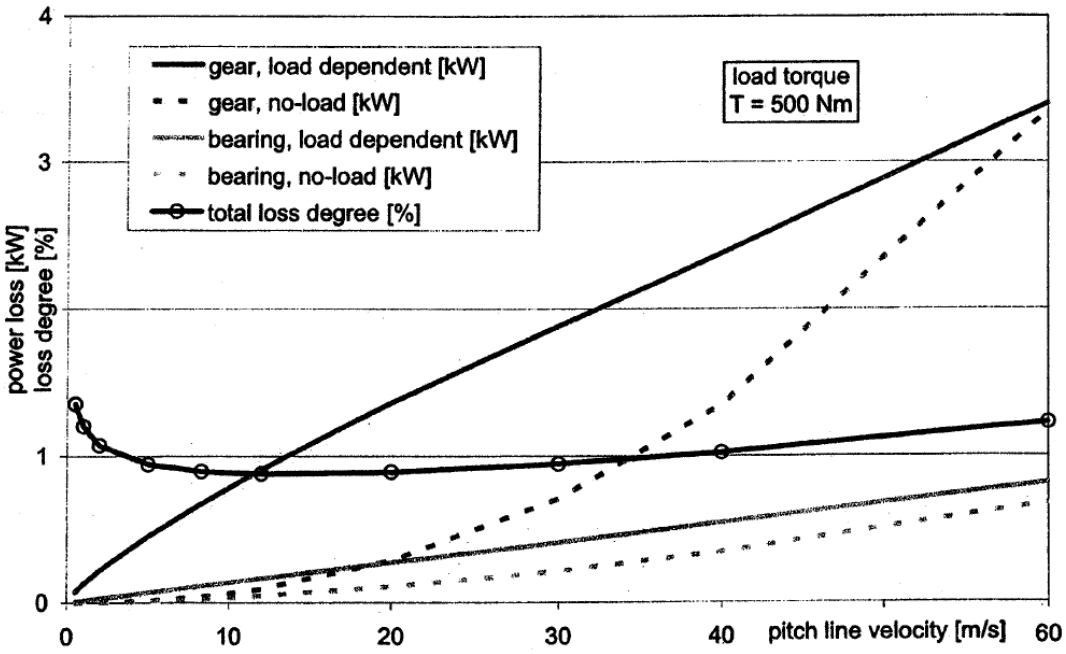

Figure 4.2: Influence of speed on power losses components in a gearbox [4].

4.2 Influence of gear tooth geometry on power losses

Tests performed by Höhn *et al.* with steel "low loss" gears relate the influence of gear tooth design and its geometric parameters on power loss. Some conclusions were taken [4]:

- The most influential parameters are transverse contact ratio ε_α and module m; the reduction of both decreases power losses but a decrease on load carrying capacity is verified;
- Increasing the pressure angle α_n favours load carrying capacity, while the decrease of loss degree (increase of efficiency) is not so evident;

- The increase of the helix angle β increases power loss, but to a limit extent; helix angle may be important when a reduction of the transverse contact ratio is necessary. As the total contact ratio [1] has to be bigger than 1 to ensure meshing continuity, in order to compensate the transverse contact ratio reduction, the increase of the helix angle will increase the overlap contact ratio. Increasing of the helix angle may also be necessary for proper load carrying capacity and noise reduction;

The influence of some of this parameters on the local gear loss factor (which directly affects the meshing gears power loss P_{VZP}, equation 4.1) was analysed in [1] within equation (4.2), where P_{IN} is the input power, μ_{mZ} is the average coefficient of friction along the path of the contact and H_{VL} is the local gear loss factor along the path of the contact. The influence of the module m_n , helix angle β, face width b and tip relief C_a is shown on Figure 4.3.

$$P_{VZP} = P_{IN} \cdot H_{VL} \cdot \mu_{mZ} \quad (4.1) \qquad H_{VL} = \int_0^b \int_A^B \frac{F_N(x,y)}{F_t} \cdot \frac{v_g(x,y)}{v_{tb}} dxdy \quad (4.2)$$

4.3 Geometry optimization for power savings

Based on conclusions taken on Section 4.2, some steps can be adopted in order to increase gears' efficiency [4]:

- Gear tooth profile shift to decrease load and sliding speed in critical areas;
- Reduction of module;
- Reduction of transverse contact ratio;
- Adoption of an helix angle for functional contact ratios;
- Increasing of tooth root fillet radius;
- Increasing of the pressure angle;
- Decreasing of the relation load/face width.

Although the pressure angle increase would bring a slightly better efficiency and a bigger load carrying capacity, it would require non conventional tools with an angle different from the typical 20 °. In order to avoid this problem, Magalhães *et al.* worked on a low-loss concept without increasing the pressure angle. The results found in [5] clearly show that it is possible to effectively increase efficiency using a conventional 20 °pressure angle. Magalhães *et al.* created three new gear tooth geometries. Later on Fernandes *et al.* [31], there were developed three other new low-loss gear tooth geometries based on C-type FZG gears: H501, H701 and H951. Maximum Hertzian pressure was imposed to the new gears and similar safety factors (calculated for K9 FZG load stage corresponding to 323,4 N·m) so that comparisons could be made properly.

[1] Total contact ratio - $\epsilon_\gamma = \epsilon_\beta + \epsilon_\alpha$

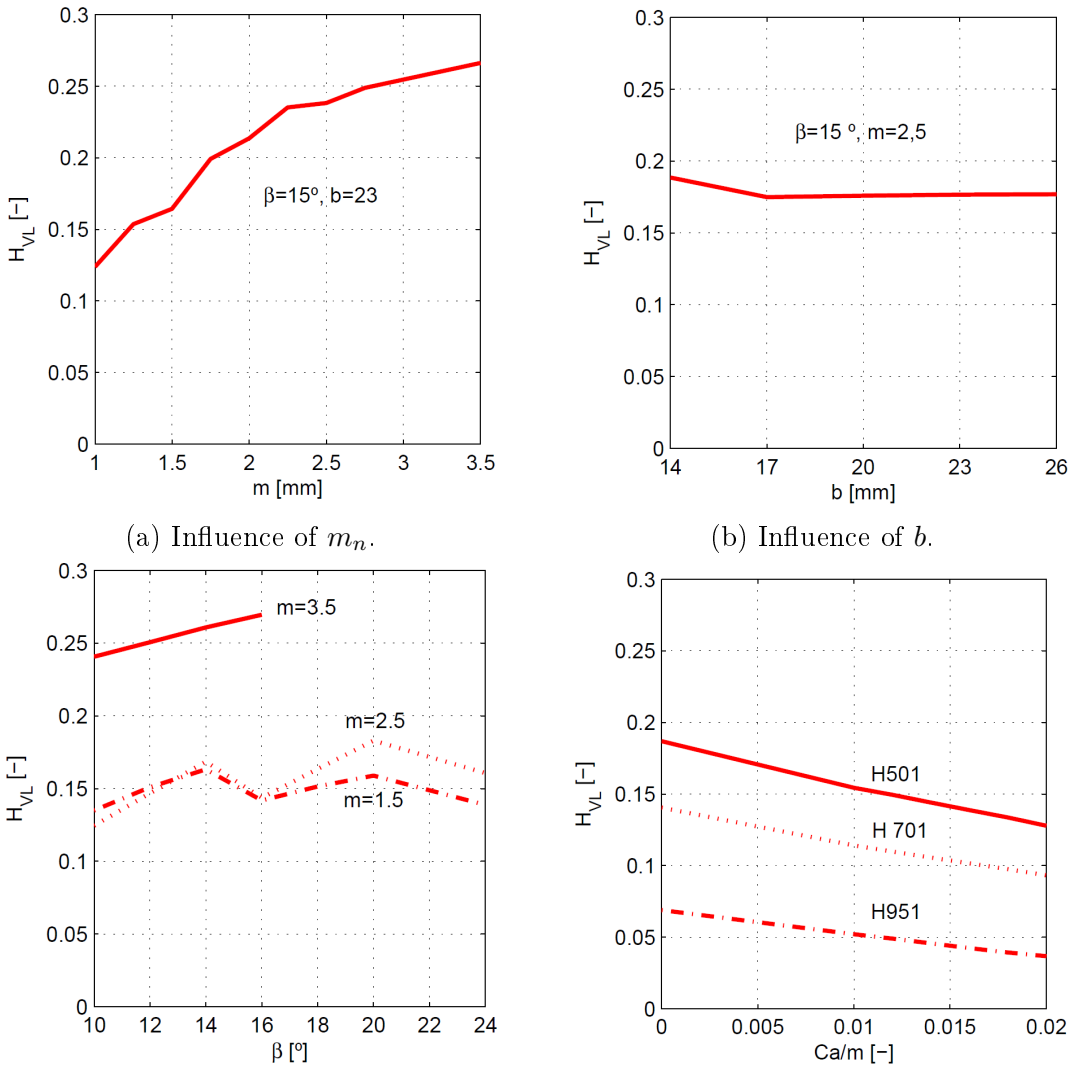

(a) Influence of m_n.

(b) Influence of b.

(c) Influence of β.

(d) Influence of C_a.

Figure 4.3: Influence of geometric parameters on local gear loss factor H_{VL} [1].

Geometric parameters and safety factors of FZG type C micro pitting gear (C14), and Fernandes low-loss helical gears are shown on Table 4.1.

Table 4.1: Geometric parameters of gears H501, H701 and H951 [31].

	Units	C14		H501		H701		951	
		Pinion	Wheel	Pinion	Wheel	Pinion	Wheel	Pinion	Wheel
a	mm	91.5							
b	mm	14		23		17		23	
m_n	mm	4.5		3.5		2.5		1.75	
α_{wt}	°	22.44		22.12		22.12		28.34	
ε_α	-	1,44		1.46		1.52		0.93	
ε_β	-	0		0.54		0.56		1.08	
ε_γ	-	1,44		2.00		2.08		2.02	
g	mm	19,10		15.55		11.53		4.98	
x	-	0,1817	0,1715	0.1809	0.0891	0.2290	0,1489	1,6915	2,0003
z	-	16	24	20	30	28	42	38	57
d	mm	72,00	108,00	72.47	108.70	72.47	108.70	68.85	103.27
d'	mm	73,20	109,80	72.47	108.70	73.20	109.8	73,2	109.80
d_a	mm	82,46	118,37	80.67	116.27	78.55	114.39	76.23	111.73
S_F	-	1,15	1,20	1.71	1,72	0.96	0.95	0.97	1.02
S_H	-	0,66	0,72	0.92	0.95	0.82	0.84	0.88	0.89
S_S	-	1,79		2.65		2.66		3.60	

4.4 Load-carrying capacity

Load carrying capacity was calculated according to VDI 2736 method for steel/plastic gear pair of 16MnCr5 and POM. An oil lubricated situation [2] was considered.

The calculation for the tooth root safety factor (S_F), tooth flank safety factor (S_H), tooth deformation safety factor (S_λ), wear safety factor (S_{W_m}), tooth root temperature ($\vartheta_{Fu\beta}$) and tooth flank temperature (ϑ_{Fla}) was performed for three different load stages (K1, K2 and K3-wear) and a rotational speed of 750 rpm on the pinion.

The calculation procedure and intermediate steps are available on Appendix A. The material meshing possibilities in terms of pinion/wheel and driver/driven are defined for four different cases on Table 4.2. VDI 2736 standard calculation method does not distiguish the influence of the material depending on the gear function as driver or driven, however different results were found between the use of "POM as wheel" and "POM as pinion" as shown on the following Section (4.4.1).

4.4.1 Material meshing simulations

The influence of the use of POM as pinion or as wheel in a plastic/steel gear pair was already discussed on Section 2.3.2 . In this section calculations were performed for both of the cases. The results for K3 load stage at 750 rpm on the pinon are shown on

[2]The heat transfer coefficients used to calculate the temperature are not for oil bath lubrication since this information is not available on VDI 2736. The considered heat transfer coefficients are the ones valid for oil mist or dry situation, which may increase the temperature to very high values, specially at temperatures found for the tooth flank.

Table 4.2: Material meshing cases.

Case No.	Material meshing	Driver/driven combination
1.1	Steel/POM	Steel/POM
1.2	Steel/POM	POM/Steel
2.1	POM/Steel	Steel/POM
2.2	POM/Steel	POM/Steel

Figure 4.4 and on Table 4.3 for a C14 gear pair.

The results show an advantage on using plastic as wheel on a steel/plastic gear pair. Although the tooth root safety factor increases when POM is used as pinion, for the case "plastic as pinion", the flank safety factor reach a value lower than 1 before reaching 10^5 cycles, while for the case "plastic as wheel", the flank safety factor reaches the value 1 after more than $3 \cdot 10^5$ cycles until failure, extending life for more than three times.

The influence on temperatures is also evident. In the case "plastic as pinion" tooth root is approximately 5 °C hotter that in the case "plastic as wheel" (check Table 4.3) but the biggest differences are found on the flank temperature: more than 30 °C. In the case "plastic as pinion" flank temperature is higher than the permissible temperature ϑ_{zul} for POM, which in practice would probably result in flank fast failure. Considering equations (4.3) and (4.4), this behaviour is not seen if the number of teeth of the pinion and the wheel is the same.

$$\vartheta_{Fu\beta} = \vartheta_0 + P \cdot \mu \cdot H_V \cdot \left(\frac{k_{\vartheta,Fu\beta}}{b \cdot z \cdot (v_t \cdot m_n)^{0,75}} \right) \cdot ED^{0,64} \tag{4.3}$$

$$\vartheta_{Fla} = \vartheta_0 + P \cdot \mu \cdot H_V \cdot \left(\frac{k_{\vartheta,Fla}}{b \cdot z \cdot (v_t \cdot m_n)^{0,75}} \right) \cdot ED^{0,64} \tag{4.4}$$

Wear is also affected by this fact as the use of POM as wheel increased the wear safety factor by 50% relatively to the one found for the use of POM as pinion.

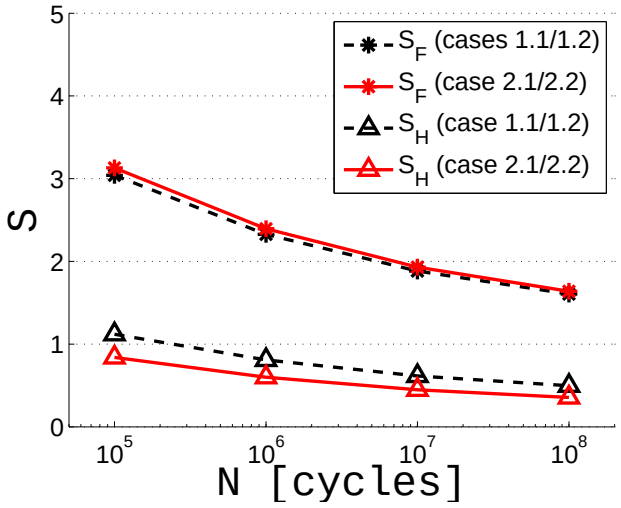

Figure 4.4: S_F and S_H for the cases "POM as pinion" and "POM as wheel".

Table 4.3: Temperatures for the cases "POM as pinion" and "POM as wheel".

-	"POM as pinion"	"POM as wheel"
$\vartheta_{Fu\beta}$ [°C]	30.69	35.51
ϑ_{Fla}[°C]	88.58	122.35
S_λ	2.03	2.03
S_{W_m} (dry) @$10^8 cycles$	0.09	0.13
S_{W_m} (dry) @$10^7 cycles$	0.90	1.35

4.4.2 Performance comparison - K1

The results for a rotational speed of 750 rpm on a POM pinion (engaged on a steel wheel) are shown in Table 4.4 and in Figures 4.5a and 4.5b.

Analysing Figure 4.5a, it is clear that, besides the module reduction in comparison with C14, the root and flank safety factors is higher for H501 gears. This happened mainly due to the reduction of service temperatures (which will increase the permissible stresses σ_{FlimN} and σ_{HlimN}, see Section 4.4.5) and to the increase of the face width b. Although an higher service temperatures reduction was found on H951 gears, tooth root safety factor was lower than the one found fo C14. The flank safety factors is slightly higher than the one found on C14, although, it is much lower when comparing with H501. This fact suggests that the module reduction when designing low loss plastic gears defines a balance between the power loss and load capacity. By one point of view, it increases the permissible stresses while reducing the service temperatures, however, by another point of view, it decreases the resistant section of the tooth root, as the flank area that supports the contact load.

Analysing wear results (Table 4.4), the difference found between C14 and H951 was very small, however, H501 shows a wear safety factor that is close to the double of the ones found for the other gear geometries. Tooth deformation results show a better performance for the H501 gears, and the lowest tooth deformation safety factor (S_λ) was found for H951 gears.

At K1 load stage, only gear H501 reaches 10^8 cycles without a wear safety factor lower than 1, however this wear results are for the dry case.

Table 4.4: Tooth root ($\vartheta_{Fu\beta}$) and flank (ϑ_{Fla}) temperatures, deformation and wear safety factors for K1 simulations at 750 rpm on the pinion.

-	C14	H501	H951
$\vartheta_{Fu\beta}$ [°C]	21.78	20.92	20.54
ϑ_{Fla}[°C]	31.73	25.81	23.42
S_λ	17.72	22.01	10.45
S_{W_m} (dry) @$10^8 cycles$	0.78	1.17	0.69
S_{W_m} (dry) @$10^7 cycles$	7.88	11.74	6.88

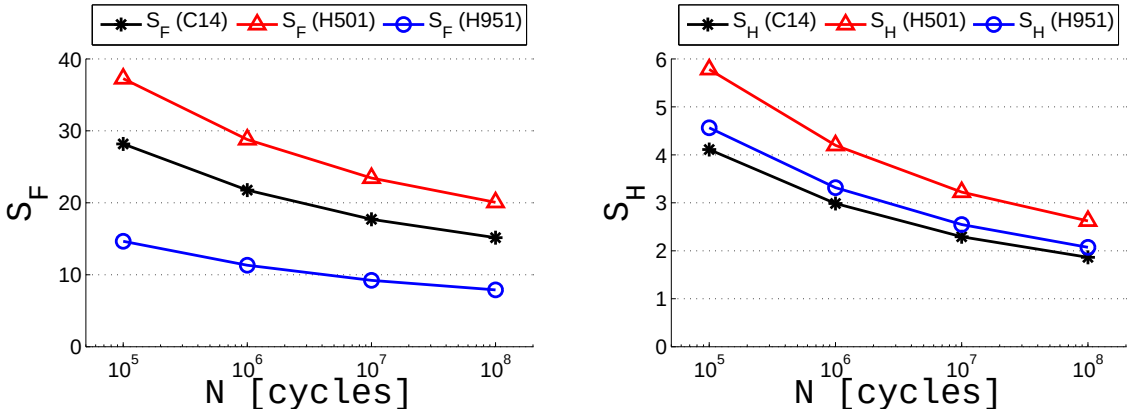

(a) S_F - Tooth root safety factor. (b) S_H Tooth flank safety factor.

Figure 4.5: Simulations performed for K1 load stage with an n_1 of 750 rpm.

4.4.3 Performance comparison - K2

The results for the simulations performed at K2 (13.7 N·m) load stage at 750 rpm on the pinion are shown in Table 4.5 and in Figures 4.6a and 4.6b.

Naturally, temperatures and stresses increased which lowered the safety factors. The maximum temperature found was 68.7 °C on C14 pinion tooth flank, compared to 31.7 °C for the same case at K1.

At K2 load stage, failure causes found are tooth flank failure for C14, and wear for H501 and H951 gears. The gear that would fail with the lower number of cycles achieved would be the C14 pinion at approximately 10^7 cycles, followed by H951, and finally H501 (although, as already said, wear results are for the dry case).

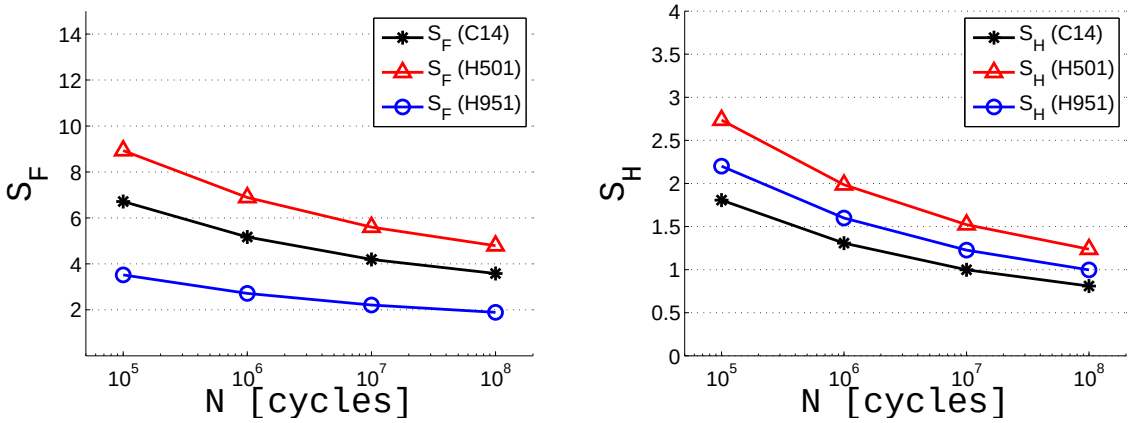

(a) S_F - Tooth root safety factor. (b) S_H - Tooth flank safety factor.

Figure 4.6: Simulations performed at K2 load stage, n_1 = 750, 1500 and 3000 rpm.

Table 4.5: Tooth root ($\vartheta_{Fu\beta}$) and flank (ϑ_{Fla}) temperatures, deformation and wear safety factors for K2 simulations at 750 rpm on the pinion.

-	C14	H501	H951
$\vartheta_{Fu\beta}$ [°C]	27.38	23.80	22.26
ϑ_{Fla}[°C]	68.69	44.11	34.21
S_λ	4.27	5.30	2.51
S_{W_m} (dry) @$10^8 cycles$	0.19	0.28	0.17
S_{W_m} (dry) @$10^7 cycles$	1.90	2.83	1.66

4.4.4 Performance comparison - K3

The results for the simulations performed at K3 (13.7 N·m) load stage at 750 rpm on the pinion are shown in Table 4.6 and in Figures 4.7a and 4.7b.

By the calculation performed, none of the gears would reach more than 10^7 cycles and all the gears would fail by tooth flank failure. The C14 pinion would fail before reach 10^6 cycles followed by H951 which would fail by the same reason after reaching just over 10^6 load cycles. The H501 appears to be the gear with higher safety factors. By the calculations performed, H501 tooth flank would fail near 10^7 cycles.

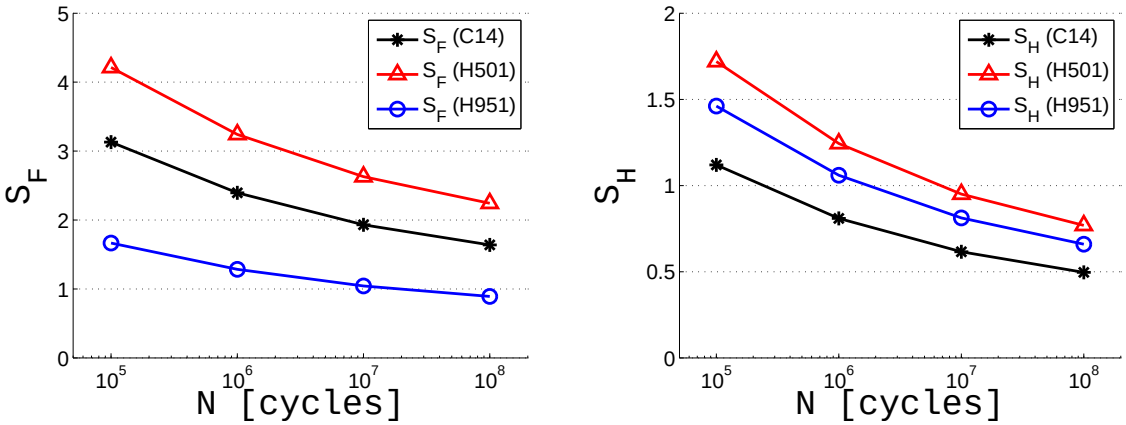

(a) S_F - Tooth root safety factor.

(b) S_H - Tooth flank safety factor.

Figure 4.7: Simulations performed at K3 load stage, $n_1 = 750$ rpm.

Table 4.6: Tooth root ($\vartheta_{Fu\beta}$) and flank (ϑ_{Fla}) temperatures, deformation and wear safety factors for K3 simulations at 750 rpm on the pinion.

-	C14	H501	H951
$\vartheta_{Fu\beta}$ [°C]	35.51	27.99	24.75
ϑ_{Fla}[°C]	122.35	70.69	49.87
S_λ	2.03	2.52	1.20
S_{W_m} (dry) @$10^8 cycles$	0.09	0.13	0.08
S_{W_m} (dry) @$10^7 cycles$	0.90	1.34	0.79

4.4.5 Wear, Deformation and Temperatures

Wear

After a large number of cycles, wear behaviour starts to be important, although these results are for the dry case and therefore may be meaningless (check Figure 4.8).

Analysing Figure 4.8, it is seen that after 10^8 all gears are considerably affected by wear. While reducing the number of cycles to 10^7, only at K2 load stage wear problems start to be relevant.

Comparing the different tooth geometries, wear effects seem to be similar on H951 and on C14 gears. The highest wear safety factors were achieved by H501 gears.

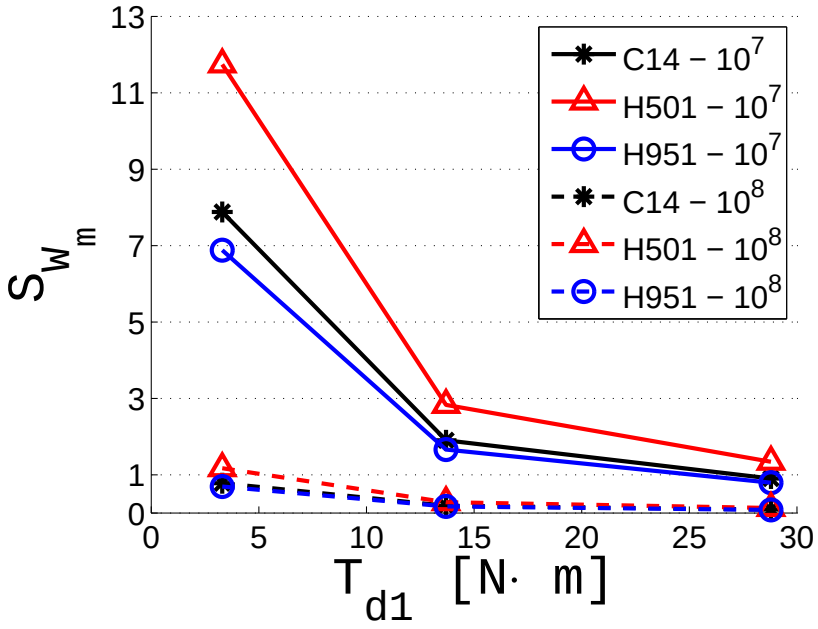

Figure 4.8: S_{W_m} - Wear safety factor for 10^7 and 10^8 cycles with n_1 = 750 rpm.

Deformation

As the temperature range found for the tooth root temperature ($\vartheta_{Fu\beta}$) is too small (between 20 and 40 °C), the deformation was considered as only torque dependent, since the changes on the elasticity modulus of POM were not considerable. Deformation results are shown on Figure 4.9.

For C14 and H501 gears, the deformation effects appear to be problematic. However, the reduction of module almost lead to a deformation failure of 951 gears. Deformation may cause other problems, like the increase of the sliding speed due to the tooth geometry changes.

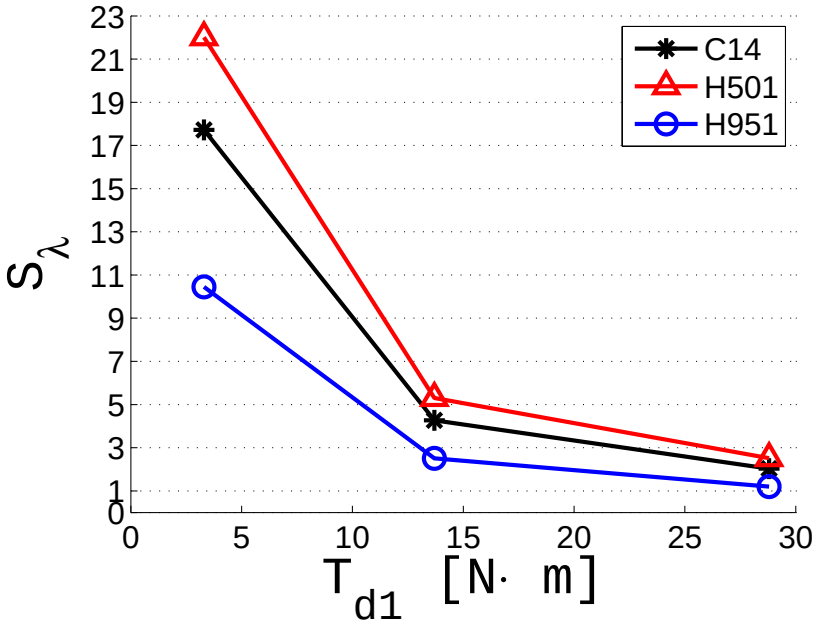

Figure 4.9: S_λ - Tooth deformation safety factor for with $n_1 = 750$ rpm.

Temperatures

Tooth temperatures increase caused by the load increase is shown on Figure 4.10a for the tooth root and on Figure 4.10b for the tooth flank.

Analysing Figures 4.10a and 4.10b the low-loss geometry effect is clear. The lowest temperatures were achieved by H951 gears, and the highest were achieved by C14 gears. At K3 load stage, flank temperature is above the permissible one for POM (90°C), while both of the low-loss gears are able to run under allowable temperatures.

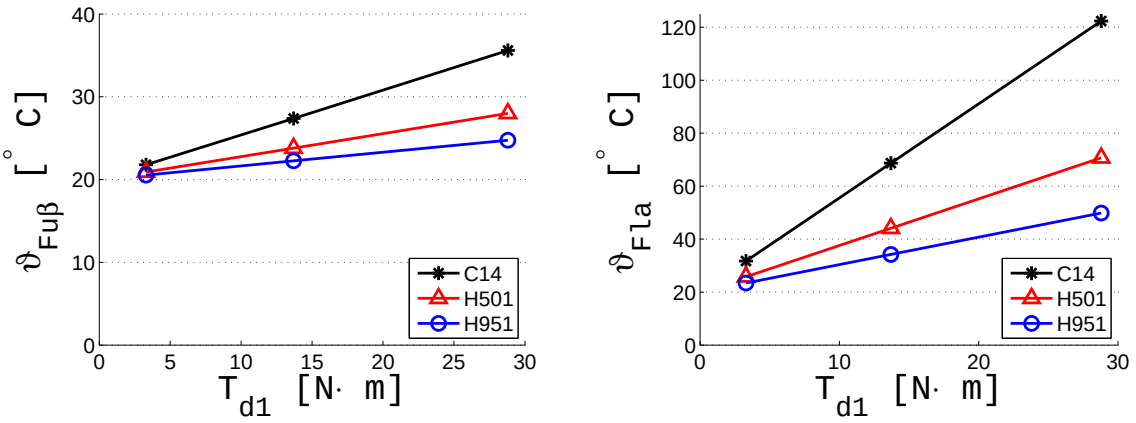

(a) Tooth root temperatures.

(b) Tooth flank temperatures.

Figure 4.10: Increase of the tooth temperatures with the applied load (K1, K2 and K3) for gears C14, H501 and H951 at 750 rpm on the pinion.

4.4.6 Life-time and Failure Causes

A summary of the failure causes (first safety factor achieving a value lower than 1) and number of cycles range where failure occurred on the simulations performed on this chapter is listed on Table 4.7.

Table 4.7: Failure causes and life-time for different tooth geometries at K1, K2 and K3 load stages, at 750 rpm on the pinion.

	C14		H501		H951	
	Cause	N_L	Cause	N_L	Cause	N_L
K1	S_{W_m}	$10^7 - 10^8$	-	$> 10^8$	S_{W_m}	$10^7 - 10^8$
K2	S_H	$10^7 - 10^8$	S_{W_m}	$10^7 - 10^8$	S_{W_m}	$10^7 - 10^8$
K3	S_H	$10^5 - 10^6$	S_H	$10^6 - 10^7$	S_H	$10^6 - 10^7$

4.4.7 Conclusions

After this simulations some conclusions can be taken:

- The use of POM as wheel and steel as pinion leads to larger safety factors because of the temperature reduction that occurs compared with the opposite situation;
- During Low-Loss gears design, the module reduction must be based on a balance defined by two distinct effecs By one point of view, it increases the permissible stresses while reducing the service temperatures, however, by another point of view, it decreases the resistant section of the tooth root, as the flank area that supports the contact load;
- H501 gears have a good balance between load capacity and power loss; gears H951 have good power saving capacities, but their load carrying capacity (specially the tooth root) was affected by the low modules used (1,75 mm);
- C14 gears always reached the highest temperatures, while H915 gears always operated at the lowest temperatures;
- H501 gears always achieved the highest safety factors;
- In the wear calculations for the dry case, all gears failed before 10^8 cycles at K2 and K3 load stages. For K1 load stage, only gear H951 shown a wear safety factor lower than one at 10^8 cycles.

Chapter 5

Experimental Procedures, Operating Conditions and Results

Two types of experimental tests were performed. The first tests evaluated the load carrying/thermal capacity at different speeds in order to have some initial information about the material "limits". We called these the "preliminary tests".

The second test phase had as main objective the material testing (S-N curve) for a specific temperature. We called these the "S-N tests".

The tests performed are resumed on Table 5.1.

Table 5.1: Gears and tests.

Gear type	Test type	Gear No.	Speed (n_1) [rpm]	Load [N·m]	Temperature [°C]
C14 (POM pinion)	Preliminary	1	750 - 4500	K1,K2	Free (K1)
		2	750 - 4500	K2,K3	Free
		3	750 - 3000	K2,K3	Free
	S-N	4	1500	K2	50
		5	1500	K3	50
		6	1500	K4	50
H501 (POM pinion)	S-N	7	1500	K4	50
		8	1500	K4	70

5.1 Materials and methods

The tests were performed on a FZG test rig, described on Section 3.2, with C14 and 501 gears that were already characterized on Section 4.3. The tested gear pairs were a POM pinion engaged on a carburized steel (16MnCr5) wheel. On this Section, test rig bearings, seals and measuring equipment used are described. The tested gears and gear material used are also described.

5.1.1 Test rig, measuring equipment and lubricant

Due to the FZG gear test rig configuration, the pinion works always as driven gear and the wheel as driver. Hereupon, on FZG test rig only the cases "POM as driving gear wheel" and "POM as driven gear pinion", are possible to be tested.

Seals and rolling bearings

The gearboxes were sealed with four Viton lip seals with an internal diameter of 30 mm and the motor shaft connection with the slave gear box was sealed with a Viton lip seal with an internal diameter of 26 mm. The shafts were supported with six cylindrical rolling bearings NJ 406 and two four point contact ball bearings QJ 308 N2MA. Four of the NJ 406 bearings were localized at the slave gearbox and two of them on the outside of the test gearbox. The QJ 308 N2MA bearings were localized on the inside of the test gearbox.

Measuring Equipment

Adding to the FZG test rig temperature sensors that allow the temperature measurement, an ETH Messtechnik DRDL-II torque transducer is assembled between the slave gear-box and the AC motor (Figures 5.2 and 5.3). The sensor interface $Valuemaster_{Base}$ allows the test data communication with a computer through Ethernet data transfer with a sample rate adjustable from 1 to 1000 Hz. The software used for data archiving was *ValueMaster Vers. 2.43*.

FZG temperatures were measured with Type K thermocouples at the locations shown on Figure 5.4. The temperatures were recorded during the tests using the software *LabVIEW SignalExpress 2010*.

The POM gear tooth temperatures were measured with a thermographic camera Flir TG165 with an accuracy of ± 1,5 % and a resolution of 0,1 °C. The emissivity used was 0.95, according to [7], which was validated with a simple experiment that is explained as follows.

Table 5.2: Technical specifications of the torque measuring.

Torque transducer type DRDL - II	
Nominal torque	50 Nm
Measurement range	5/10/20/50 Nm
Non-linearity	$< 0.1\%$
Hysteresis	$< 0.1\%$
Accuracy	0.01 %
Temperature sensitivity	0.01 %/°K
Torque Measuring Module Type $Valuemaster_{Base}$	
Non-linearity	0.1%
Accuracy	0.02 %
AD converter resolution	11 bit + 1 bit for leading sign

An oil container with a mercury glass thermometer (0,5 °C resolution), and a POM gear pair were placed in a room for 4 hours in order to stabilize temperatures. After that, oil was dropped on the pinion in order to simulate in-test measurements (oil bath lubrication). The pointing direction of the measurement and the resulting temperatures are shown on Figure 5.1.

During the measurements made, various pictures were taken. The results from the thermographic camera showed some variations when lightly changing the pointing direction. This behaviour was not found during the experiment made to measure the emissivity.

It is known that the tooth root and the tooth flank should have different temperatures which may be a possible cause for this variations. The criteria used while choosing the result for analysis was always to choose the highest temperature found.

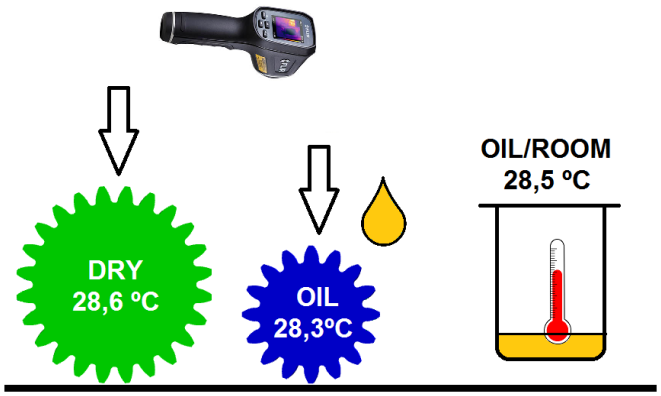

Figure 5.1: Experiment for thermographic camera calibration and resulting temperatures.

Lubricant

The chosen lubricant was an ISO VG-150 BP Energol GR-XP 150. It was chosen according to the information given in Section 2.4.4: high viscosity to avoid hygroscopy problems, mineral oil since most of the tests were made into the recommended service temperatures for mineral oils (20-60 °C), with low polarity since POM is a polar polymer. The main properties of the lubricant used are shown on Table 5.3. Viscosity and thermoviscosity are shown as a function of the temperature on Figure 5.5. The lubricant datasheet can be found in Appendix C.

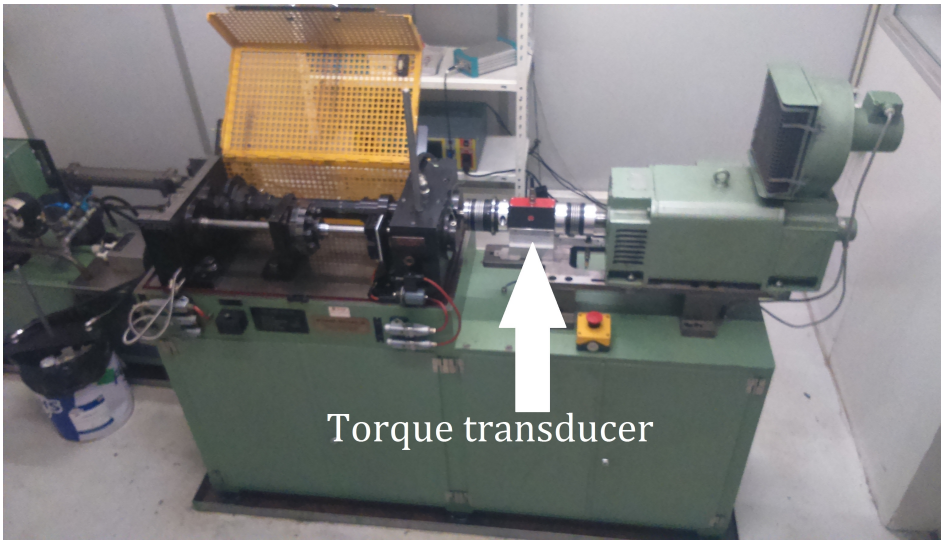

Figure 5.2: Schematic view of FGZ test rig .

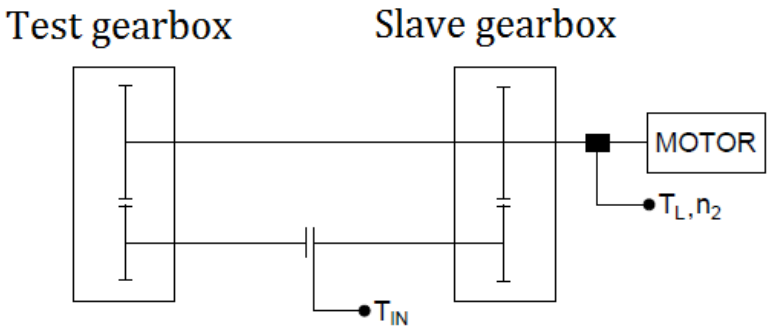

Figure 5.3: Schematic view of the FGZ test rig with the torque measuring transducer [1].

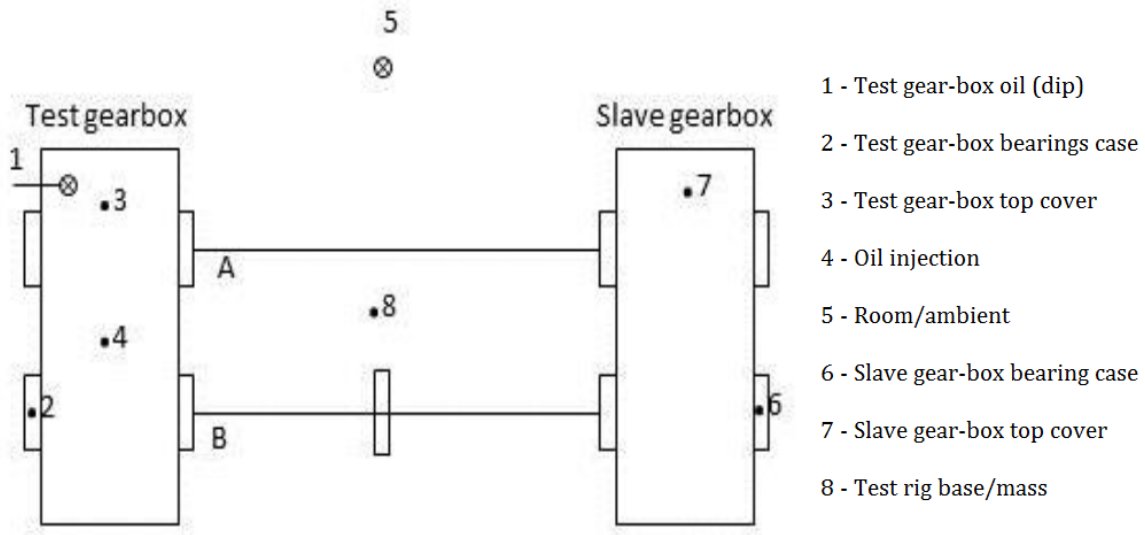

Figure 5.4: Type K thermocouples locations.

Table 5.3: BP Energol GR-XP 150 oil properties (according to the manufacturer).

Property	Value	Unit
Kinematic Viscosity @40°	150.00	mm^2/s
Density @15 °C	0.89	-
Viscosity Index	-	>95
Flash point	220	°C
Limit temperature	180.00	°C
Pour point	-18.00	°C

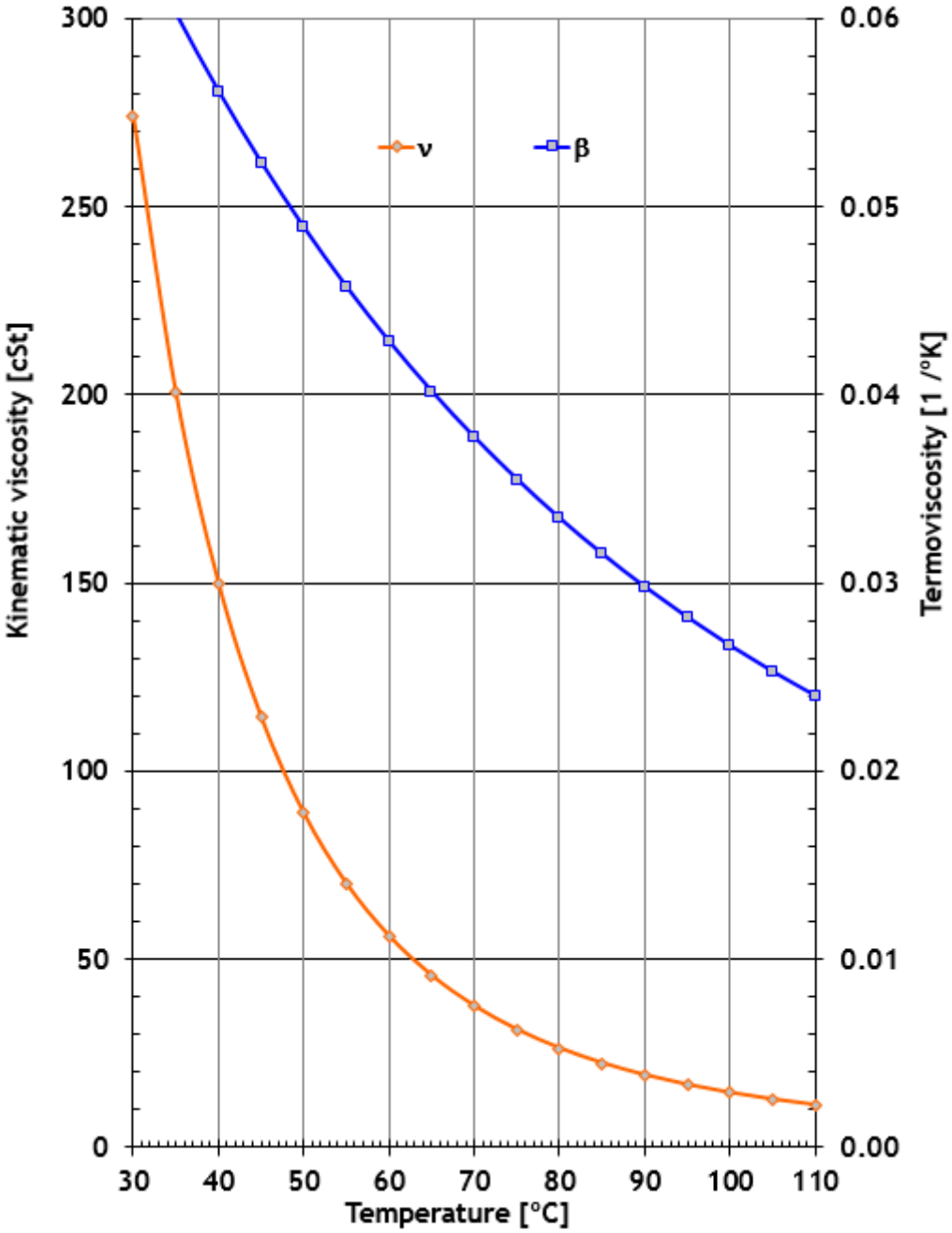

Figure 5.5: Kinematic viscosity and thermoviscosity variation with temperature.

5.1.2 Gears Material

Gears were made of POM, material that was identified via FTIR (Fourier Transform Infrared). FTIR analysis provides a spectrum that is a molecular fingerprint for organic, polymeric, and some inorganic materials [2].

The monomer (molecule that forms the basic unit for polymers) of POM is shown on Figure 5.6, and a comparison between the FTIR experimental results and the ones found on [2] is shown on Figure 5.12.

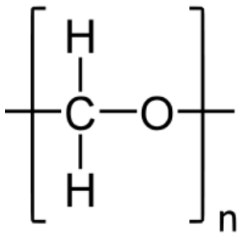

Figure 5.6: POM monomer [2].

Ed Hare suggests some reasons for the peaks found on the FTIR rsults:

- the peak that happens at the wave number 903 $cm^{-}1$ is due to the C-O-C symmetric absorption. A similar peak happened at 881.2 $cm^{-}1$ in our experimental results.
- the peak found at 1097 $cm^{-}1$ is due to the C-O-C asymmetric stretch. A similar peak happened at 1089.6 $cm^{-}1$ in our experimental results.
- the peak at 2923 $cm^{-}1$ is due to the CH_2-O asymmetric stretch. A similar peak happened at 2920.5 $cm^{-}1$ in our experimental results.

Based on this facts, and on the analysis of Figure 5.12, we concluded that the material tested was POM.

Some properties of POM were already given during Chapter 2. More detailed properties of POM are given on Appendix D.

5.1.3 Gears

Gear tooth geometry was already described in Section 4.3. In this Section, the surface roughness measurements and the weighting process of the tested gears are described.

Roughness measurements were performed in all the gears before and after the tests. Roughness was measured in three teeth performing three roughness radial profiles each as shown on Figure 5.7 (center and borders). A topography was also performed at one teeth by gear. Topographys can be found in Appendix E. The analysed teeth were always the same, before and after the tests performed on the FZG.

The weighting was also made before and after FZG tests. Each weighting was repeated three times for each pinion and an average value was considered. A reference weight was used in every measurement.

Figure 5.7: Roughness measuring positions.

Tables 5.4 and 5.5 [1] show the obtained results after roughness and weighting procedures. Figure 5.8 shows that roughness profiles for *pinion 1, 2 and 3* in new condition are similar. Figure 5.8 clearly shows the roughness reduction after the end of the tests. More detailed information about roughness can be found in Appendix E.

Table 5.4: Roughness and weight data of POM *pinions 1, 2 and 3*.

Pinion No.	Load Stage	Speed n_1 [rpm]	R_a	R_q	R_z	R_{max}
Before run-in						
1	K1,K2	750 - 4500	2.30	2.90	13.12	16.66
2	K2,K3	750 - 4500	2.13	2.70	13.89	16.03
3	K2,K3	750 - 3000	1.62	1.97	9.42	10.32
After fail						
1	K1,K2	750 - 4500	1.87	2.33	9.98	14.40
2	K2,K3	750 - 4500	1.72	2.15	9.48	12.39
3	K2,K3	750 - 3000	1.37	1.75	7.90	8.70

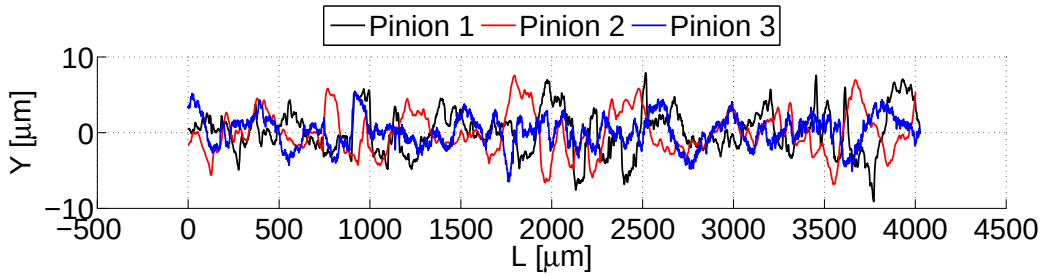

Figure 5.8: Roughness profiles from the POM *pinions 1, 2 and 3* in unused condition.

[1] Weight data for *pinions 1, 2, 3, 7 and 8* is meaningless due to tooth breakage. Roughness data for *pinion 8* is not presented due to unavailability of the measuring equipment during the time when this work was performed.

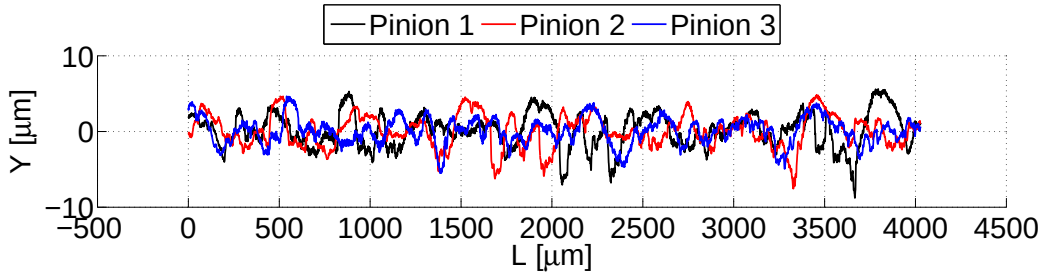

Figure 5.9: Roughness profiles from the POM *pinions 1, 2 and 3* after failure.

Table 5.5: Roughness and weight data from POM *pinions 4, 5, 6, 7 and 8.*

Gear No.	Load Stage	Speed n_1 [rpm]	R_a	R_q	R_z	R_{mx}	Ref. Weight [g]	Weight [g]
Before run-in								
4	K2	1500	1.56	1.92	8.76	10.18	92.360	95.419
5	K3	1500	1.62	2.03	9.56	10.80	92.360	95.360
6	K4	1500	2.04	2.61	11.85	15.72	92.358	95.359
7	K4	1500	1.53	2.05	8.85	15.81	-	(broken)
8	K4	1500	1.41	1.79	8.99	12.89	-	
After fail/run-in								
4	K2	1500	1.37	1.67	7.13	8.56	92.357	95.436
5	K3	1500	1.16	1.47	6.21	8.33	92.359	95.349
6	K4	1500	1.38	1.72	8.10	10.43	92.357	95.295
7	K4	1500	1.40	1.86	8.47	13.34	-	(broken)

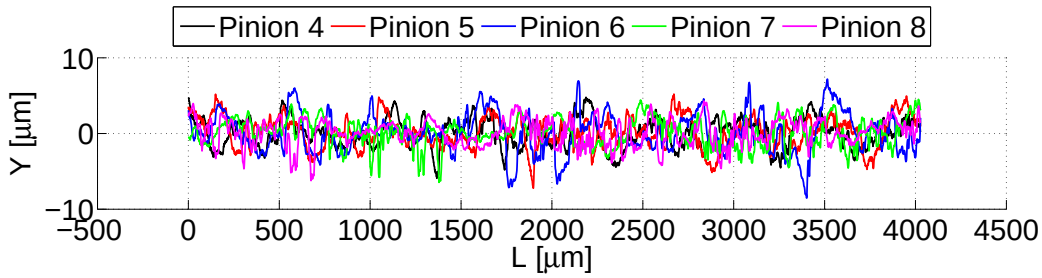

Figure 5.10: Roughness profiles from the pinions 4, 5 and 6 in unused condition.

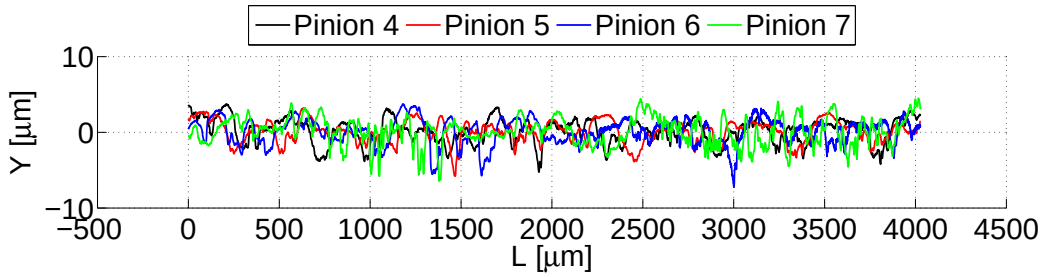

Figure 5.11: Roughness profiles of pinions 4, 5 and 6.

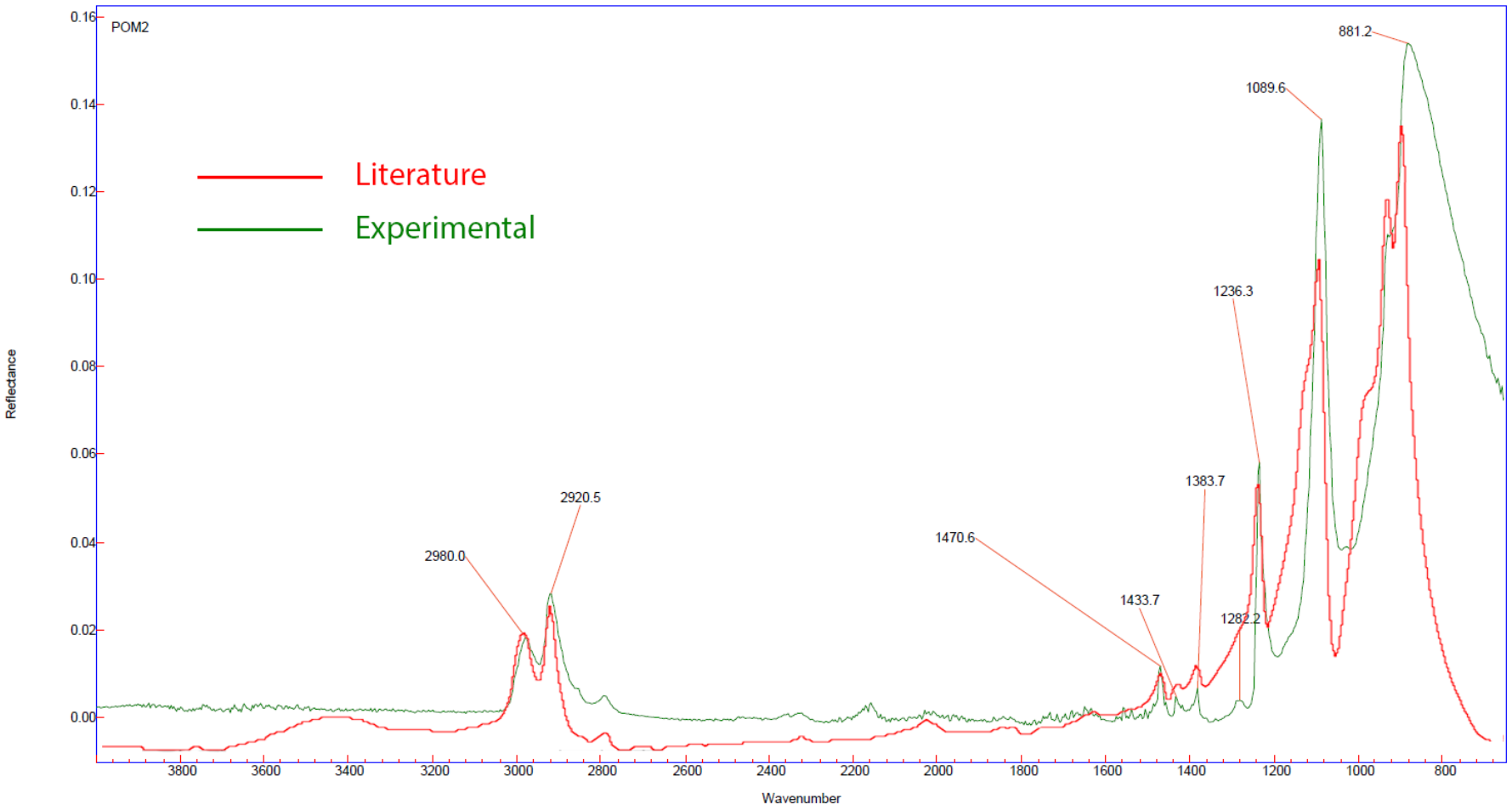

Figure 5.12: FTIR comparison between the experimental results and the results found in [2].

5.1.4 Wear measurement

Wear in steel gears can be measured by the mass loss after tests. The tested gears were weighted before and after the tests. However, some results (e.g. the increase of the weight after-run on *pinion 4*) have suggested controversy for this method.

A simple experiment was made in order to evaluate this situation. An oil container was placed inside an oven with a plastic pinion made of the same material of the gears used on the tests, submerged in lubricant ((Energol GR-XP 150) at 55 °C. Measurements were then taken for 9 days. The results for the weighting experiment are shown on Figure 5.13.

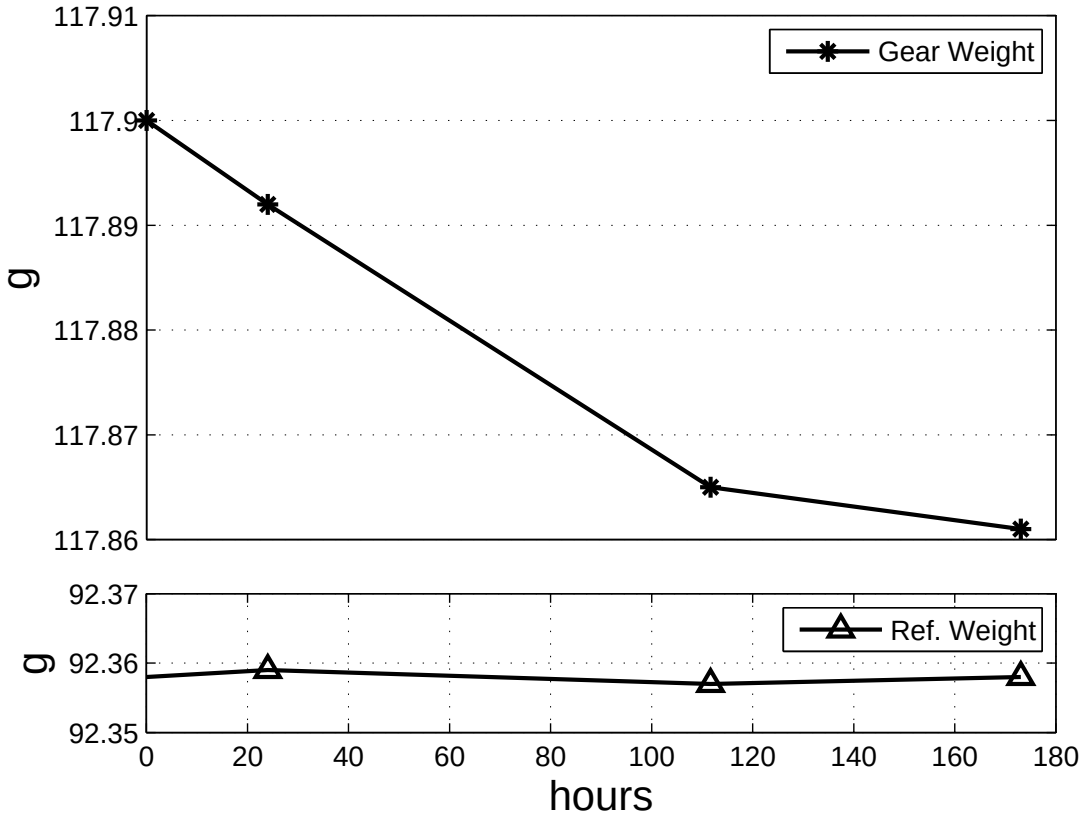

Figure 5.13: Weight of POM pinion.

By the results shown in Figure 5.13 it is seen that weight reduced when the gear was submerged into oil during more than 8 days. As this method did not appear to be coherent, it was decided to evaluate wear visually recurring to an optical microscope.

Zoomed photos (50x) from the flank area below and above the pitch circle were taken in order to evaluate wear. For that, an approximation to the depth of the cavity generated by wear was measured on photos as shown on Figure 5.14. It is known that there are some problems with this method. Considerable length that may be ignored (red area on Figure 5.14) and is also impossible to measure the wear depth at the middle of the face width (where wear is more effective) without performing a tooth cut in every gear. However, a direct comparison can be made, and the wear on broke pinions could now be analysed. The results obtained by weighting method are still shown for the S-N

tests performed with C14 gears where no tooth breakage happened. However, wear results and discussion are based on the obtained photos.

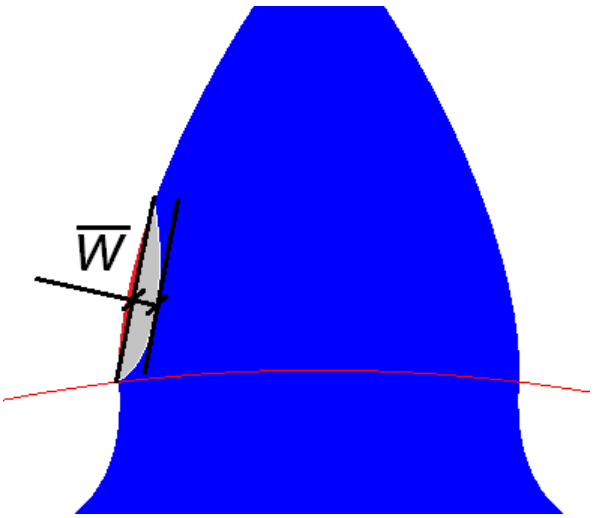

Figure 5.14: Distance $\overline{w}$ [μm] measured to evaluate wear.

5.2 Preliminary Tests - Load and Thermal capacity

Three pinions were tested during preliminary tests. The procedure was not fixed during this experiments and suffered some adaptations based on the obtained results and experimental observations. The main focus was to understand the limits of C14 plastic gears in terms of speed, load and temperature.

5.2.1 Operating Conditions and Results

Pinion 1

The test procedure adopted on the first test is shown on Figure 5.28. A POM pinion was engaged on a steel wheel (16MnCr5) and the first load stage K1 was set. The speed was set to 750 rpm on the pinion, followed by 1500, 3000, and 4500 during 3 hours at each speed. The main objective of this test was to find a limit load/speed combination that would lead to failure.

As fail did not occur on K1 load stage, the test continued to K2 load stage with a pre-defined number of cycles (instead of a fixed test time), for the same speeds used on K1 load stage tests.

On K2 load stage, temperatures were pre-set to the same ones obtained before on K1 load stage since a small increasing on temperature was expected. The temperature control system was turned off after 1,5 hours at 750 rpm, and after 1 hour at 1500 rpm. Differently from what was expected, oil temperature significantly decreased. The two last speed stages at K2 (3000 and 4500 rpm) were fully made with temperature control at K1 temperatures and failure occurred at 4500 rpm, between $2.295 \cdot 10^6$ and $2.475 \cdot 10^6$ cycles. The aspect of *pinion 1* after the test is shown on Figure 5.15. Immediately[2] after the test, the tooth temperature was 81.9 °C and the oil temperature was 69.1 °C, as shown on Figures 5.16 and 5.17 respectively. The total power losses are shown on Figure 5.18.

Pinion 2 and Pinion 3

Based on information obtained with *pinion 1*, tests continued with a POM pinion engaged on a steel gear with the fixed number of cycles principle for different speeds, increasing load. As it was observed that K1 load stage would lead to higher oil temperatures than K2, K1 load stage was suppressed. Tests started at K2 load stage, followed by K3. As temperature critically affects plastic gears running life-time, the tests were run with free temperature after pre-heating to the temperature of the previous load stage, allowing the time to reach the stabilization temperatures to be reduced. The flow chart of the test procedure used with *pinion 2* and *pinion 3* is shown on Figure 5.29.

[2]A temperature measurement of the tooth was always made at the end of the tests using a thermographic camera. To measure it, it was always necessary to open the top cover of the test gearbox of the FZG test rig, always during less than one minute.

This time a failure did not occur on K2 load stage. *Pinion 2* resisted until K3 and failed at 4500 rpm after a number of cycles between $1.26 \cdot 10^6$ and $1.44 \cdot 10^6$, again by tooth breakage. The teeth aspect after *pinion 2* failure is shown on Figure 5.19. Immediately after the test the tooth temperature was 66.3 °C and the oil temperature was 52.5 °C and as shown on Figures 5.20 and 5.21 respectively . The average power loss in *pinion 2* tests after temperatures stabilization is shown on Figure 5.22.

As two failures had already happened at 4500 rpm, following the test procedure, the last speed was suppressed. With *pinion 3*, 180 000 cycles were made at 750 and 1500 rpm, and 2× 180 000 cycles were made at 3000 rpm.

While repeating tests made with *pinion 2* (excluding the ones at 4500 rpm), different temperatures were found. The oil temperature was always more than 8 °C higher despite a maximum increase on the ambient temperature of 5 °C. The maximum difference on oil temperature when comparing with the tests between *pinion 2* and *pinion 3* was found at K2 load stage, at 3000 rpm: 25 °C. *Pinion 3* failed at K3 load stage at 3000 rpm $1.23 \cdot 10^6$ cycles, with the oil bath at 58.1 °C (it had no time to stabilize since the last speed stage had only 50 minutes), with a tooth temperature of 67.4 °C as shown on Figure 5.24. The damage at *pinion 3* is shown on Figure 5.23. The temperatures recorded during the tests of *pinion 3* are shown on Figure 5.25 [3] . Besides the increase of the oil temperature, total power losses did not change so much and even decreased. The total power losses are shown on Figure 5.26 [4].

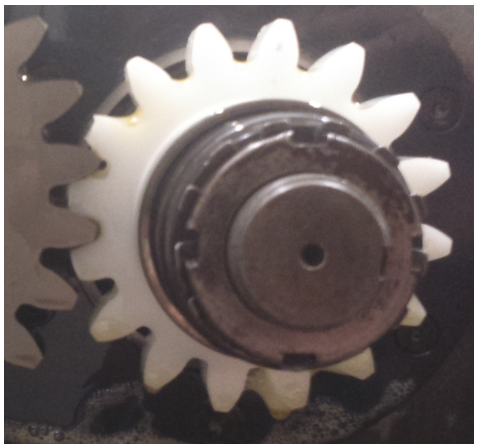

Figure 5.15: Tooth flank breakage fail of *pinion 1*.

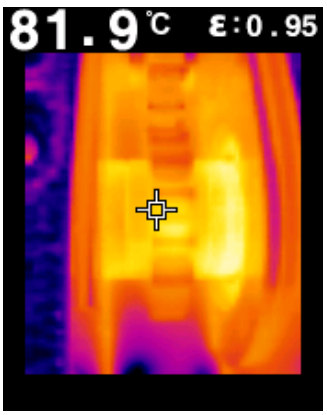

Figure 5.16: Tooth temperature after *pinion 1* failure.

[3]FZG base temperatures (biggest heat transfer surface of the test rig) are shown since the oil temperature reduction at 3000 rpm can be explained by it: the test started after a stoppage of more than eight hours, which decreased the test rig body temperature.

[4]Data was not recorded at 1500 rpm.

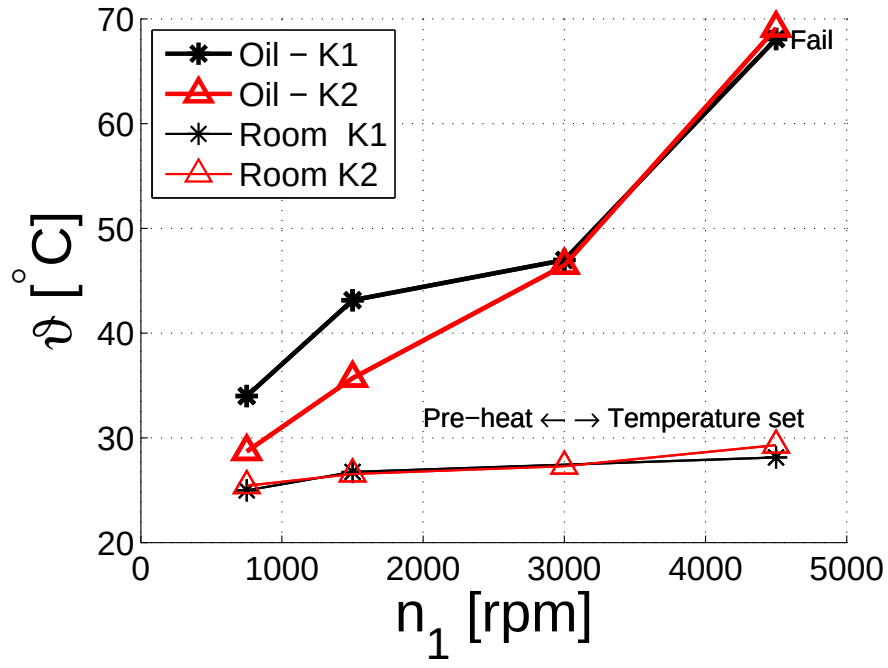

Figure 5.17: Oil and ambient stabilization temperatures with *pinion 1*.

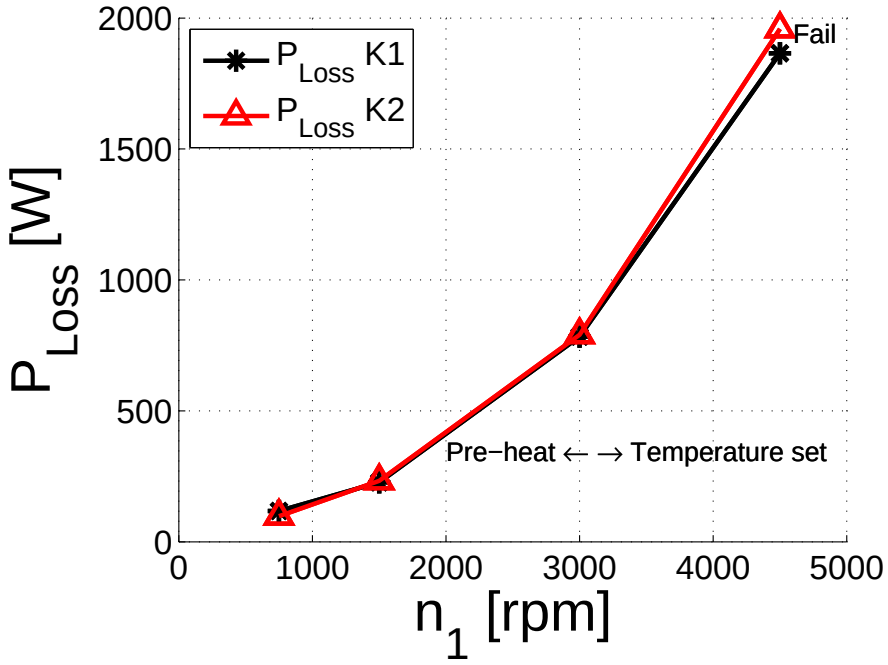

Figure 5.18: Total power loss during tests performed with *pinion 1*.

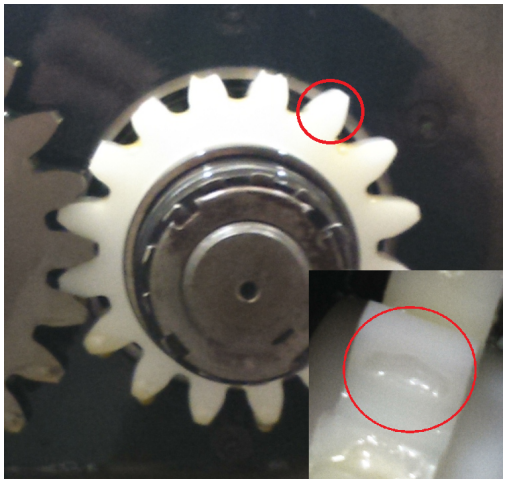

Figure 5.19: *Pinion 2* aspect after the test.

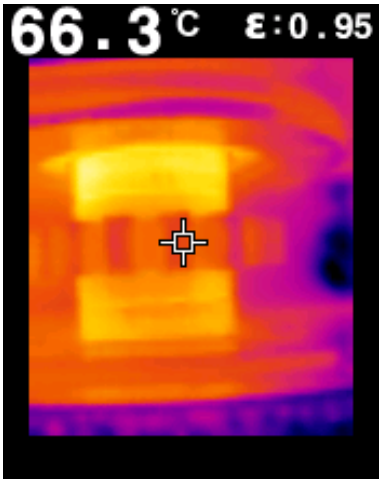

Figure 5.20: Thermographic photo after failure of *pinion 2*.

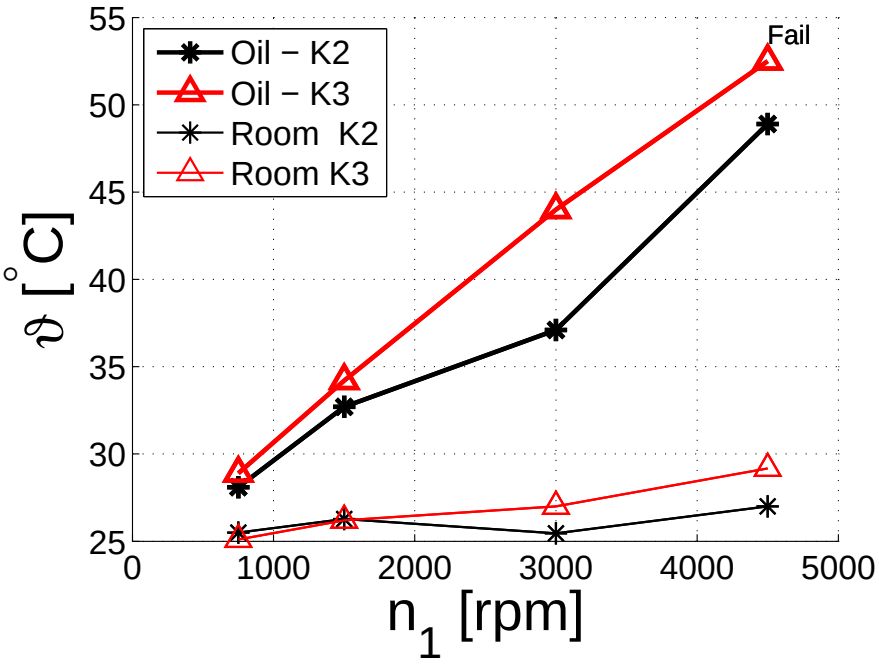

Figure 5.21: Stabilization temperatures on tests performed with *pinion 2*.

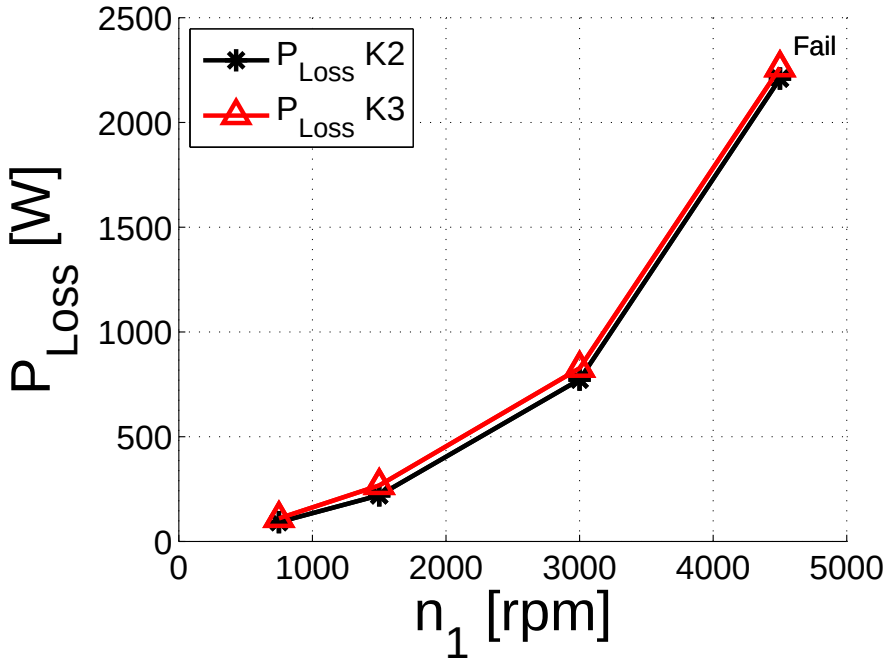

Figure 5.22: Total power loss on tests performed with *pinion 2*.

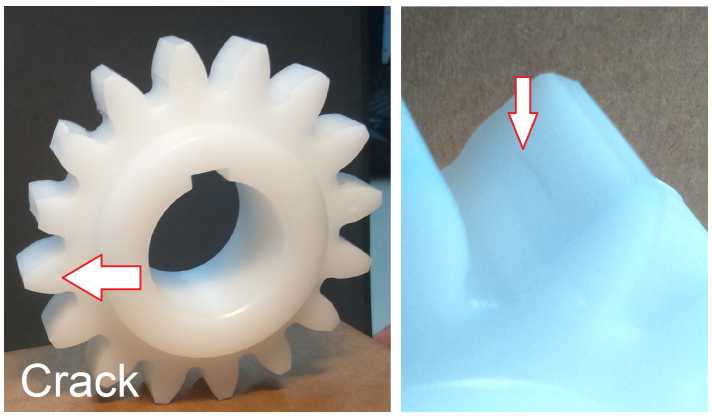

Figure 5.23: Tooth flank breakage fail of *pinion 3* and grown crack.

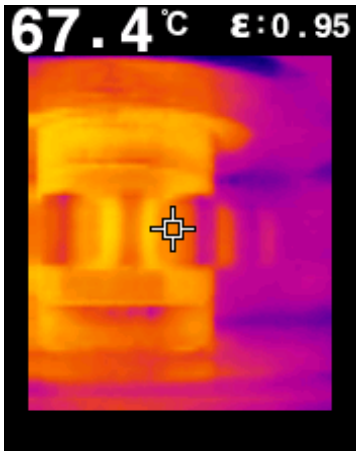

Figure 5.24: Tooth temperature after *pinion 3* failure.

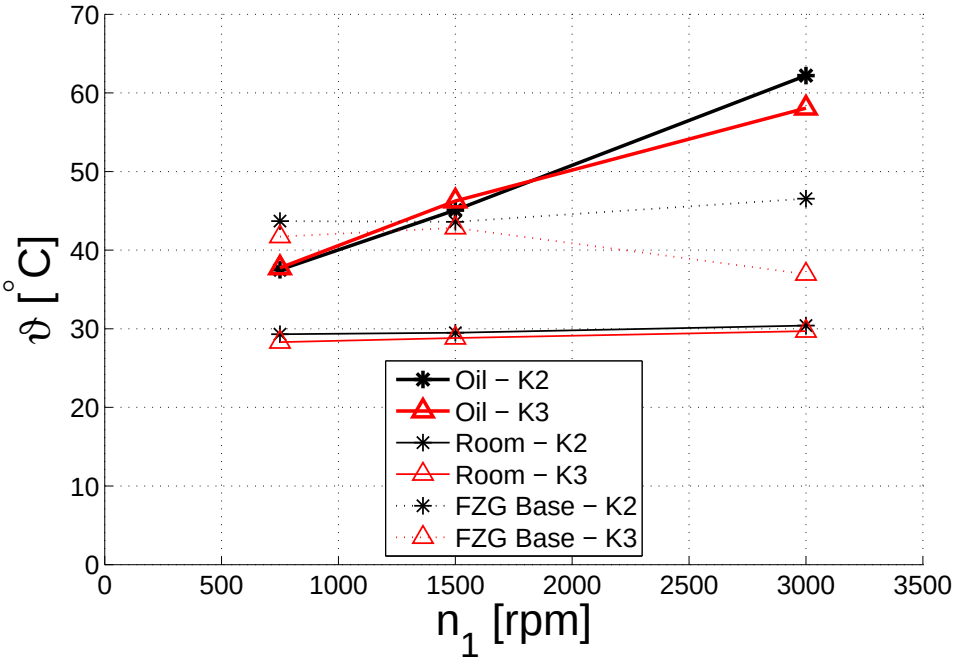

Figure 5.25: Oil bath, room, and FZG base temperatures during pinion 3 tests.

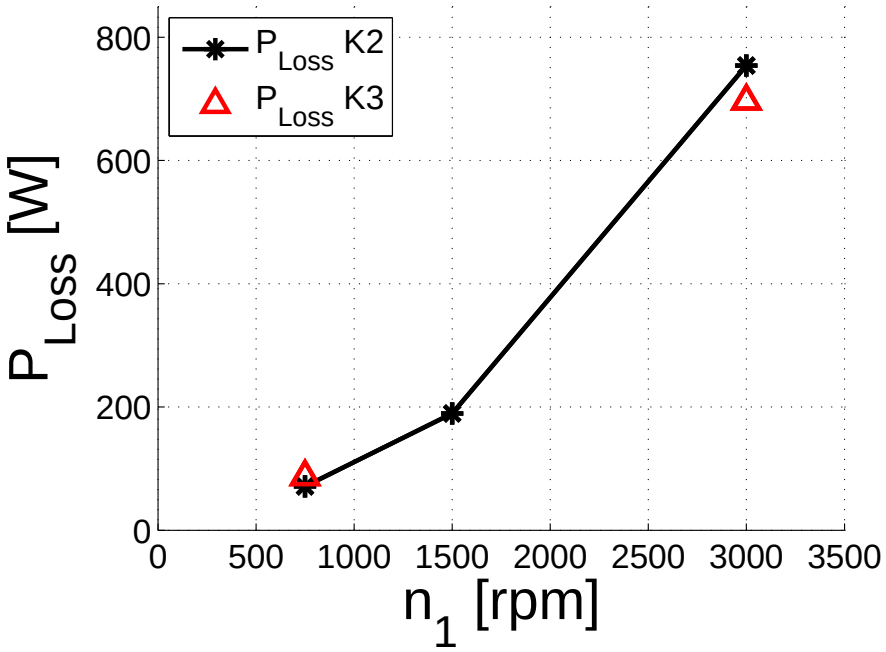

Figure 5.26: Total power loss during pinion 3 tests.

5.2.2 Specific Film Thickness Calculation

Specific film thickness was calculated using the method explained in Section 2.5 (Myers solution) for the centre of the meshing line. The values for R_q considered on the plastic pinion for this calculation were average values obtained in the three measured teeth for the cases "new" and "after test". For the steel wheel, the R_q value considered was and experimental and average which was kept constant for all the calculations. The results are shown on Figure 5.27.

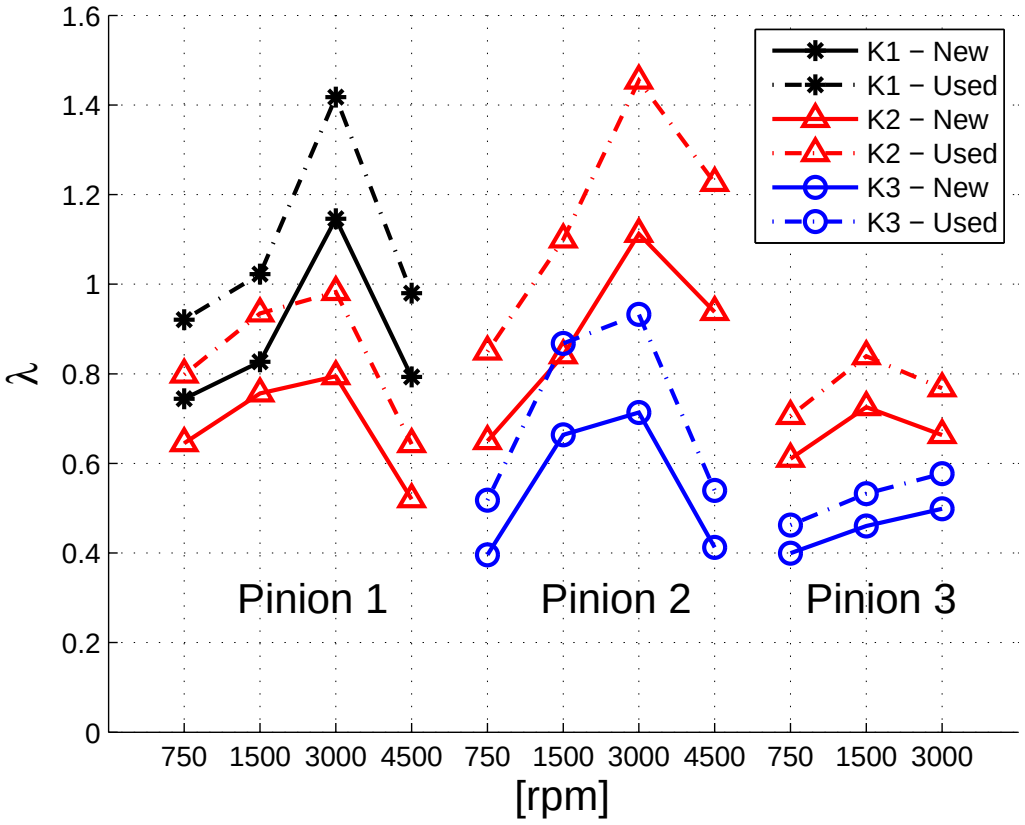

Figure 5.27: Calculated specific film thickness Λ for the preliminary tests.

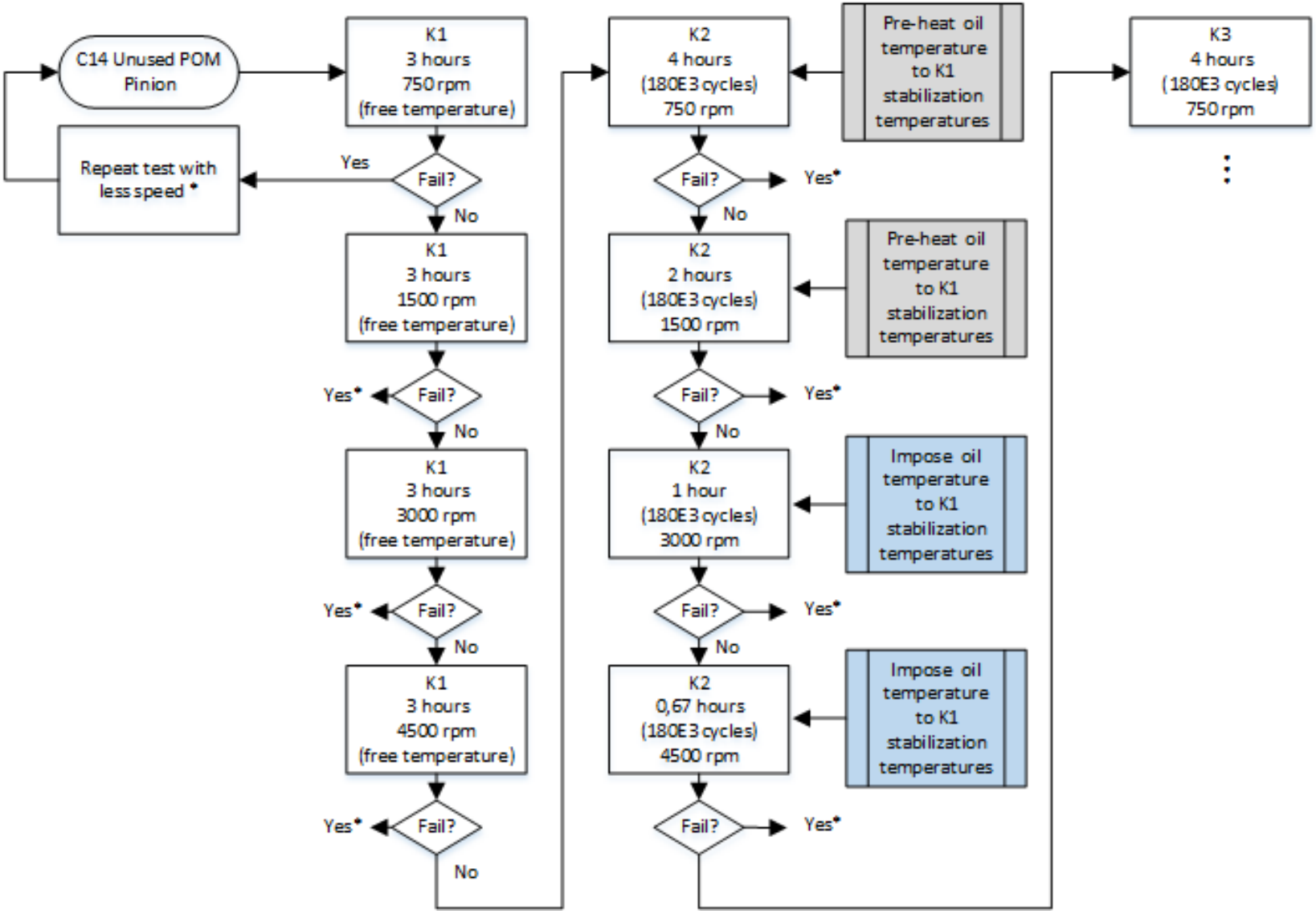

Figure 5.28: Flow chart of the *pinion 1* tests procedure.

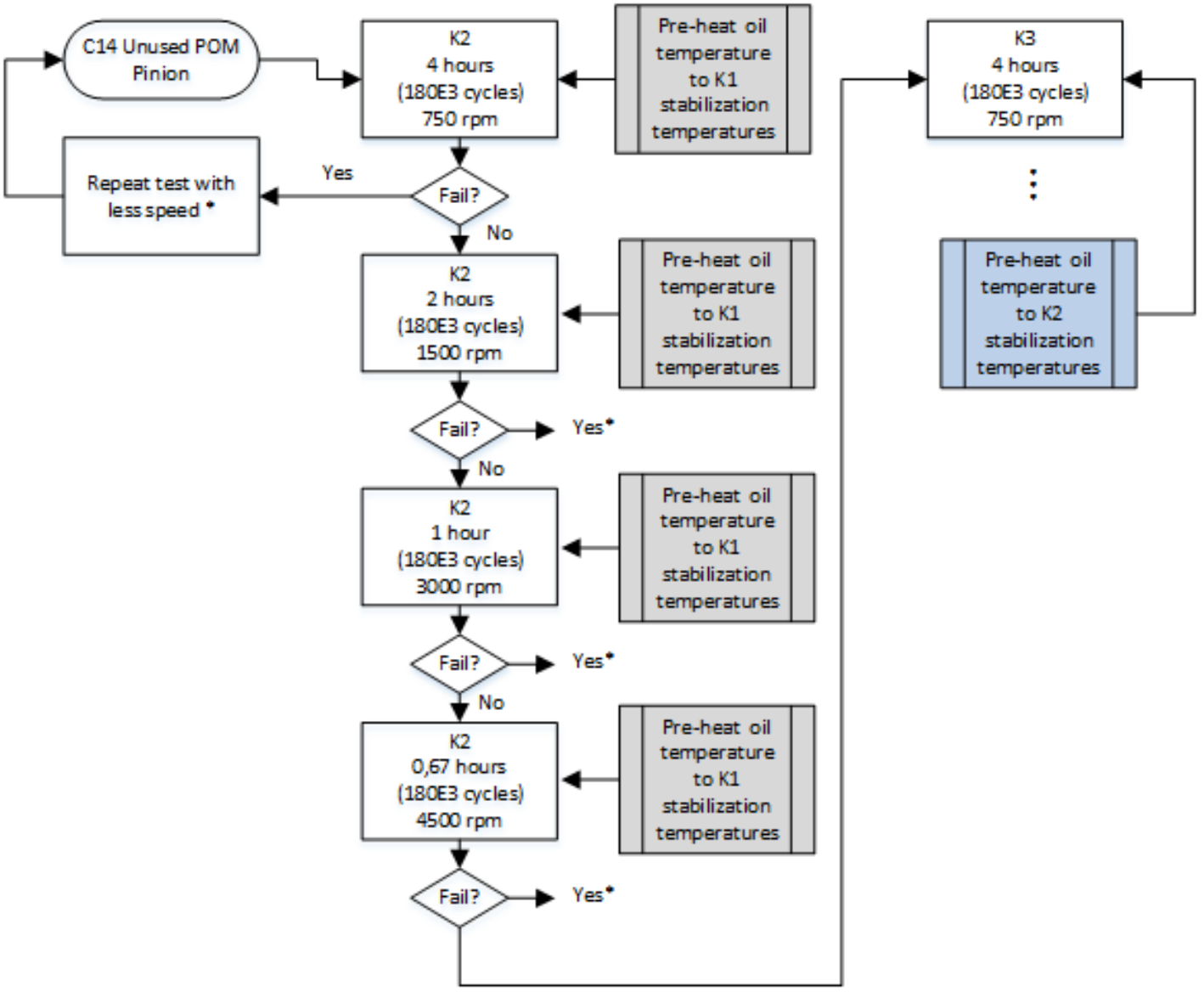

Figure 5.29: Flow chart of test procedure made with *pinion 2* and *pinion 3*.

5.2.3 Wear

To evaluate wear, photos were taken from *pinion 1, pinion 2, pinion 3* and a new unused C14 pinion for comparison. Results are shown on Figures 5.31 - 5.30.

(a) Tooth profile below the pitch circle. (b) Tooth profile above the pitch circle.

Figure 5.30: Tooth profile of a new C14 pinion.

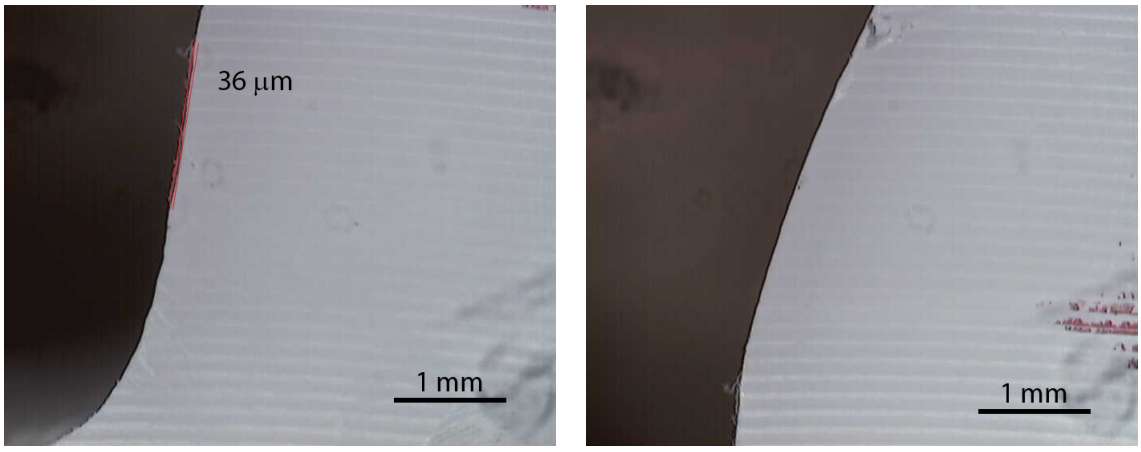

(a) Tooth profile below the pitch circle. (b) Tooth profile above the pitch circle.

Figure 5.31: Tooth profile of *pinion 1* after tests.

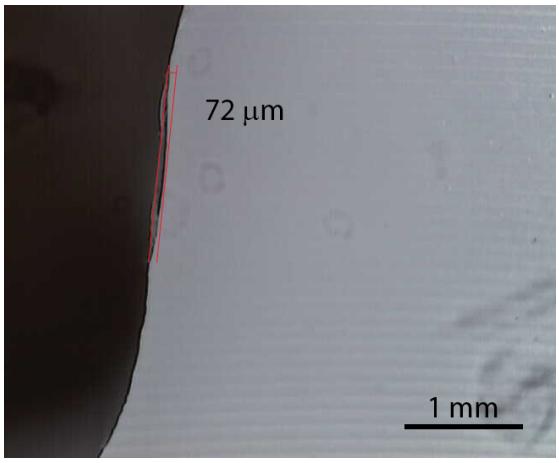

(a) Tooth profile below the pitch circle.

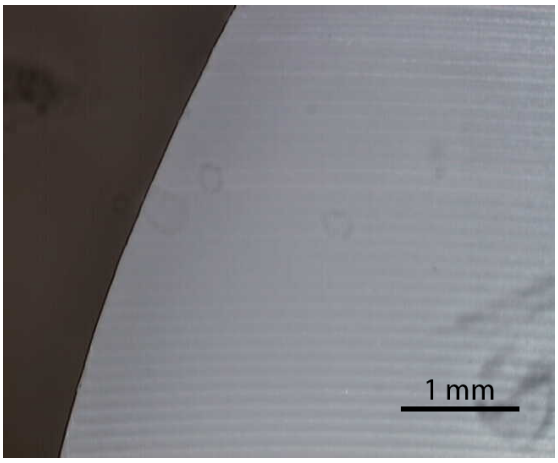

(b) Tooth profile above the pitch circle.

Figure 5.32: Tooth shape of *pinion 2* after tests.

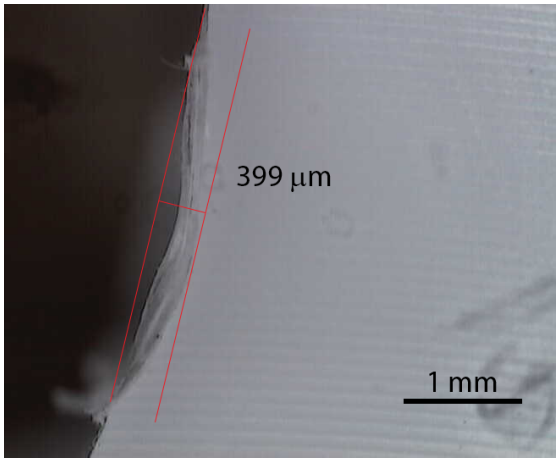

(a) Tooth profile below the pitch circle.

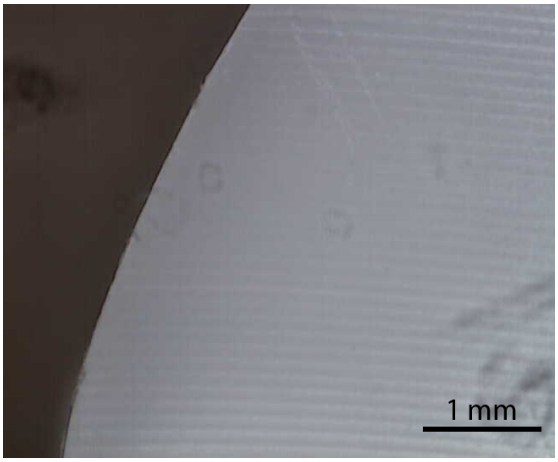

(b) Tooth profile above the pitch circle.

Figure 5.33: Tooth (next to broke tooth) profile of *pinion 2* after tests.

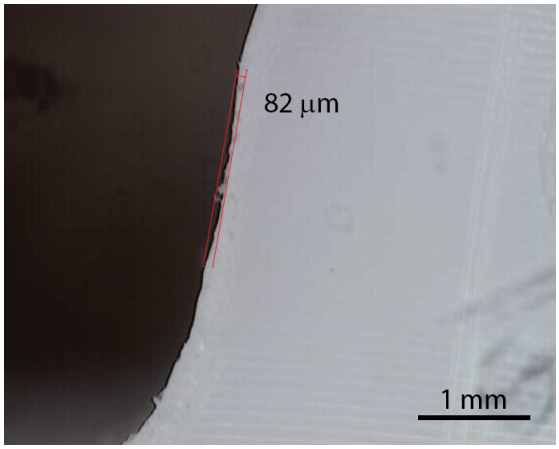

(a) Tooth profile below the pitch circle.

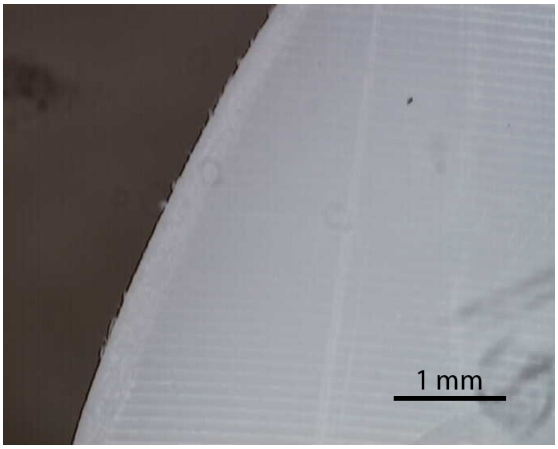

(b) Tooth profile above the pitch circle.

Figure 5.34: Tooth profile of *pinion 3* after tests.

5.2.4 Discussion

Pinion 1

As the failure mode was always tooth flank breakage, with engagement continuity being guaranteed, the FZG test rig could not detect the exact failure moment and stop the electric motor. Because of that, the number of cycles considered was the last 120 thousand cycles (last speed stage at K2).

The position of the pinion after the test(Figure 5.15) suggests that the failure happened during the stoppage. This aspect will be discussed ahead on this section.

A decrease on oil temperature was verified when load was increased (at 750 and 1500 rpm without temperature control). As the loads are low (3.3 N·m on K1 and 13.7 N·m on K2), the effect of load increasing on the total power loss is not easily detected since the largest part of the power loss is load independent. Total power loss was lightly lower on K2 before the temperature control (at 750 and 1500 rpm) However, when temperature was pre-set to K1 load stage stability values, power loss on K2 load stage reached similar values at 3000 rpm to the ones obtained on K1, and only became noticeably different (1865.37 W on K1 versus 1958.674 W on K2) at the last speed stage. It seems that similar temperatures lead to similar power loss which may be related with the viscosity variation effect on churning power loss.

As seen on Figure 5.27, at 4500 rpm and K1 load stage, the specific film thickness decreased, which means that the temperature effect (viscosity reduction) prevailed to the speed effect (increase of the film thickness). It is important to note that K1 load stage tests were performed under free-temperature conditions on the test gear-box, this suggests the existence of a critical speed between 3000 and 4500 rpm that results on the reduction of the specific film thickness.

As seen on Figure 5.31, wear was found below the reference circle (near the tooth root). However, above the reference circle wear effects were not observed. Analysing Figure 5.35 it is seen that specific sliding is higher on the tooth root which may be a possible explanation. Deformation is also a possible cause which will be discussed on the S-N tests.

Pinion 2 and 3

The failure mode was the same one found on *pinion 1*, although holes appeared on one flank which could have leaded to the final tooth breakage. It seems that high flank local temperatures[5] combined with high Hertzian stresses form small holes that easily grow.

The broken teeth aspect suggest that, starting on these holes, a crack was then formed and grown by the bending stresses leading to the final failure, as shown on Figure 5.36.

[5]Flank local temperatures may be higher than the ones measured with the thermographic camera since it is very hard to measure a small area of a tooth. Variations of 5 °C were common during measurements at the end of the tests. The chosen temperature for results analysis was always the biggest one found. For better understanding, an aproach to tooth temperature distribution was already shown on Figure2.4.

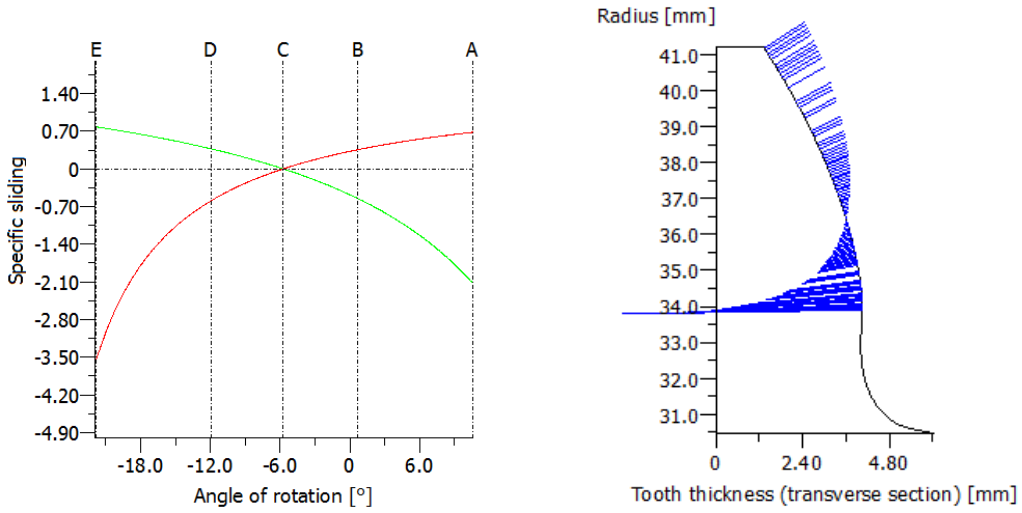

(a) C14 gear pair. (b) C14 pinion.

Figure 5.35: Specific speed for C14 pinion (max/min=-3.5865/0.6801) and wheel (max/min=-2.1259/0.7820) at K2 load stage. [3].

A zoomed crack is shown on Figure 5.37.

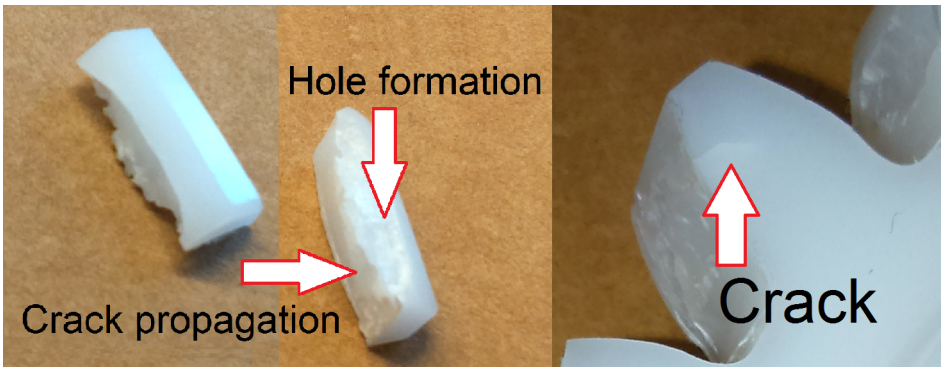

Figure 5.36: Broken tooth - failure mode (*pinion 2*).

Figure 5.37: Crack found on *pinion 2*.

An increase on oil temperature was verified while increasing load, however, power losses remained very similar in both of the load stages K2 and K3.

Once again it is shown on Figure 5.27 the existence of a critical speed that decreases specific film-thickness. The specific film reduction happened on K2, and K3 load stages in free-temperature conditions at 4500 rpm, as it had already been verified for K1 tests on *pinion 1*.

When comparing to *pinion 1*, wear on *pinion 2* was more effective, specially on the teeth next to the critically damaged ones (broken or with drilled flanks). A huge difference can be seen when comparing Figures 5.32 and 5.33 which suggest that the load was larger on the teeth next to the damaged ones. This effect can possibly be explained by the after failure run: because of the big mass removal on the flank (holes found), and the broken teeth, the load distribution by tooth was affected increasing the load on the following teeth, this load increasing may also have increased tooth deformation which created a critical situation for this specific teeth.

The difference on wear between the teeth next to the damaged ones and the teeth far from the damaged ones was not found above the reference circle. Once again, the tooth flanks were not affected by wear above the reference circle.

The wear found on *pinion 3* is very similar to the one found on *pinion 2* (Figures 5.32 and 5.34). In fact, applied loads were the same and the number of cycles was very similar. This aspect suggests these two factors are determinant to wear.

Failure at stoppage

A power loss increase is expected after tooth breakage since tooth profile changes result in very high sliding speeds. To understand what happened to the power losses after failure, the broken *pinion 2* was assembled again on the FZG test rig. After 20 minutes the test was paused in order to check if some tooth would break at stoppage. As there were the same number of broken teeth, the test continued for more 40 minutes.

A mean value of power loss was calculated within 10 minutes time periods so that the power loss changes could be eventually observed.

It is known that the first tooth breakage happened between $1.32 \cdot 10^6$ and $1.44 \cdot 10^6$, so, power losses between $1.32 \cdot 10^6$ and $1.60 \cdot 10^6$ were analysed. Results are shown on Figure 5.38. After 60 minutes, it was clear that power loss increased, but, in fact, we can not conclude that the tooth breakage happened at the test ending since during the first 10 minutes after failure the total power losses decreased.

As the meshing gears' power losses P_{VZP} is a small part of the total power losses, the effect of increasing the tooth sliding speed may not be noticeable. The oil bath temperature had to be analysed, so that a sudden temperature increasing could be possibly noted. Results are shown on Figure 5.39.

Figure 5.39 clearly shows that the temperature increased dramatically after Test 2 (original tests on *pinion 2*). Until the end no more teeth got broken, although, damage on tooth flank increased (Figure 5.40): the existing hole became bigger, and another hole was found at the following tooth; wear dramatically increased near tooth root. The obtained temperatures clearly suggest that failure happened during stoppage.

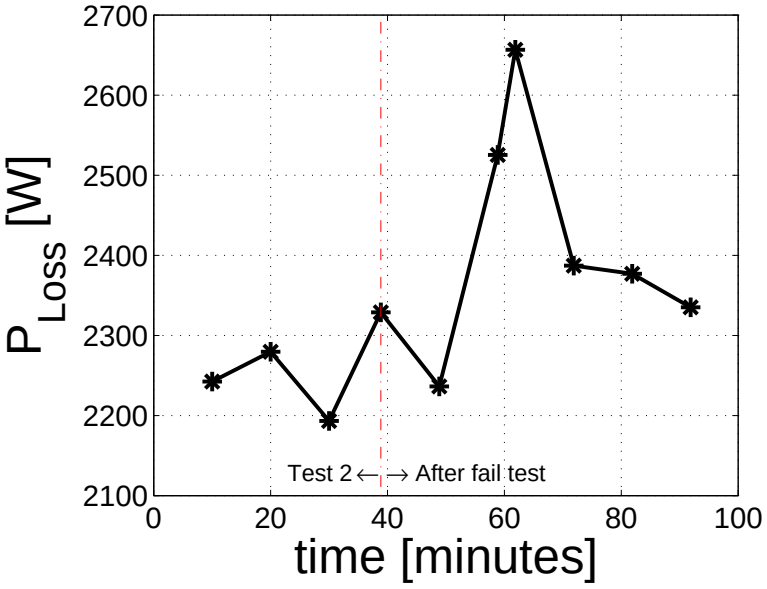

Figure 5.38: Average power loss in 10 minutes periods during the last half hour of the test and during the "after failure" test performed with *pinion 2* (4500 rpm, K3 load stage).

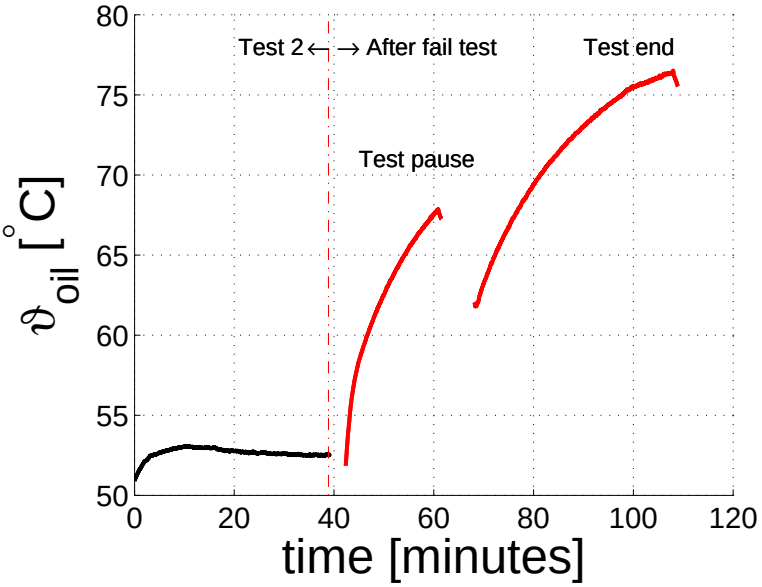

Figure 5.39: Oil temperature before and after failure on *pinion 2*.

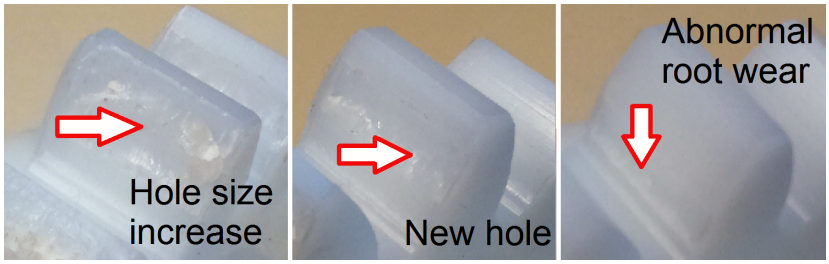

Figure 5.40: Damage found after the "after failure" test performed with *pinion 2*.

5.3 S-N tests

An S-N curve, relates the fatigue limit stress with the number of load cycles. With the increasing of the load cycles, the materials limit stresses tend to decrease. Some materials such as steel, show an endurance limit stress below which the fatigue life is infinite (fatigue limit stress remains constant while increasing the number of cycles). For steel this endurance limit is generally near 10^7 cycles as shown on Figure 5.41. For other materials, this limit may not exist, or exist for a huge number of cycles.

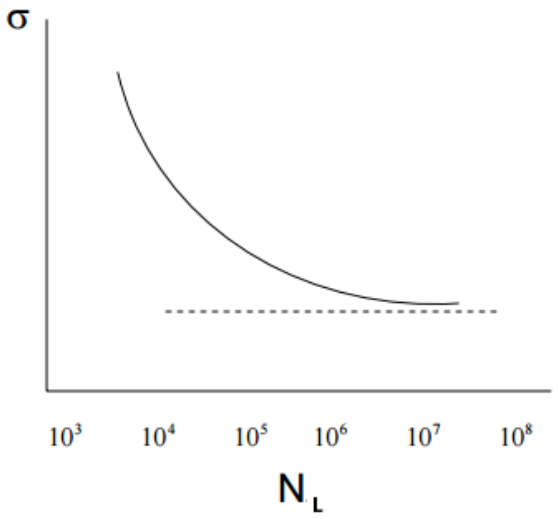

Figure 5.41: An example of an S-N curve.

In order to obtain an S-N curve for the tested material,as the fatigue strength of thermoplastics have an high dependence on the the service temperature it was decided to perform tests with controlled oil bath temperature. Once again, a POM pinion was meshed with a steel wheel (16MnCr5). The gears tested were three C14 pinions and two H501 pinions.

5.3.1 Operating Conditions and Results

All the tests were performed at 1500 rpm on the pinion, at K2, K3 and K4 load stages. The maximum number of cycles per test was 10 million (if a fail would not occur before). The test procedure is shown on Figure 5.42.

To avoid failure at stoppage, the FZG vibrations sensor was readjusted running in a broke pinion in order to stop after tooth breakage. Even after this adjustment, it was decided to stop periodically the tests in order to evaluate the damage on the tested gears. The motor stoppage and start was always made slowly: 1 minute for a progressive reduction of the speed from 1000 to 300 rpm, 2 minutes running in at 300 rpm, and 30 seconds for a progressive motor stoppage.

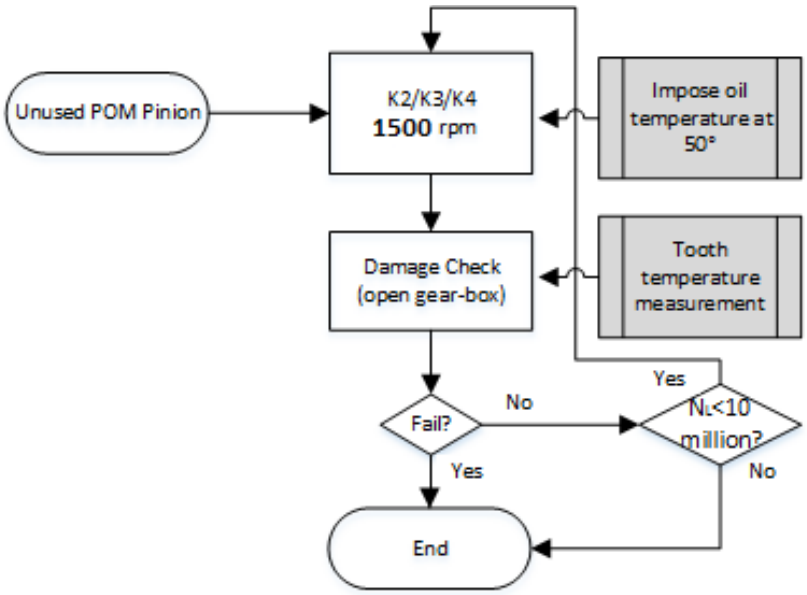

Figure 5.42: Flow chart of S-N tests.

5.3.2 Results

K2 Load Stage - *Pinion 4*

At K2 load stage, the gearbox check was made every 25 hours (10^6 cycles). The tested pinion reached 10 million cycles and a failure did not occur. At the end of the test, no observable damage was found at the pinion, besides some wear on the tooth root (Section 5.3.4).

The tooth temperature measured at the end of the test was 60.8 °C, as shown on Figure 5.43. The average total power loss after temperature stabilization was 208.48 W.

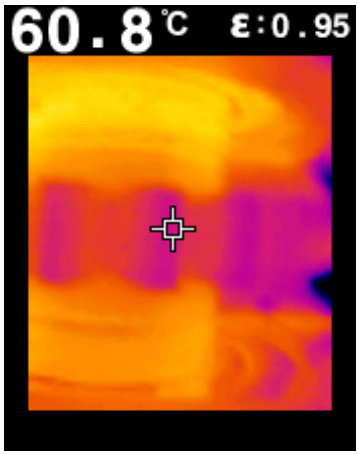

Figure 5.43: Thermographic photo at the end of K2 load stage S-N test.

K3 Load Stage - *Pinion 5*

At K3 load stage, verifications started to be made after 1 million cycles within 5.55 hours ($0.5 \cdot 10^6$ cycles). As a damage development was not observed, after the pinion reach $4 \cdot 10^6$ cycles it was decided to increase the verification period to 8.33 hours ($0.75 \cdot 10^6$ cycles). After $5.507 \cdot 10^6$ cycles two cracks were found at the tooth flank and the test was stopped.

In order to check the crack dimensions, a topography was performed in one of the cracks using a 3D optical microscope. Figure 5.45 shows the shape of the crack tip, and Figure 5.48 shows two roughness profiles. By analysing Figure 5.48, a deep valley with approximately 50 μm is clearly shown. The length of this valley is around to 2 mm. After this analysis, it was concluded that the damage was sufficient to be considered a failure and end the test.

The damaged tooth flank is shown on Figure 5.46. The tooth temperature at the end of the test was 58.8 °C as shown on Figure 5.47. The average total power loss measured was 239.17 W.

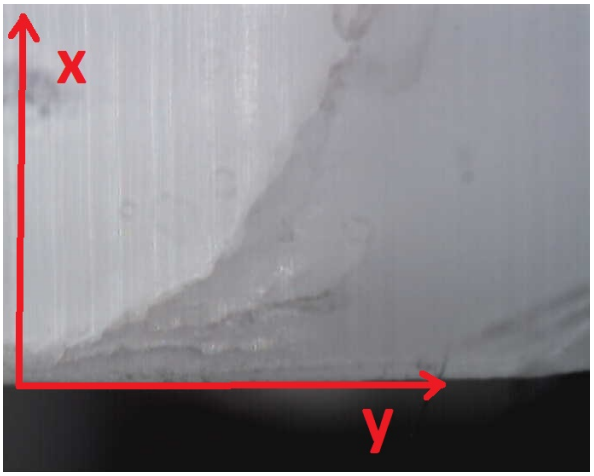

Figure 5.44: Top view of the right crack (Figure 5.46) found on *pinion 5*.

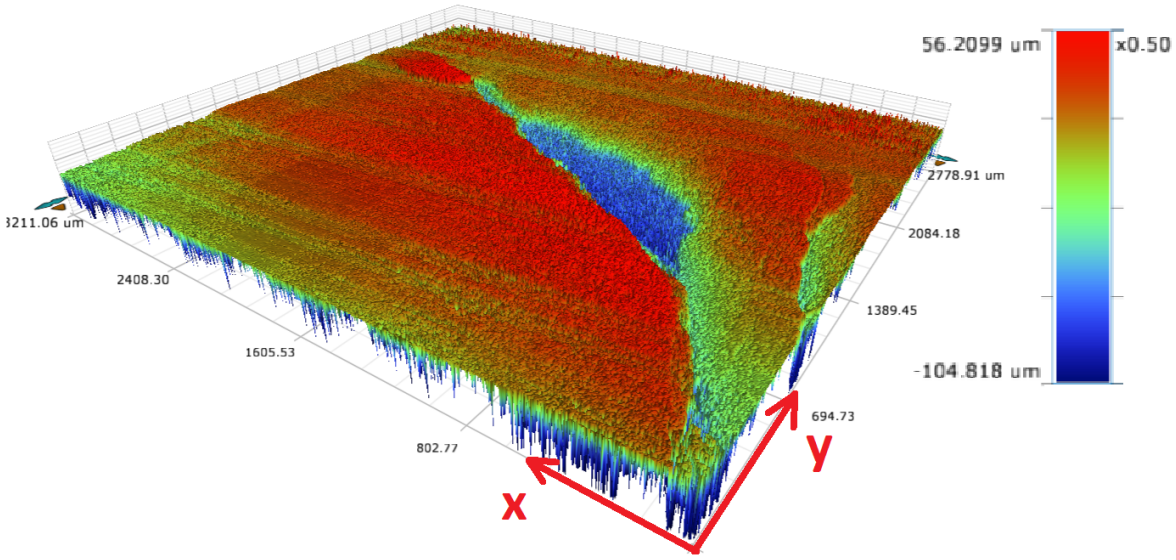

Figure 5.45: Topography of a crack found at the end of K3 load stage S-N test (*pinion 5*).

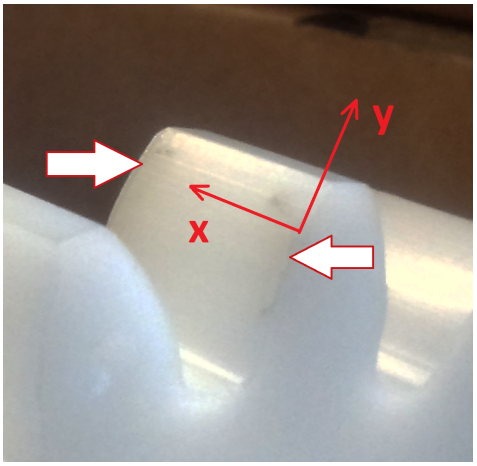

Figure 5.46: Two cracks found at the end of K3 load stage S-N test (*pinion 5*).

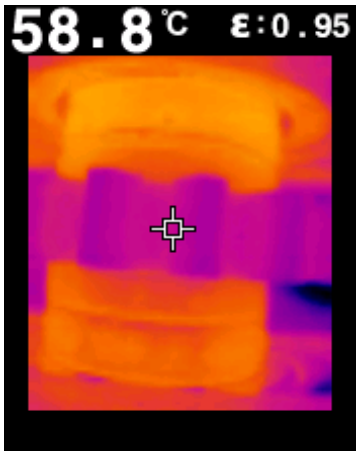

Figure 5.47: Thermographic photo at the end of K3 load stage S-N test (*pinion 5*).

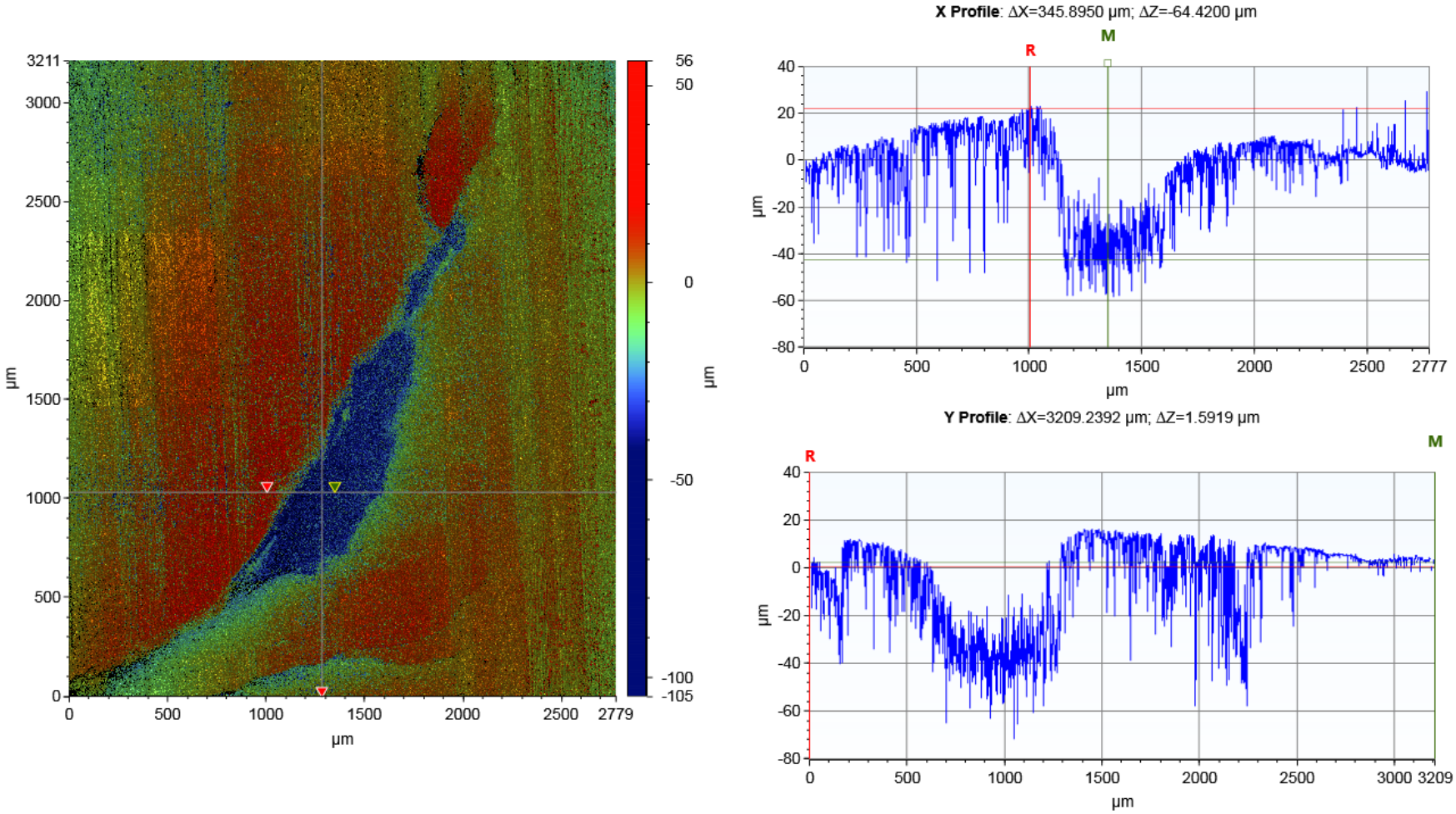

Figure 5.48: Roughness profiles of a crack found at the end of K3 load stage S-N test (*pinion 5*).

K4 Load Stage - *Pinion 6*

On the tests performed with *pinion 6* two verifications were made. The first was made after 5.5 hours ($N_L = 0.5 \cdot 10^6$ cycles) with no damage observed despite some plastic chips could already be observed (the plastic chips were removed from the oil at the end of the test and are shown on Figure 5.49). The second verification was made after 13.8 hours ($N_L = 1.75 \cdot 10^6$ cycles) and various cracks were found in two tooth flanks. The damage found was similar to the one found before on K3 load stage, but more severe. The damaged tooth flank is shown on Figure 5.50. The tooth temperature at the end of the test was 59.2 °C as shown on Figure 5.51. The average total power loss measured was 254.41 W.

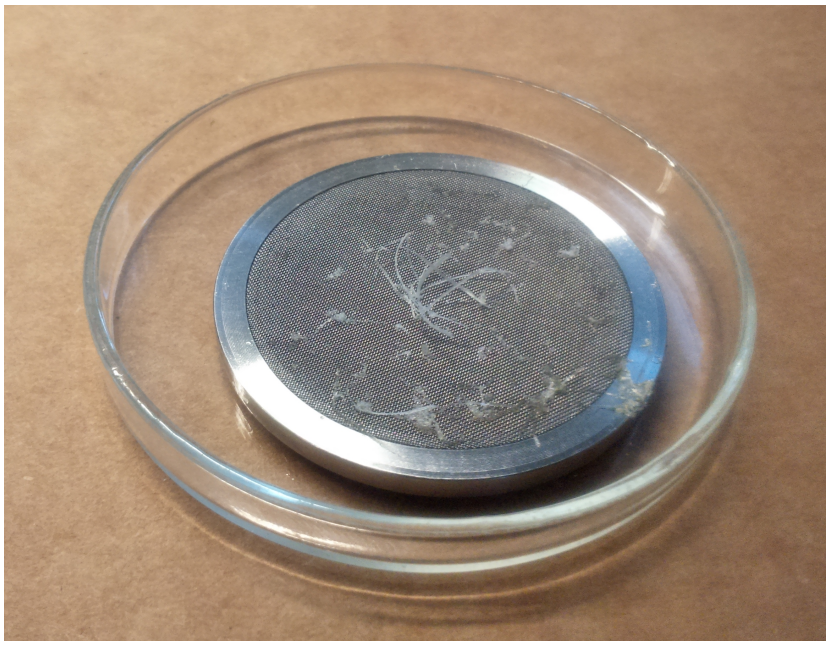

Figure 5.49: Plastic chips removed from the oil after the test.

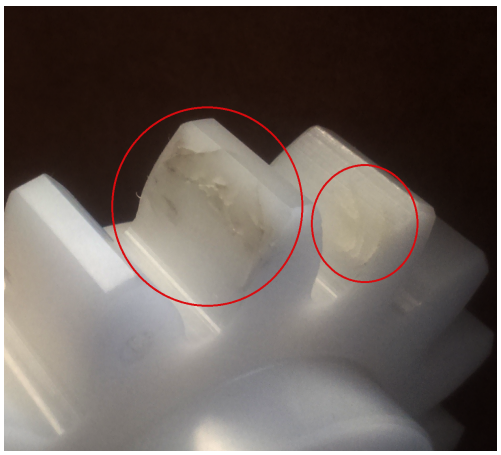

Figure 5.50: Various cracks found at the end of K4 load stage S-N test.

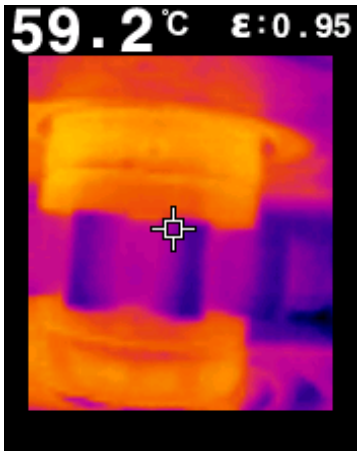

Figure 5.51: Thermographic photo at the end of K3 load stage S-N test.

K4 Load Stage - *Pinion 7*

The test was performed with an H501 pinion in the same conditions of the test made with a C14 pinion at K4 load stage. The first verification was made after 13.8 hours ($N_L = 1.25 \cdot 10^6$ cycles) and no damage was found. After the first verification of the test gearbox, the test was interrupted every 5.5 hours ($0.5 \cdot 10^6$ cycles). When the number of cycles where *Pinion 6* had failed was reached, a black spot (Figure 5.52) appeared on a tooth loaded flank. On the following test interruption, two new similar black spots where found as shown on Figure 5.52. The test continued until a tooth breakage happened between $3.25 \cdot 10^6$ and $3.75 \cdot 10^6$ cycles). At the end of the test, more black spots were found on the unloaded tooth flanks of the tooth immediately before and on the tooth immediately after the broke tooth. On the loaded flanks, the tooth immediately after the broke tooth showed no damage. However, the tooth immediately after it had a superficial crack. The damaged unloaded and loaded flanks are shown on Figures 5.53 and 5.54.

The tooth temperature at the end of the test was 60.1 °C (Figure 5.55). The average power loss after temperature stabilization was 299.21 W.

(a) Black spot found on *pinion 7* after $1.75 \cdot 10^6$ cycles.

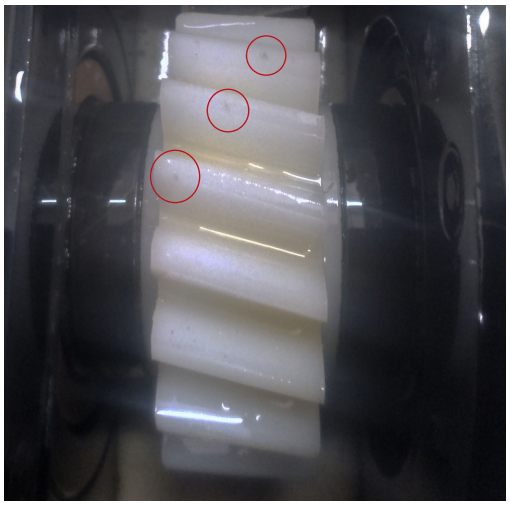

(b) Three black spots found after $2.25 \cdot 10^6$ cycles.

Figure 5.52: Black spots found on unloaded flanks.

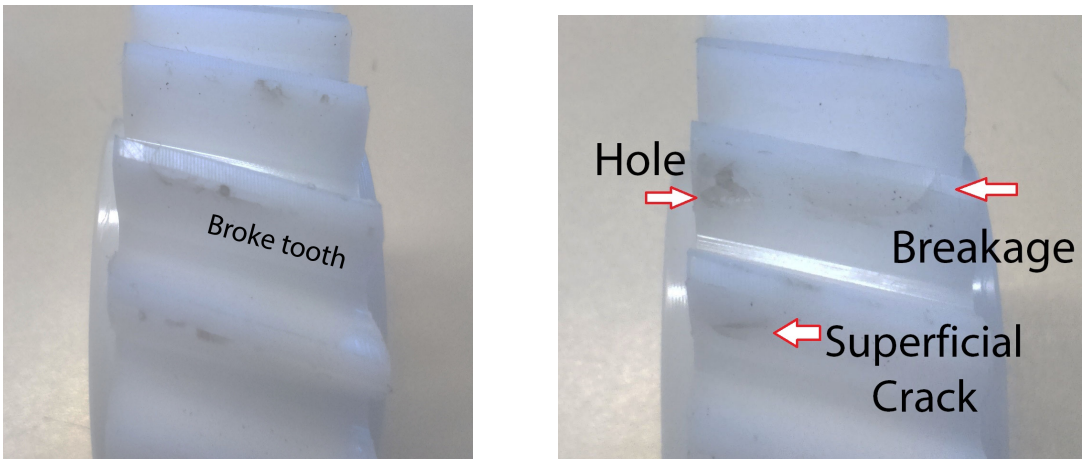

(a) Unloaded flanks. (b) Loaded flanks.

Figure 5.53: Damage at the end of the tests performed with *pinion 7*.

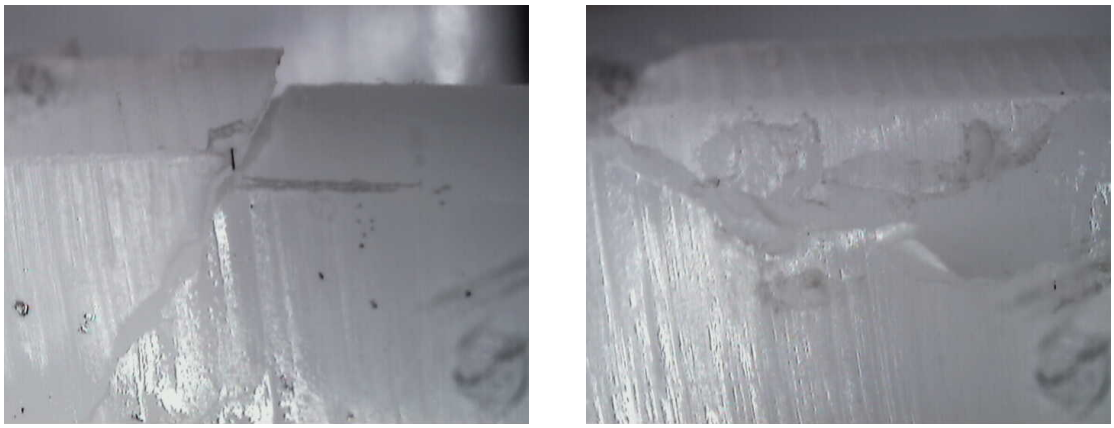

(a) Unloaded flank. (b) Loaded flank.

Figure 5.54: Tooth breakage on *pinion 7*.

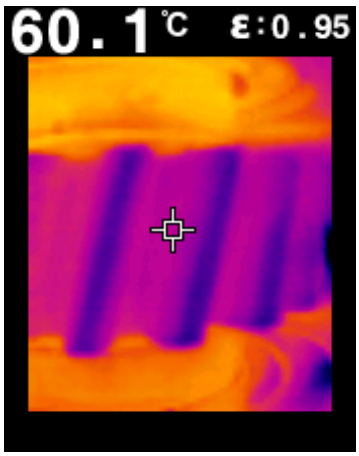

Figure 5.55: Tooth temperature at *pinion 7* after the test.

K4 Load Stage - *Pinion 8*

Repeating the procedure made on the previous S-N tests, *pinion 8* was tested at 1500 rpm and at K4 load stage. The difference when comparing with the previous S-N tests was related to the on the oil temperature that was increased from 50 to 70 °C in order to show the temperature influence on the number of cycles achieved. The first verification was made after 5.5 hours ($N_L = 0.5 \cdot 10^6$ cycles) and two cracks crossing two teeth from one flank to the other were found as shown on Figure 5.56a. Although the damage level being already critical, it was decided to continue the test for more 2.5 hours ($N_L = 0.75 \cdot 10^6$ cycles). At at the end of the test four breakages were found, as shown on Figure 5.56b.

The tooth temperature at the end of the test was 82.5 °C (Figure 5.57). The average power loss after temperature stabilization (before first verification) was 257.52 W.

(a) Cracks found on *pinion 8* after $0.5 \cdot 10^6$ cycles.

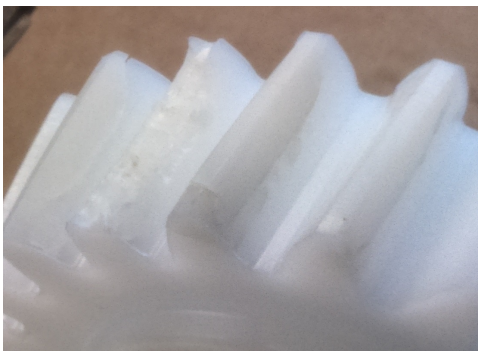

(b) Four tooth breakages after $0.75 \cdot 10^6$ cycles.

Figure 5.56: Damage found on *pinion 8*.

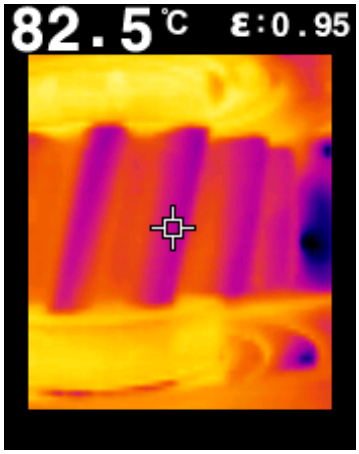

Figure 5.57: Tooth temperature at the end of the test of *pinion 8*.

5.3.3 Specific Film Thickness Calculation

As on preliminary tests, film thickness was calculated at the contact center. The calculation was performed only for C14 gears. Results are shown on Figure 5.58.

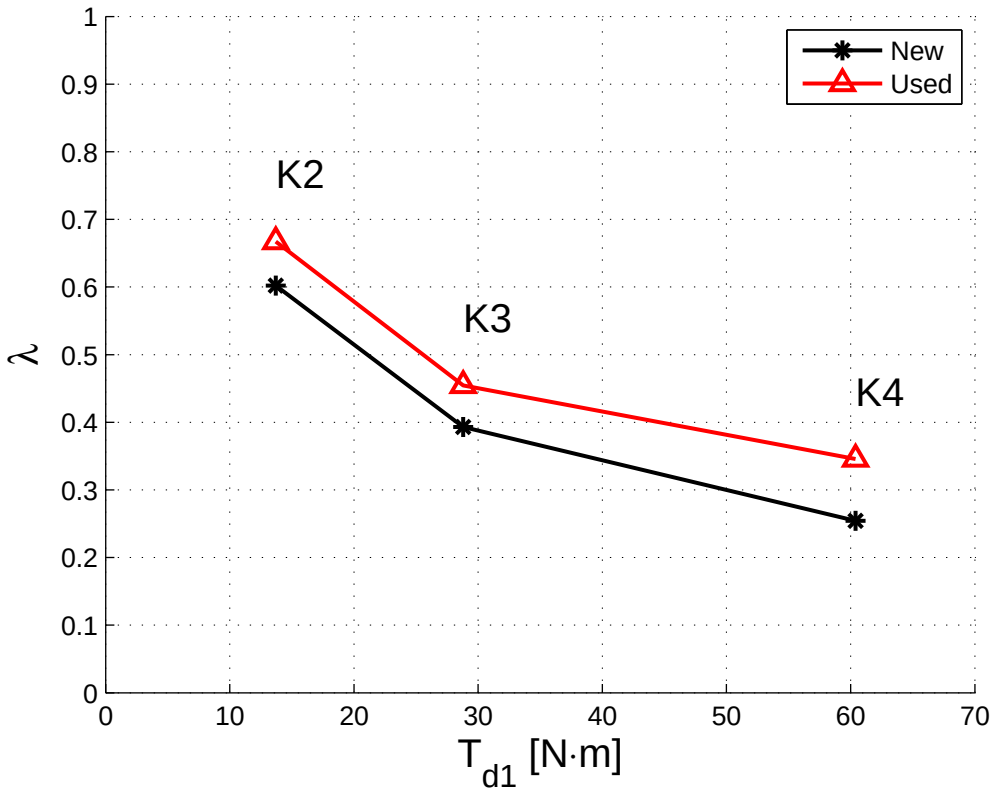

Figure 5.58: Calculated specific film thickness Λ for the S-N tests (n_1=1500 rpm; C14 POM pinions; $\vartheta_o il$=50°C).

5.3.4 Wear

For the S-N tests, as there was no tooth breakage mass loss data is presented for the tests performed with C14 gears (*pinions 4, 5 and 6*). For helical gears, wear evaluation recurring to microscope images took into account the helix angle β. For helical gears, the measured distance $\overline{w}$ on the photo must be multiplied by $cos(\beta)$ so that the measured length has the equivalent direction to the one measured for C14 gears. The distance to be considered for wear analysis $w \cdot cos(\beta)$, is shown on photos between parentheses. The resulting measurements are shown on Figures 5.59 - 5.63. Mass loss results are shown on Figure 5.66.

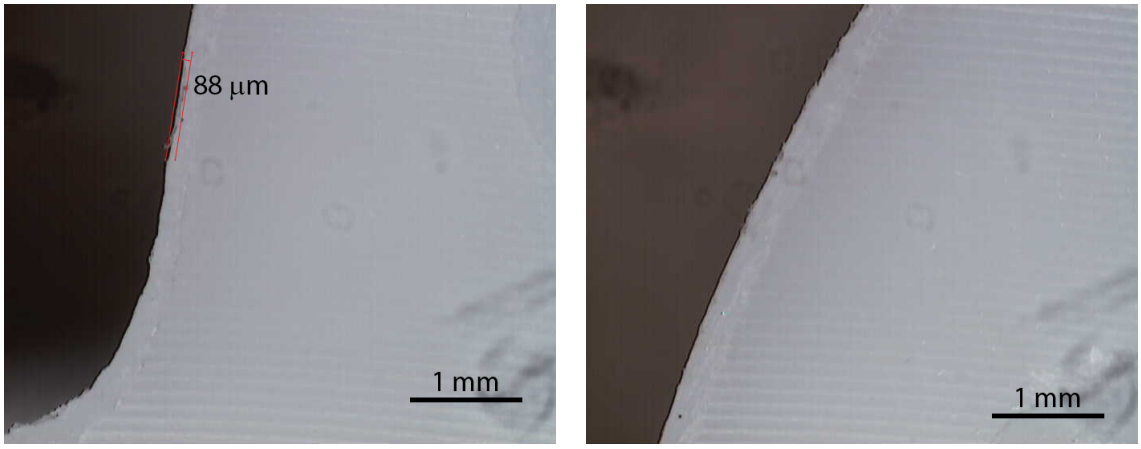

(a) Tooth profile below the pitch circle. (b) Tooth profile above the pitch circle.

Figure 5.59: Tooth shape of *pinion 4* after the test.

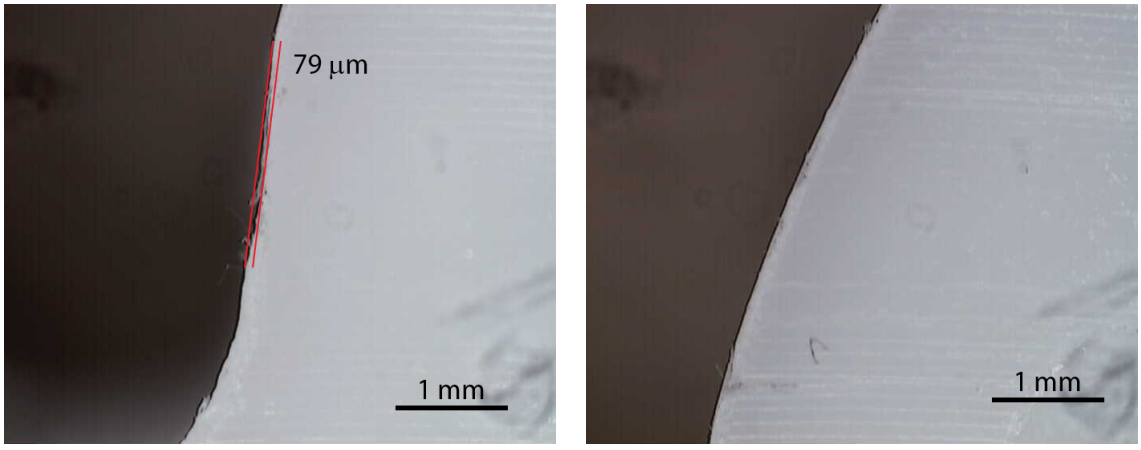

(a) Tooth profile below the pitch circle. (b) Tooth profile above the pitch circle.

Figure 5.60: Tooth shape of *pinion 5* after the test.

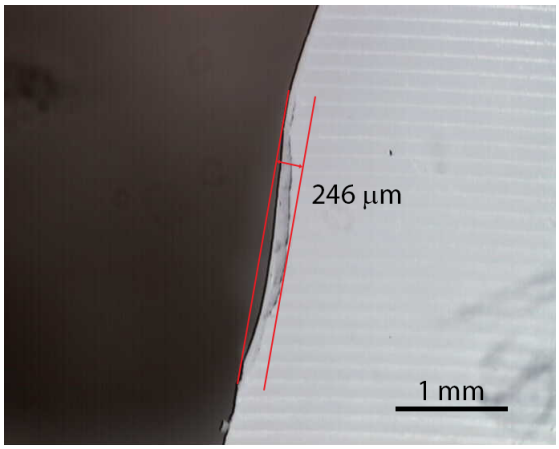

(a) Tooth profile below the pitch circle.

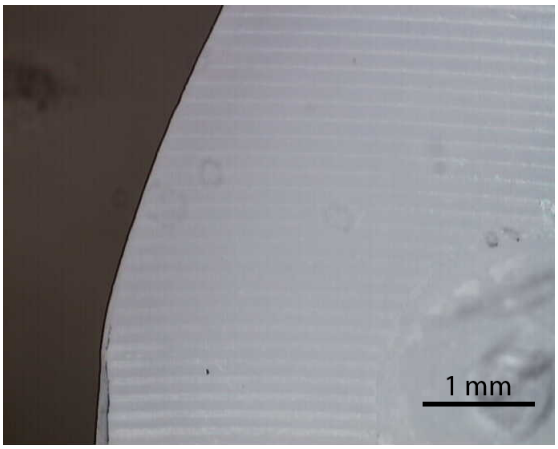

(b) Tooth profile above the pitch circle.

Figure 5.61: Tooth shape of *pinion 6* after the test.

(a) Tooth profile below the pitch circle.

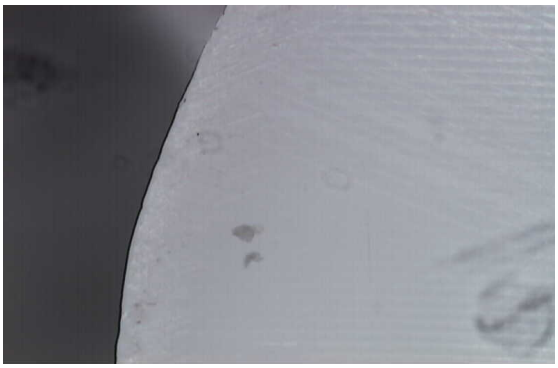

(b) Tooth profile above the pitch circle.

Figure 5.62: Tooth shape of a new H501 pinion.

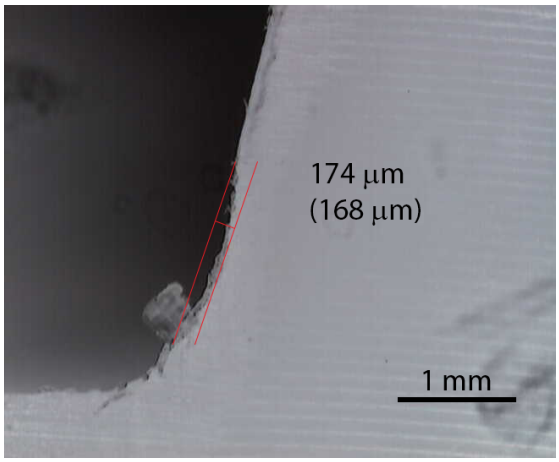

(a) Tooth profile below the pitch circle.

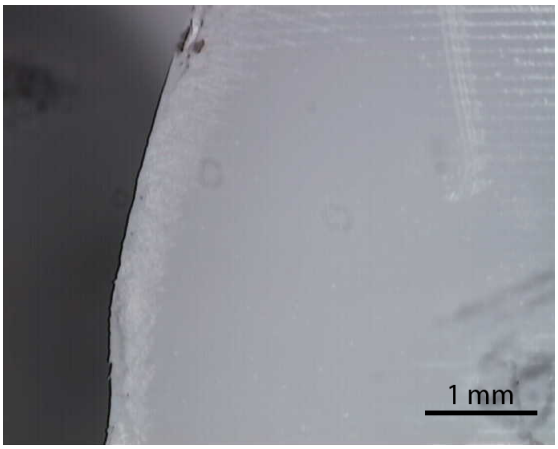

(b) Tooth profile above the pitch circle.

Figure 5.63: Tooth shape of *pinion 7* after run in.

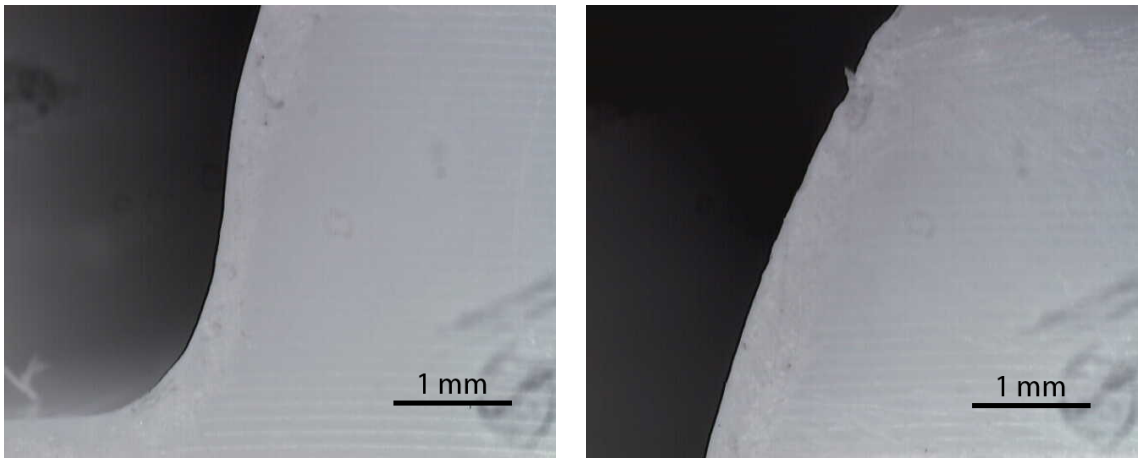

(a) Tooth profile below the pitch circle. (b) Tooth profile above the pitch circle.

Figure 5.64: Tooth shape of *pinion 8* after run in on the tooth immediately after the broken teeth.

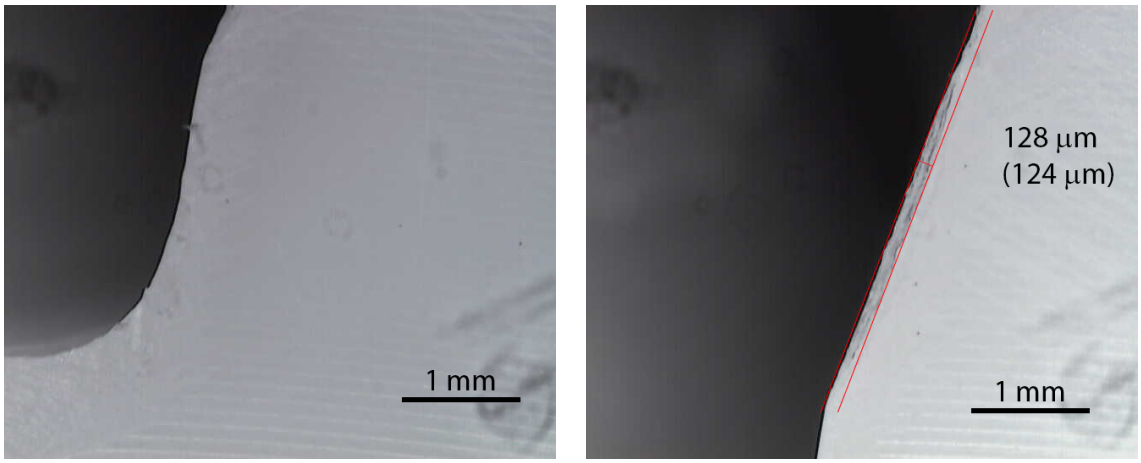

(a) Tooth profile below the pitch circle. (b) Tooth profile above the pitch circle.

Figure 5.65: Tooth shape of *pinion 8* after run in a tooth far from the broken teeth.

5.3.5 Discussion

Tooth temperature

The results obtained for C14 gears, show that tooth temperature decreased while applied load changed from K2 to K3 load stage and increased while the applied load increased from K3 to K4 as shown on Figure 5.67. This results can be explained by the oil temperature.

When oil temperature was pre-set to be at 50 °C, it suffered variations of ± 1.5 °C as show on Figure 5.68. As the maximum variation found on tooth temperature was 3.0 °C, adding to the measuring variations with the thermographic camera that depend on the pointing direction, the tooth temperature variations found might be meaningless.

Analysing results for H501 gear tests with an oil temperature at 70 °C *pinion 8*, tooth temperature increased more than 10 °C relatively to the oil. For the lubrication case

tested, oil bath lubrication, experimental results shown that the tooth temperature increase relatively to the oil temperature was always bigger than 8 °C.

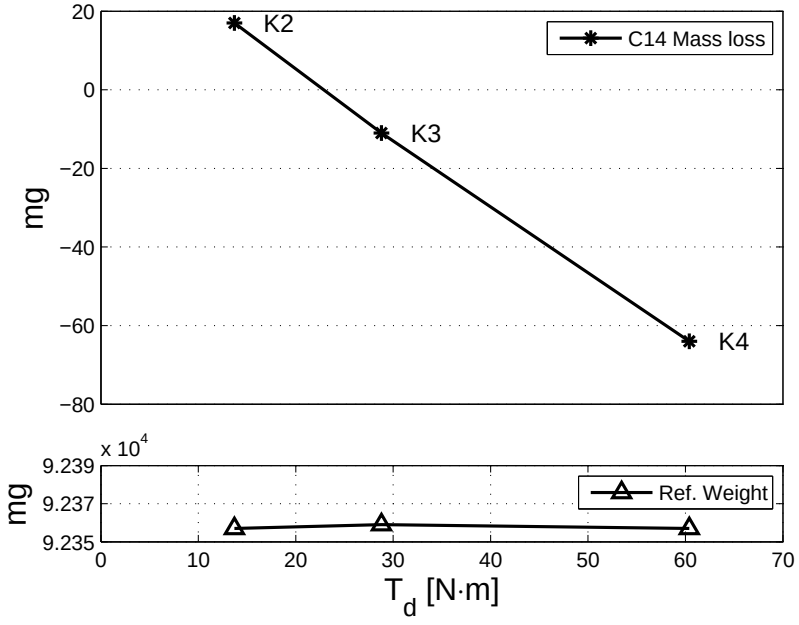

Figure 5.66: Mass loss during S-N tests with C14 gears (n_1=1500 rpm;$\vartheta_o il$ = 50 °C).

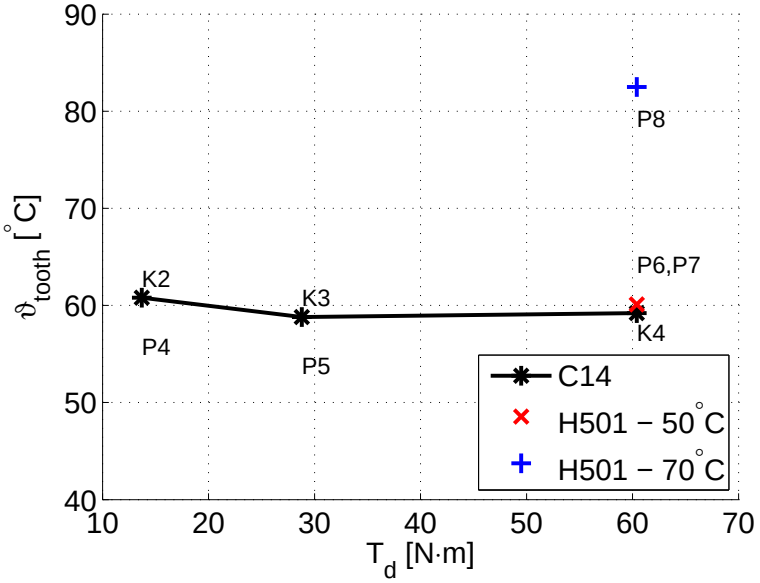

Figure 5.67: Tooth temperature measured at the test (n_1=1500 rpm).

Power Loss

As on preliminary tests, power loss changed slightly with the load increase. The average total power loss is shown on Figure 5.69. It is seen that power increased with low loss gears for K4 load stage. This aspect may be related with the increase of the churning losses. As the face width of 501 gears is higher than the one of gears C14, the oil level for the same oil volume used in tests (1 l) was higher, increasing churning losses. Low

loss gears have lower gear meshing losses, although, for the load stages applied, it seems that this effect was not noticeable. This aspect suggests the necessity of reducing the no load dependent power losses for a better analysis.

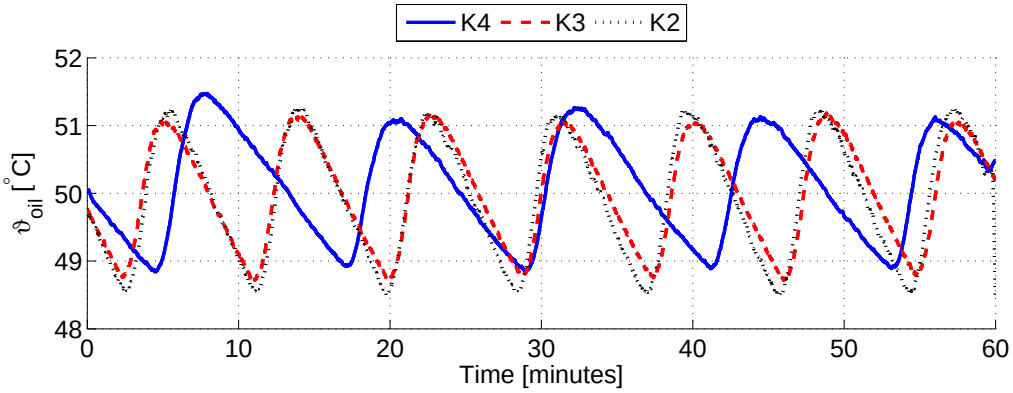

Figure 5.68: Oil temperature at the last hour of C14 S-N tests.

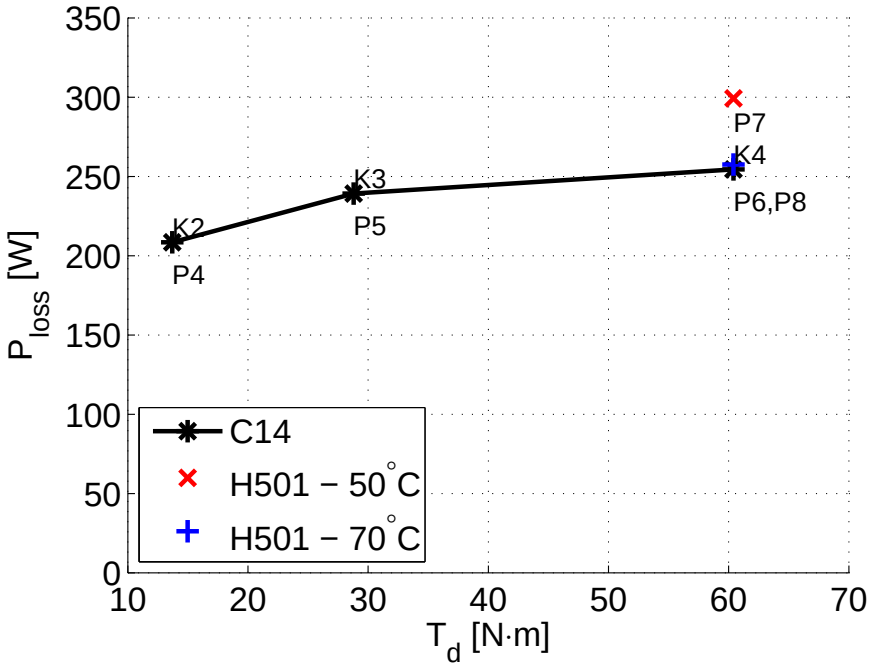

Figure 5.69: Total power loss on of C14 S-N tests.

Film Thickness and Wear

Once again wear was not observed above the pitch circle, differently from the tooth flank zone below the pitch circle, where wear was effective.

Considering data shown on microscope photos on Section 5.3.4, wear depth rate can be calculated as shown on equation (5.1), resulting in a length per hour.

$$\Delta\overline{w} = \frac{\overline{w}}{N_L} \cdot n \cdot 60 \tag{5.1}$$

The results for wear rate are shown on Figure 5.70.

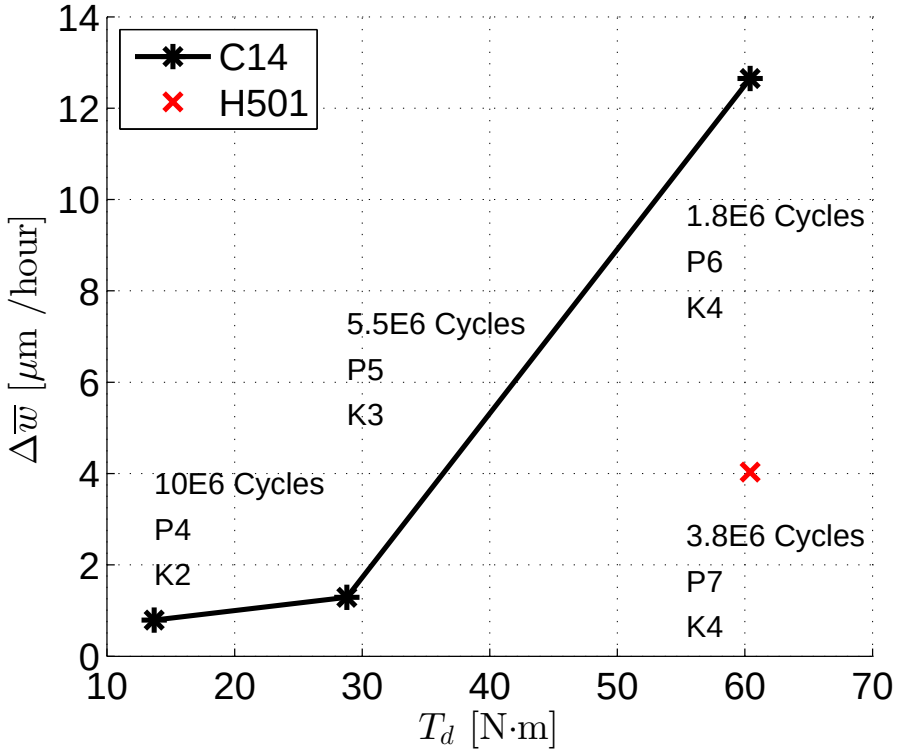

Figure 5.70: Wear rate for S-N tests.

As seen in previous works by other authors (in [9] for example) for the dry case, Figure 5.70 suggests the existence of a critical load that dramatically increases wear rate. This value seems to be between K3 and K4 load stages.

Comparing C14 with H501 tests at 50 °C, wear rate is more than three times lower, which can prove the better wear performance of low loss gears. As the wear rate tends to increase with the number of cycles, since *pinion 7* completed more than two times the number of cycles of *pinion 6*, this achievement has even more relevance.

For H501 tests at 70 °C, as the test finished after $0.75 \cdot 10^6$ cycles, wear was not measurable on the teeth far from the damaged ones. However, for the tooth next to the damaged ones, considerable wear was observed over the pitch circle. This may be related with a possible long time running after tooth breakage.

Taking the calculated specific film thickness values as reference, when λ was below 0.5, it was observed considerable wear; however other factors must be taken into account (tooth deformation is a possible cause and is analysed ahead on this section. When comparing the tooth root of *pinion 4* to *pinion 5*, Figures 5.59 and 5.60 respectively, it is seen that besides the similarity of the values found on wear depth $\overline{w}$, the area affected at the tooth flank is much higher on *pinion 5*, which indicates clearly that wear was more severe on K3 load stage,in spite of the lower number of cycles.

Calculating wear by VDI 2736 calculation process shown on Appendix A for *pinion 6* and *pinion 7* experimental conditions, resulted on wear safety factors of 3.69 and 1.71 respectively, which expresses the opposite of the results experimentally found.

This may be related to an high dependence of this calculation on the number of cycles (check Appendix A, Section A).

Tooth deformation

To evaluate the hypothesis considered on the preliminary tests about the wear increasing due to tooth deformation, specific sliding was calculated recurring to *KISSsoft*® [3], at K2, K3 and K4 load stages, 1500 rpm on the pinion, for a POM/Steel and a Steel/Steel C14 gear pairs. The results obtained for the pinion are shown on Table 5.6.

	POM/Steel		Steel/Steel	
Load Stage	Maximum (tooth tip)	Minimum (base circle)	Maximum (tooth tip)	Minimum (base circle)
K2	0.786	-3.424	0.696	-3.418
K3	0.826	-3.431	0.706	-3.418
K4	0.898	-3.444	0.716	-3.419

Table 5.6: Specific sliding for C14 POM pinion at different load stages [3].

Analysing Table 5.6, it is seen that the specific sliding value (in module) increases with load increasing for both of the cases. Comparing the POM/Steel with the Steel/Steel gear pair, it is clear that this increase is more effective when plastic is present.

In order to compare the tooth deformation, transmission error was analysed. The transmission error evaluates the difference found on the angular displacement of a gear pair relatively to the theoretical displacement. As an example, for a gear ratio (i) of 1.5, if the wheel rotates 1 rad, the pinion should rotate 1.5 rad, which in practice does not happen. The difference between the theoretical and the practical angular displacements represent the transmission error.

By the contact analysis performed by *KISSsoft*®, it was verified that the transmission error calculated is approximately the inverse of the stiffness of the system. This verification was made after applying the torque on the pinion that would result on a unitary force on the tooth ($T_d = r_{b1} \cdot 10^3$). The results that prove this fact are shown on Figure 5.71[6]. Repeating the transmission error calculation for K4 load stage, the obtained result shows the displacement on the base circle due to tooth deformation. Results for POM/Steel and Steel/Steel gear pairs are shown on Figures 5.72.

Comparing the deformation on both cases, the differences found are considerable. At a POM/Steel gear pair the maximum displacement found on the base circle is approximately 360 μm against 13 μm for a Steel/Steel gear pair. Converting the displacement on the base circle to angular displacement, the transmission error is 0.0106 rad for a plastic/steel gear pair, comparing with 0.0004 rad for the steel/steel case.

Normal force along the meshing line was analysed. The resulting data shown on Figure 5.73, reveals a large difference between D and B for the two distinguished cases.

[6]Inverse values for the transmission error result in stiffness values for the case where $T_d = r_{b1} \cdot 10^3$ ($0.16^{-1} = 6.25$; $0.28^{-1} = 3.57$, values taken from Figure 5.71

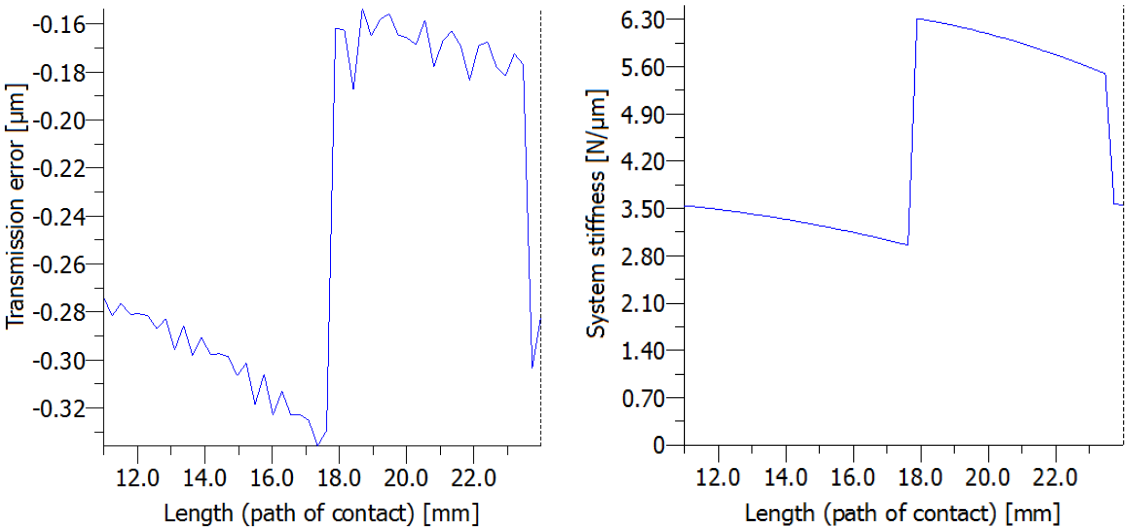

(a) Transmission error. (b) System stiffness.

Figure 5.71: Transmission error and the inverse of the system stiffness for a POM/Steel gear pair with $T_d = 0.034N \cdot m$ (Results obtained with: *KISSsoft*®).

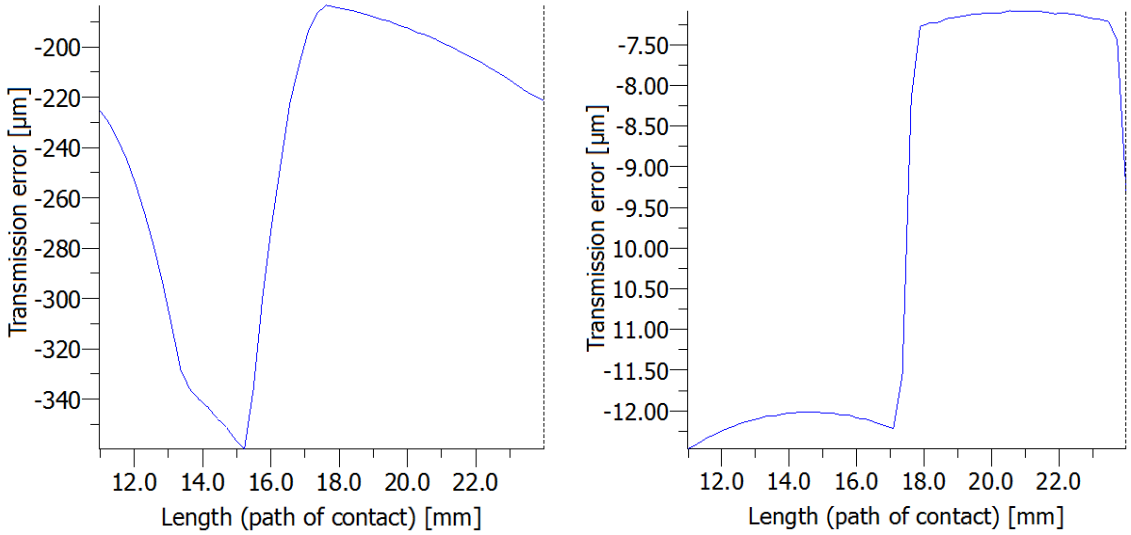

(a) POM/Steel gear pair. (b) Steel/Steel gear pair.

Figure 5.72: Displacement on the base circle at K4 load stage (Results obtained with: *KISSsoft*®).

Comparing both of the graphs, normal force on POM/Steel gear pair is larger from E to C and the load distribution is asymmetric. Another observation made relates to the distance to the meshing line at which the load is stil effective. Results from the contact analysis show that for the POM/Steel gear pair, this length is more than 4 mm.

Specific sliding was analysed for the same cases. The results shown on Figure 5.74 reveal the existence of a secondary sliding on the POM/Steel gear pair, which is not so effective on the Steel/Steel gear pair. Probably, due to the "extension" of the meshing line due to tooth deformation, specific sliding gains some importance during the disengagement. This fact may have increased wear on that zone. This behaviour seems to increase with load. The specific sliding graphs along the tooth profile for K2

and K3 load stages are shown on Figure 5.75. The maximum/minimum values were already shown on Table 5.6.

Increasing the system stiffness or reducing the sliding speed on the base circle can soften this problem.

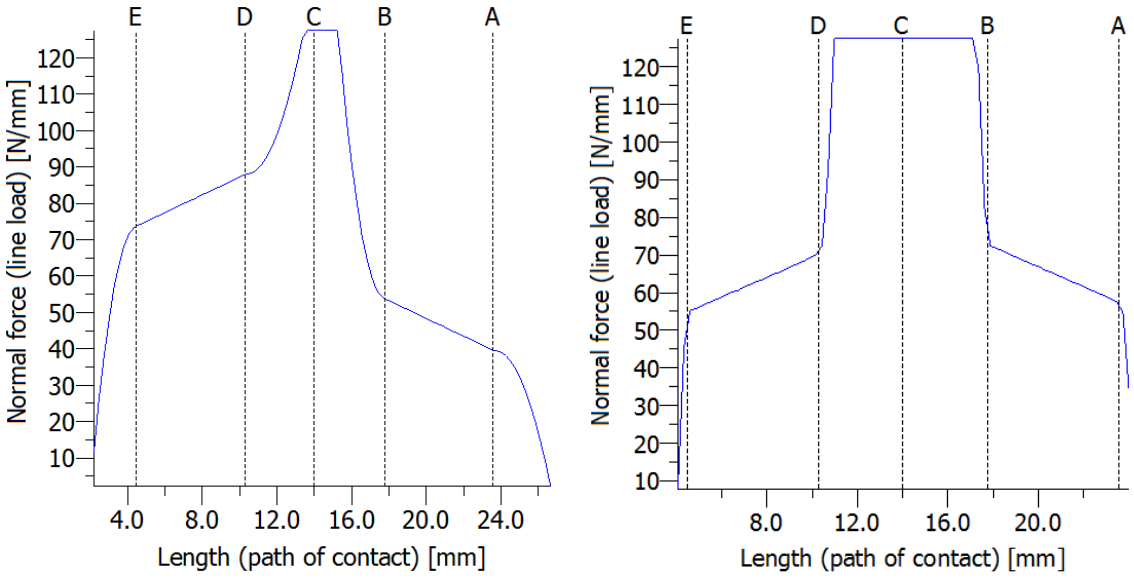

(a) POM/Steel gear pair. (b) Steel/Steel gear pair.

Figure 5.73: Normal force along the meshing line at K4 load stage ($\mu = 0$; Results obtained with: *KISSsoft*®).

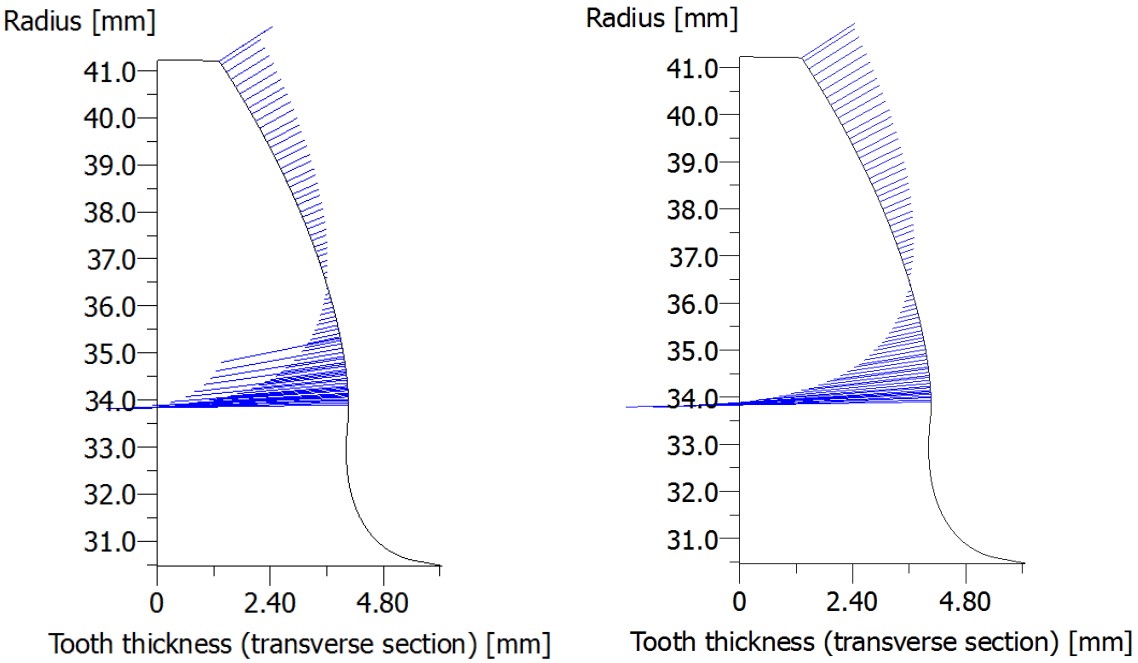

(a) POM/Steel gear pair. (b) Steel/Steel gear pair.

Figure 5.74: Specific sliding at K4 load stage (Results obtained with: *KISSsoft*®).

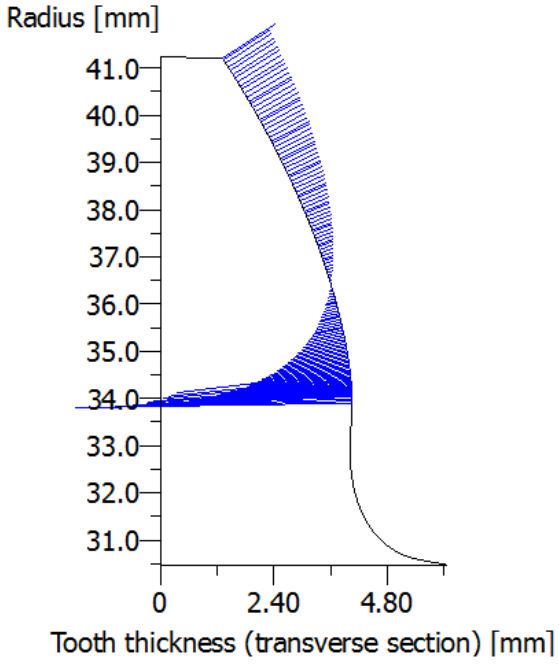

(a) K2 load stage.

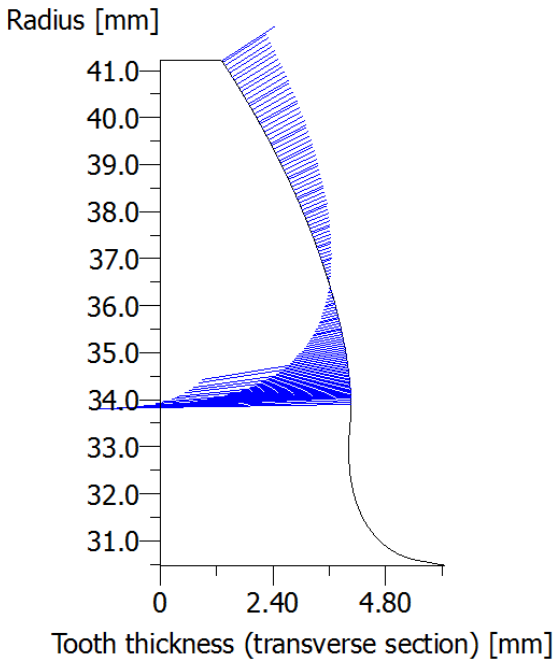

(b) K3 load stage (Results obtained with: *KISSsoft*®).

Figure 5.75: Specific sliding for the pinion of a C14 POM/Steel gear pair (Results obtained with: *KISSsoft*®).

Failure modes and causes

The failure modes found were all quite similar. Differently from what happened on preliminary tests where the failure suggests overheating of the tooth flank, the aspect of the failures of the S-N tests suggests a failure due to the exceeding of the fatigue stress on the tooth flanks.

It seems to start with one or more small cracks that are formed due to very high hertzian stresses. This small crack (Figure 5.76a) grows perpendicularly to the surface creating huge cracks inside the tooth. When two cracks join inside the tooth some material pieces are released from the surface, creating spalls as seen on *pinion 6* and *pinion 7* (Figures 5.76b and 5.77). The tooth breakage happens when a crack crosses the whole tooth from one flank to the other as verified on *pinion 8* .

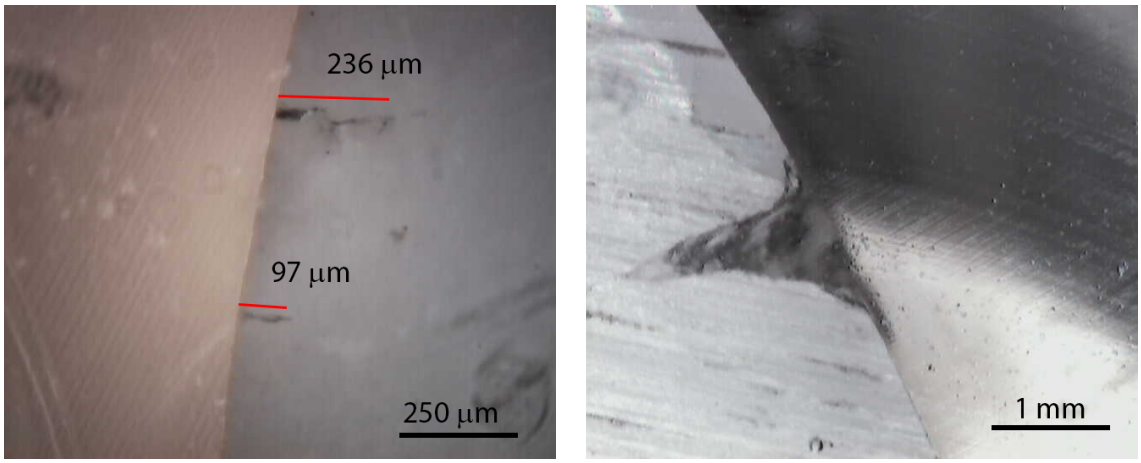

(a) Small cracks perpendicular to the tooth flank (near the base circle).

(b) Spall after the joint of two cracks (above the reference circle).

Figure 5.76: Tooth cut performed on *pinion 6* (C14).

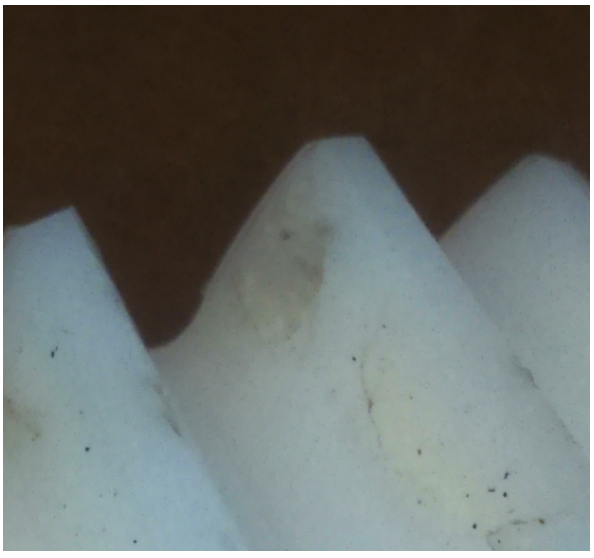

Figure 5.77: Huge spall at the on the tests made with *pinion 7*.

5.3.6 S-N curve

As all the failures were on the tooth flank, the S-N curve obtained relates to the fatigue superficial stresses over the tooth flank, or hertzian stresses (σ_{HlimN}). To calculate the stresses it was used the method present on Appendix A to evaluate tooth flank load capacity. POM S-N curve theoretical approximation was the same one considered for the calculations on Chapter 4 (PA66 data for oil lubricated conditions multiplied by a 0.9 coefficient). The temperature considered for the theoretical curve was the average tooth temperature of the tests performed with oil temperature at 50 °C: 59.73 °C. For the last test made with an oil temperature of 70 °C the temperature considered for the theoretical approximation was the tooth temperature measured: 82.5 °C.

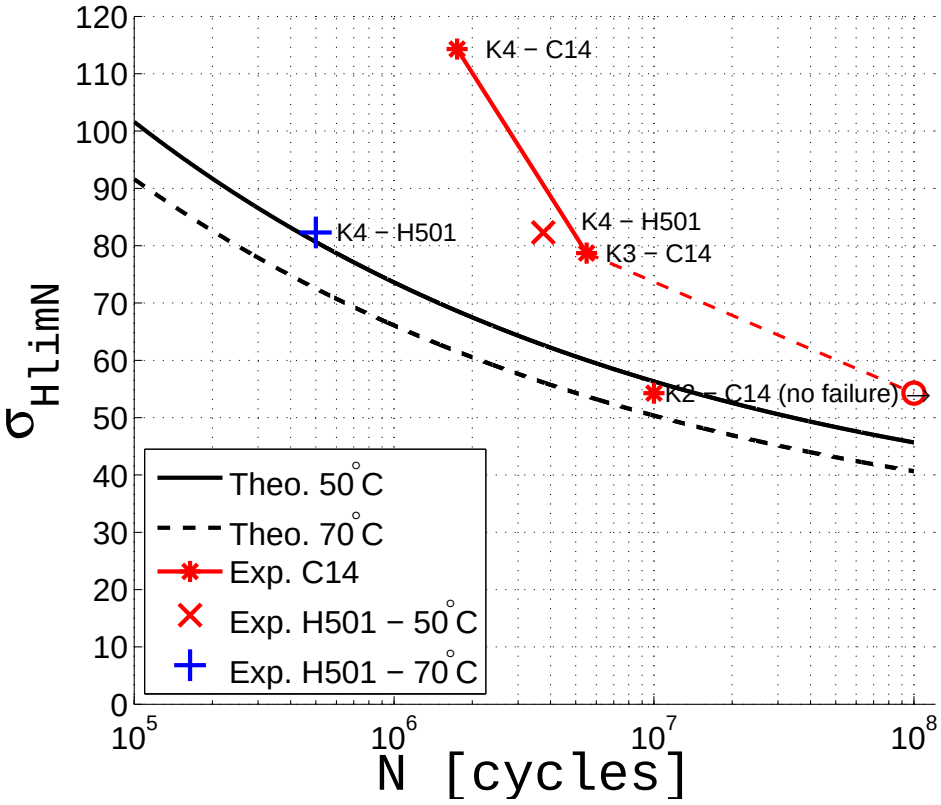

Figure 5.78: S-N curve: experimental and theoretical comparison.

Figure 5.78 shows that the approximation considered for POM is not consistent if we compare it to the experimental values obtained.

It is important to note that K4 load stage applied on a C14 gear, leads to a deformation safety factor S_λ (calculated by VDI 2736) that is lower than one. This effect does not happen if the same load is applied on a H501 low loss pinion.

As with C14 gears there was no failure at K2 load stage, the obtained S-N curve only has two points at K3 and K4 load stages. To show an eventual achievement of a life time equals to 10^8 cycles at K2 load stage, a red circle was plotted in order to simulate this situation.

Chapter 6

Conclusions and Future Work

It is important to note that the results found on this work need statistical approval. Experimental tests performed on this work should be repeated in order to validate the following conclusions.

6.1 Conclusions

6.1.1 Materials and Methods

- During the tests performed, Mineral oil Energol XP - 150 has shown no evidence of chemical incompatibility with POM;
- Mass loss may not be a consistent method to evaluate wear due to high mass variations verified in no-running conditions during the weighing experiment (Section 5.1.4);
- Based on the experimental calibration performed with the thermographic camera used on experimental tests(Section 5.1.1), the value of 0.95 can be considered as a good approximation for POM emissivity;

6.1.2 Preliminary Tests

- K1 load stage leaded to higher free oil temperatures than K2 load stage in tests performed with the same gears;
- At K3 load stage, speeds higher than 4500 rpm leaded to tooth flank breakage;
- Flank breakage seems to have happened after the propagation of a crack on the tooth flank which grows after the formation of a small hole that continuously grows, mainly due to high heating;
- Even after tooth flank breakage, engagement continuity was still guaranteed on the FZG test rig tests;

- At 3000 and 4500 rpm, a plastic pinion meshed with a steel gear might have failed during rotation stoppage;
- By Myers solution for film thickness calculation, a critical value of speed that decreases the specific film thickness was located between 3000 and 4500 rpm (POM pinion meshed with a steel gear - C14);
- Wear was not observed at the region above the reference circle, this may be related with the tooth deformation;
- After tooth flank breakage, wear dramatically increased on the teeth next to the broken ones;

6.1.3 S-N Tests

- During the tests performed, tooth temperature increase relatively to the oil temperature was not highly affected by load increasing on K2, K3 and K4 load stages;
- At K4 load stage with a speed of 1500 rpm on the pinion, total power loss increased when using 501 low loss gear with the same volume of oil, this aspect might be related with the oil level increasing;
- Wear rate dramatically increased at K4 load stage when compared to K2 or K3;
- Failure at 50 °C on K3 and K4 load stages happened after the propagation of small cracks perpendicular to the tooth flank surface;
- Low loss H501 tooth geometry increased 2 times more the number of cycles comparing with C14 for the same running conditions;
- The increase of the oil temperature from 50 °C to 70 °C on the test performed with an H510 pinion, leaded to a reduction of the life time in more than 4 times.

6.1.4 General Conclusions

Based on all the experimental tests made, some conclusions can be taken:

- Loads above K3 (28.8 N·m) might be critical for a C14 and H501 POM/Steel oil lubricated gear pairs;
- Oil temperatures above 68 °C, which resulted in tooth temperatures above 80 °C, might be critical for a C14 and H501 POM/Steel oil lubricated gear pairs;
- Due to the low load stages (K1, K2, K3 and K4) that can be applied to plastic gears, FZG test rig total power loss was not considerably affected by load dependent losses; Based on this fact, rotational speed has a determinant contribute on the oil temperature due to a possible big portion of the churning losses on the total power loss;

6.2 Future Works

6.2.1 Polymer gears

- Evaluate the power loss with injected oil lubrication on FZG test rig (to eliminate churning losses);
- Evaluate the deformation influence on wear;
- Evaluate compatibility with other oils;
- Evaluate mass variations of a polymer gear and oil bath influence on it;
- Repeat the S-N tests for statistical validation;
- Perform S-N tests for the dry case.

6.2.2 Low-Loss Polymer gears

- Testing and comparing 901 low loss gear model with the obtained results;
- Evaluate the influence of low loss geometry on flank wear
- Evaluate the possibility to reach the same or better results replacing the steel wheel by a polyamide one;

Bibliography

[1] C. M. C. G. Fernandes, *Power Loss in Rolling Bearings and Gears Lubricated with Wind Turbine*. PhD thesis, Faculdade de Engenharia da Universidade do Porto, Rua Dr. Roberto Frias - Porto, 2015.

[2] E. Hare, "Ftir analysis." Published Online, SEMLab, Inc (http://www.semlab.com/papers/ftiranalysis.pdf). Web. 2015-06-25.

[3] KISSsoft®, *Release 03/2013B*. KISSsoft AG, Bubikon, Switzerland, 2013.

[4] B.-R. Höhn, K. Michaelis, and A. Wimmer, "Low loss gears," *Gear Technology*, vol. 24, no. 4, pp. 28–35, 2007. cited By 7.

[5] L. Magalhães, R. Martins, C. Locateli, and J. Seabra, "Influence of tooth profile and oil formulation on gear power loss," *Tribology International*, vol. 43, no. 10, pp. 1861 – 1871, 2010. 36th Leeds–Lyon Symposium Special Issue: Multi-facets of Tribology.

[6] L. Magalhaes, R. Martins, J. Seabra, and R. Gonçalves, "Low torque loss gears: Austempered ductile iron versus carburized steel," *Proceedings of the Institution of Mechanical Engineers, Part J: Journal of Engineering Tribology*, vol. 225, no. 12, pp. 1209–1216, 2011. cited By 0.

[7] A. Pogačnik and J. Tavčar, "An accelerated multilevel test and design procedure for polymer gears," *Materials & Design*, vol. 65, no. 0, pp. 961 – 973, 2015.

[8] K. Mao, "A new approach for polymer composite gear design," *Wear*, vol. 262, no. 3–4, pp. 432 – 441, 2007.

[9] K. Mao, W. Li, C. Hooke, and D. Walton, "Friction and wear behaviour of acetal and nylon gears," *Wear*, vol. 267, no. 1–4, pp. 639 – 645, 2009. 17th International Conference on Wear of Materials.

[10] K. Terashima, N. Tukamoto, and N. Nishida, "Development of plastic gears for power transmission. (design on load-carrying capacity).," *Bulletin of the JSME*, vol. 29, no. 250, pp. 1326–1329, 1986. cited By 6.

[11] N. Tsukamoto, "argument on plastic gears for power transmission," *JSME International Journal, Series C: Dynamics, Control, Robotics, Design and Manufacturing*, vol. 38, no. 1, pp. 1–8, 1995. cited By 12.

[12] VDI 2736: Blatt 1. Thermoplastische Zahnräder. Werkstoffe, Werkstoffauswahl, Herstellverfahren, Herstellgenauigkeit, Gestalten. VDI Richtlinien. Duesseldorf: VDI-Verlag GmbH, 2014.

[13] VDI 2736: Blatt 2. Thermoplastische Zahnräder. Stirnradgetriebe. Tragfähigkeitsberechnung. VDI Richtlinien. Duesseldorf: VDI-Verlag GmbH, 2014.

[14] N. Tsukamoto, "Investigation about the strength of plastic gear (6th report; endurance limit and damage state of nylon gear for power transmission).," *Bulletin of the JSME*, vol. 28, no. 241, pp. 1528–1534, 1985. cited By 3.

[15] CES EduPack *version 14.3.5 (2014)* Granta Design, Cambridge, United Kingdom, 2014.

[16] N. TSUKAMOTO and K. TERASHIMA, "Development of plastic gears for power transmission : Various methods of lengthening the life of plastic gears and their effect," *Bulletin of JSME*, vol. 29, no. 247, pp. 249–255, 1986.

[17] J. A. de Sousa Ferreira Brandão, *Gear tooth flank damage prediction using high-cycle fatigue and wear models.* PhD thesis, Faculdade de Engenharia da Universidade do Porto, Rua Dr. Roberto Frias - Porto, 2015.

[18] GE Plastics. A Guide to Plastic Gearing. One Plastics Avenue Pittsfield, MA 01201 USA, 2009.

[19] A. A. Carey and A. J. Hayzen, "The dielectric constant and oil analysis." Published Online, Machinery Lubrication (http://www.machinerylubrication.com/Read/226/dielectric-constant-oil-analysis). Web. 2015-04-21.

[20] R. Gianattasio, "Lubrication tips for plastic gears and more." Published Online, Motion System Design (http://machinedesign.com/mechanical-drives/lubrication-tips-plastic-gears-and-more). Web. 2015-04-21.

[21] V. Shkol'nikov, L. Bronshtein, Y. Shekhter, and O. Drozdova, "Electrical and viscosity properties of mineral oil components," *Chemistry and Technology of Fuels and Oils*, vol. 13, no. 7, pp. 479–481, 1977.

[22] N. TSUKAMOTO, "A study on oil-bath lubrication for plastic gears," *Transactions of the Japan Society of Mechanical Engineers Series C*, vol. 55, no. 514, pp. 1432–1437, 1989.

[23] K. D. Dearn, T. J. Hoskins, L. Andrei, and D. Walton, "Lubrication regimes in high-performance polymer spur gears," *Advances in Tribology*, vol. 2013, 2013. cited By 3.

[24] J. KL, "Regimes of elastohydrodynamic lubrication," *J Mech Eng Sci*, vol. 12, no. 1, pp. 9–16, 1970. cited By 77.

[25] T. Myers, R. Hall, M. Savage, and P. Gaskell, "The transition region of elastohydrodynamic lubrication.," *Proc. R. Soc. Lond., Ser. A*, vol. 432, no. 1886, pp. 467–479, 1991.

[26] VDI 2736: Blatt 4. Thermoplastische Zahnräder. Ermittlung von Tragfähigkeitskennwerten an Zahnrädern. VDI Richtlinien. Duesseldorf: VDI-Verlag GmbH, 2014.

[27] I. Moriwaki, A. Ueda, M. Nakamura, K. Yoneda, and D. Iba, "New japanese standard {JIS} b 1759 on load capacity of plastic gears," in *International Gear Conference 2014: 26th–28th August 2014, Lyon* (P. Velex, ed.), pp. 1172 – 1178, Oxford: Chandos Publishing, 2014.

[28] S. Beermann, "Estimation of lifetime for plastic gears," KISSsoft AG, October,2007.

[29] H. Winter and K. Michaelis, "Fzg gear test rig. description and test possibilities.," *IN: SECOND INT. SYMP. ON THE PERFORMANCE OF AUTOMOTIVE FUELS AND LUBRICANTS, (WOLFSBURG, FED. REP. GERMANY: JUN. 5-7, 1985)*, vol. 4 , Coord. European Council Dev. Perform. Tests Lubr. & Engine Fuels, 1985, Paper TL2, p.27-42., 1985. cited By 0.

[30] H. Winter and K. Michaelis, "Fzg gear test rig. description and test possibilities.," *IN: SECOND INT. SYMP. ON THE PERFORMANCE OF AUTOMOTIVE FUELS AND LUBRICANTS, (WOLFSBURG, FED. REP. GERMANY: JUN. 5-7, 1985)*, vol. 4 , Coord. European Council Dev. Perform. Tests Lubr. & Engine Fuels, 1985, Paper TL2, p.27-42., 1985. cited By 0.

[31] C. M. Fernandes, P. M. Marques, R. C. Martins, and J. H. Seabra, "Gearbox power loss. part ii: Friction losses in gears," *Tribology International*, no. 0, pp. –, 2014.

[32] K. Michaelis and B.-R. Höhn, "Influence of lubricants on power loss of cylindrical gears©," *Tribology Transactions*, vol. 37, no. 1, pp. 161–167, 1994.

[33] S. M. O. Tavares and P. M. S. T. de Castro, "Cálculo da capacidade de carga de engrenagens cilíndricas." Faculdade de Engenharia da Universidade do Porto, 2013.

Appendix A

VDI 2736 - Calculation procedure

The calculation procedure followed VDI 2736 guideline proceedings. It started with the calculation of the geometric parameters followed by tooth root and flank temperatures. The operating temperatures allow to obtain the material properties, which combined with the intended number of cycles leads to the safety factors in terms of tooth root, tooth flank, deformation and wear. Figure A.1

Tooth temperatures calculation

In this step, two different temperatures were calculated, tooth root temperature $\vartheta_{Fu\beta}$, and tooth flank temperature ϑ_{Fla}.

Tooth root temperature $\vartheta_{Fu\beta}$ was calculated according with Equation **??**

$$\vartheta_{Fu\beta} = \vartheta_0 + P \cdot \mu \cdot H_V \cdot \left(\frac{k_{\vartheta,Fu\beta}}{b \cdot z \cdot (v_t \cdot m_n)^{0,75}} \right) \cdot ED^{0,64} \tag{A.1}$$

The parameters for tooth root temperature are:

- ϑ_0 is the ambient temperature in °C. For the following calculations it was considered 20 °C;
- P is the nominal output in watts and depends on torque and rotational speed applied. The reference gear used to calculate the power was the pinion, it can be obtained multiplying the torque in $N \cdot m$ and the rotational speed in rad/s on the pinion;
- μ is the coefficient of friction and it is suggested in [13] as presented on Table A.1. It was considered 0,055 which is a value between the ones for circulating oil and oil mist. This value is a trying approach to the oil bath case;
- H_V is the degree of tooth loss and can be calculated with the Equation (A.2). It is dimensionless;
- $k_{\vartheta,Fu\beta}$ is the heat transfer coefficient of the plastic gear for the tooth flank temperature calculation.It may be found on Table A.3. As our case is not circulation

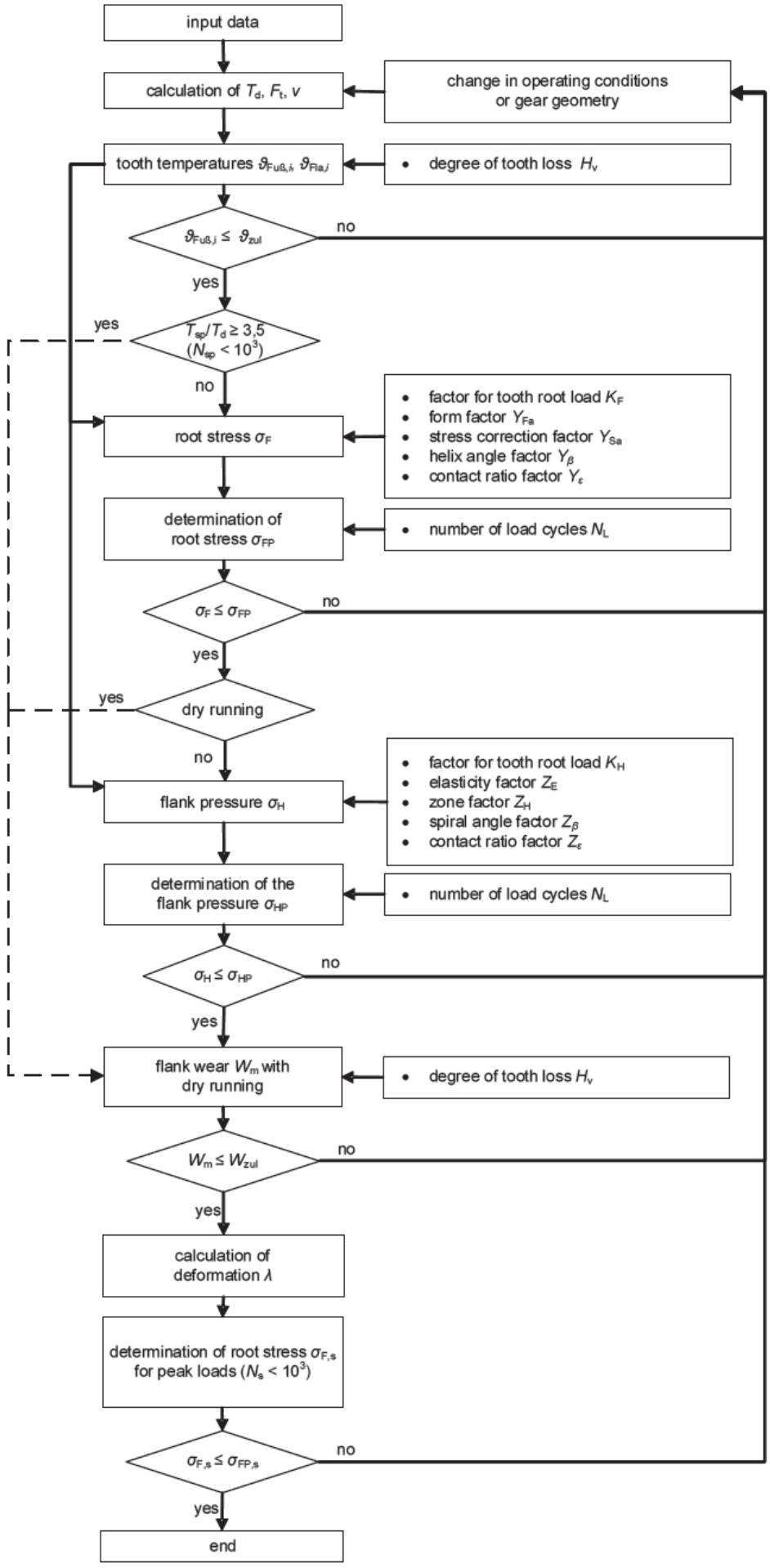

Figure A.1: Flow chart for cylindrical plastic gears calculation [13].

Table A.1: Coefficient of friction μ [13].

Lubrication	Pairing	μ
Circulating oil	all	0,04
Oil mist	all	0,07
Grease	all	0,09
Dry	plastic/steel	0,20
	PA/PA)	0,40
	POM/POM	0,28
	POM/PA	0,18
	PA/PBT	0,35
	POM/PBT	0,18

oil (it is oil bath), the value for dry/Grease/oil mist was used, which is more critical and general than the use of the value 0.

- b, z, and m_n are geometric parameters of the gear (face width, teeth number, and normal module respectively);
- v_t is the tangential velocity. It was taken the pinion as reference gear for this calculation, so it can be calculated according to Equation (A.3).
- $R_{lambda,G}$ is the heat transfer resistance of the mechanism and may be found on Table A.4;
- A_G is the area of the heat dissipating surface in m^2. For our calculations it was considered 1,4 m^2 as reference value as exemplified in [32];
- ED is the relative tooth-engagement time in minutes within a period of ten minutes divided by ten minutes. For continuous operation it has the value of 1, which was the value used.

H_V can be calculated as presented in Equation (A.2).

$$H_V = \frac{\pi \cdot (u+1)}{z_2 \cdot \cos(\beta_b)} \cdot \left(1 - \varepsilon_1 - \varepsilon_2 + \varepsilon_1^2 + \varepsilon_2^2\right) \tag{A.2}$$

The parameters for Equation (A.2) are:

- z_2, teeth number for the gear;
- u, the gear ratio z_2/z_1;
- ε_1 and ε_2, the partial radial contact ratios for gear and pinion;
- β_b, the helix angle at the base circle;

Table A.2: Values calculated of H_V, for C14, 501 and 951 gears.

Gear type	H_V
C14	0,1951
501	0,16392
951	0,1048

Table A.3: Heat transfer coefficients $k_{\vartheta,Fu\beta}$ and $k_{\vartheta,Fla}$ of the plastic gear in $K \cdot (m/s)^{0,75} \cdot mm^{1,75}/W$ [13].

Lubrication	Pairing	$k_{\vartheta,Fu\beta}$	$k_{\vartheta,Fla}$
Circulating oil	all	0	0
Dry/Grease/oil mist	plastic/plastic	$2,1 \cdot 10^3$	$9,0 \cdot 10^3$
	plastic/steel	$0,9 \cdot 10^3$	$6,3 \cdot 10^3$

$$v_t = d_1 \cdot \pi \cdot n/(60 \cdot 10^3) \tag{A.3}$$

By a similar way, tooth flank temperature may be calculated. The Equation (A.4) was used to obtain tooth flank temperatures.

$$\vartheta_{Fla} = \vartheta_0 + P \cdot \mu \cdot H_V \cdot \left(\frac{k_{\vartheta,Fla}}{b \cdot z \cdot (v_t \cdot m_n)^{0,75}}\right) \cdot ED^{0,64} \tag{A.4}$$

To make possible the running of the system, ϑ_{Fla} must be lower than ϑ_{zul}, which is the permissible temperature for thermoplastic gears. As we are going to test POM in continuous operation, the value ϑ_{zul} of 90 °C was considered as suggested in [12].

Tooth root load-carrying capacity

On this step, root stress σ_F is calculated and evaluated in safety factor form.

Root stress is given by Equation (A.5).

$$\sigma_F = K_F \cdot Y_{Fa} \cdot Y_{Sa} \cdot Y_\varepsilon \cdot Y_\beta \cdot \frac{F_t}{b \cdot m_n} \tag{A.5}$$

Table A.4: Heat transfer resistance of the mechanism housing in $K \cdot m^2/W$ [13].

Mechanism	$R_{lambda,G}$
Open with unimpeded entry of air	0
Partially open housing	0,015 ... 0,045
Closed housing	0,060

$$K_F = K_A \cdot K_v \cdot K_{F\beta} \cdot K_{F\alpha} \tag{A.6}$$

The parameters for Equation (A.5) are:

- K_F, the factor for tooth root load. K_F results from the multiplication of four other factors (see Equation (B.7)):
  - K_A, the application factor;
  - K_v, the dynamic factor;
  - $K_{F\beta}$ the width factor;
  - $K_{F\alpha}$ the face factor;
- Y_{Fa}, the form factor;
- Y_{Sa}, the stress correction factor;
- Y_ε, the contact ratio factor;
- Y_β, the helix angle factor;
- F_t, tangential force applied;
- b and m_n, respectively face width and normal module.

K_A, the application factor

The application factor can be found on DIN 3990 and depends on service (running) conditions. It takes into account some external dynamic forces that may make the situation more critical. A suggestion for K_A is present on Table A.5, with some examples of possible applications.

K_v, $K_{F\beta}$, and $K_{F\alpha}$ the dynamic, width and face factors

Calculations made shown that, in our case this factors can be assumed equal to one.

Y_{Fa}, the form factor

Form factor takes into consideration the influence of tooth shape on the nominal bending stress for loads applied on the tooth tip. Values for Y_{Fa} are suggested on Figure A.2 for reference profiles as per DIN 867 ($h_{fP} = 1,25 \cdot m_n; h_{aP} = 1,0 \cdot m_n; \rho_{fP} = 0,25 \cdot m_n$) from DIN 3990. The equivalent number of teeth z_n can be assumed equals to z for spur gears, while for helical gears, z_n should be calculated using Equation (A.7).

$$z_n = \frac{z}{\cos(\beta_b)^2 \cdot \cos(\beta)} \tag{A.7}$$

Table A.5: Application factor possibilities [33].

	Driven machine			
Driving machine	Uniform belt transmissions uniformly loaded, light elevators, machine-tools positioning, ventilators...	Minor shocks: belt transmissions non uniformly loaded, mixers for non homogeneous materials...	Moderate shocks: runer extrusion, wood machine-tools, gears for elevators, simple piston pump...	High shocks: Gears for excavators, heavy machines for steel mill applications, cold rolling mills...
Uniform: turbines, electric motors with low starting torque	1	1,25	1,50	1,75
Minor shocks: turbines, electric motors with high starting torque	1,10	1,35	1,60	1,85
Moderate shocks: combustion motor with multiple cylinders	1,25	1,50	1,75	2,00
High shocks: combustion motor with one cylinder	1,50	1,75	2	>= 2,25

Y_{Sa}, the stress correction factor

The stress correction factor takes into account the notch effect for load application at the tooth tip. By the same way as for Y_{Fa}, values for Y_{Sa} may are suggested on Figure A.3 for reference profile as per DIN 867.

Y_ε and Y_β, the contact ratio and helix angle factors

Contact ratio factor takes into account the modified lever arm and the modified notch effect. It depends on the radial contact ratio and is calculated according to Equation (A.8)

$$Y_\varepsilon = 0,25 + \frac{0,75}{\varepsilon_\alpha} \tag{A.8}$$

Helix angle factor takes into account the favourable meshing conditions found in helical teeth. It can be calculated with Equation (A.9).

$$Y_\beta = 1 - \frac{\varepsilon_\beta \cdot \beta}{120°} \tag{A.9}$$

If $\varepsilon_\beta > 1$, set $\varepsilon_\beta = 1$
If $\beta > 30°$, set $\beta = 30\ °$

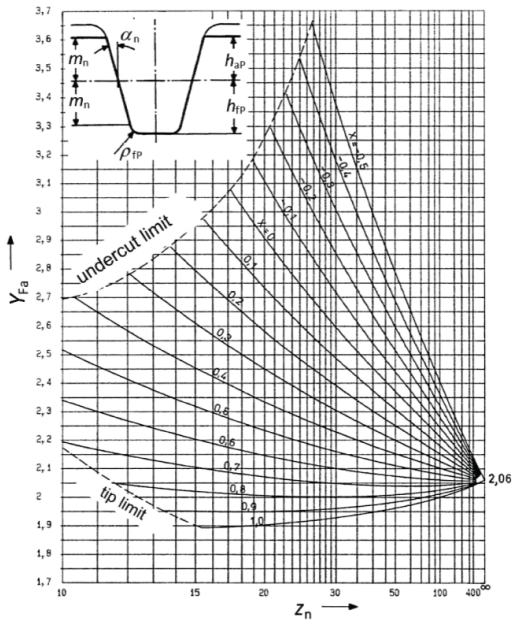

Figure A.2: Y_{Fa} values for reference profiles as per DIN 867 [13].

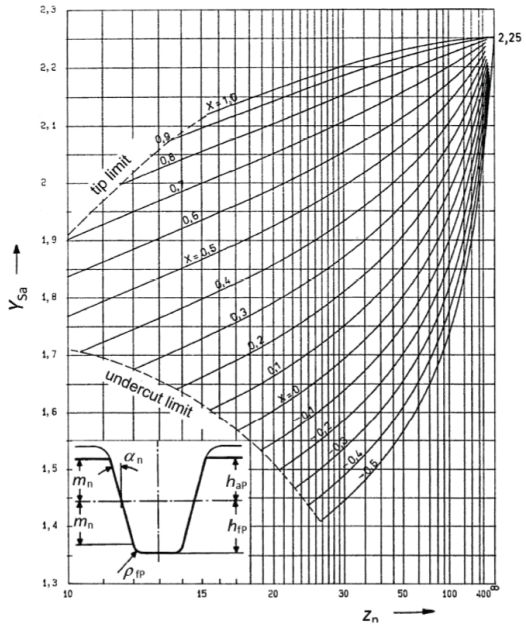

Figure A.3: Y_{Sa} values for reference profiles as per DIN 867 [13].

σ_F and S_F tooth root stress and tooth root safety factor

Once that we have a value for σ_F calculated with Equation (A.5), the tooth root safety factor may be obtained dividing the obtained stress value by σ_{FlimN}, the permissible fatigue stress under pulsating solicitations (check Equation (A.11)). σ_{FlimN} decreases with the increasing of the operating temperature and with the number of load cycles applied until a specific moment as shown in Figure A.6.

For faster and more precise calculation, the graphic consultation was avoided, and it was used Equation (A.10) given in [13].

$$\sigma_{FlimN} = 30 - 0,22 \cdot \vartheta_{Fu\beta} + (4600 - 900\vartheta_{Fu\beta}^{0,3}) \cdot N_L^{-1/3} \tag{A.10}$$

$$N_L \in [10^5; 10^8]$$

$$S_F = \frac{\sigma_F}{\sigma_{FlimN}} \tag{A.11}$$

In [13], it is suggested a minimum safety factor $S_F = 2$ for continuous operation where number of cycles $N_L = 10^8$ is mandatory. For intermittent operation it is suggested a minimum safety factor of $S_F = 1,6$.

Tooth root load-carrying capacity

On this step, flank pressure σ_H is calculated and evaluated in a safety factor form.

Flank pressure $sigma_H$ is given by Equation (A.12):

$$\sigma_H = Z_E \cdot Z_H \cdot Z_\varepsilon \cdot Z_\beta \cdot \sqrt{\frac{F_t \cdot K_H}{b_w \cdot d_1} \cdot \frac{u+1}{u}} \tag{A.12}$$

The parameters for Equation (A.12) are:

- Z_ε, elasticity factor that takes into account elastic modulus and Poisson's ration of the materials present on gear pair. It is calculated with Equation (A.13);

$$Z_E = \sqrt{\frac{1}{\pi \cdot \left(\frac{1-\nu_1^2}{E_1} + \frac{1-\nu_2^2}{E_2}\right)}} \tag{A.13}$$

  The values considered for steel were $E = 206GPa$ and $\nu = 0,3$. For POM, E can be found on Figure A.8 and a value of $\nu = 0,35$ was considered as suggested in [13].

- Z_H, the zone factor, takes into account the flank curvature radius at the contact point since it converts some peripheral force at the reference cylinder to normal force on the pitch cylinder. Figure A.4 is suggested on [13] (according to DIN 3990) for determining Z_H values. It is valid for internally or externally toothed cylindrical gears with a pressure angle of 20 °;

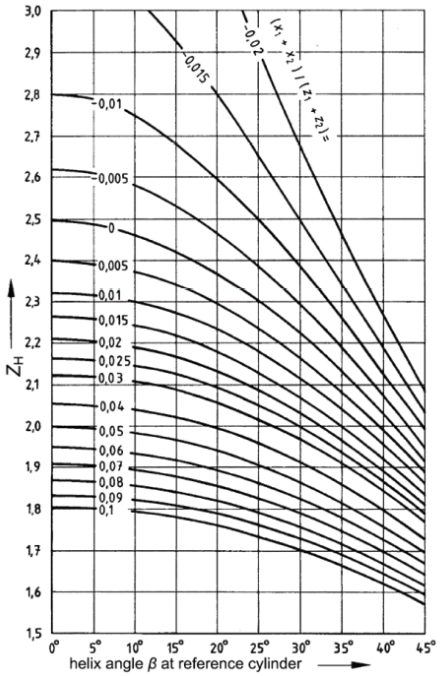

Figure A.4: Suggested values of Z_H for $\alpha_n = 20°$ (DIN 3990) [13].

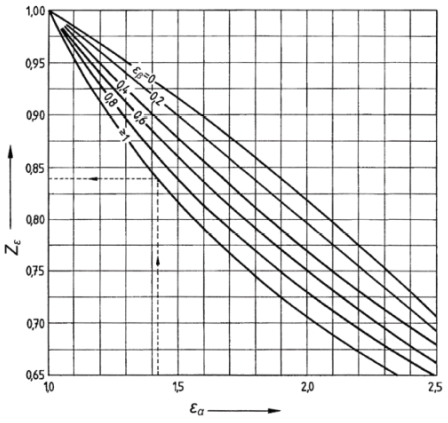

Figure A.5: Suggested values of Z_ε for $\alpha_n = 20°$ (DIN 3990) [13].

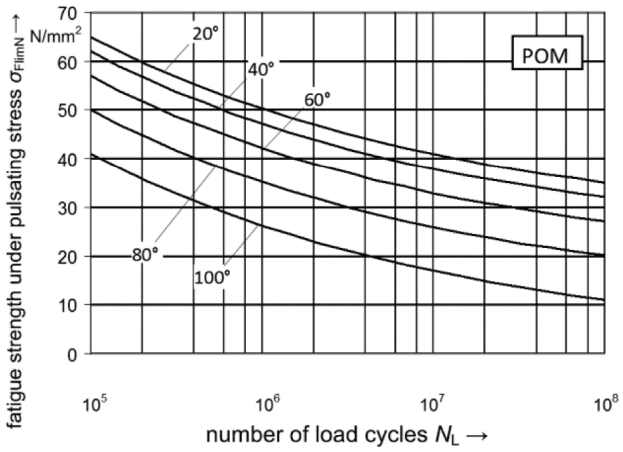

Figure A.6: Suggested values of σ_{FlimN} for POM for different tooth root operating temperatures and number of cycles [13].

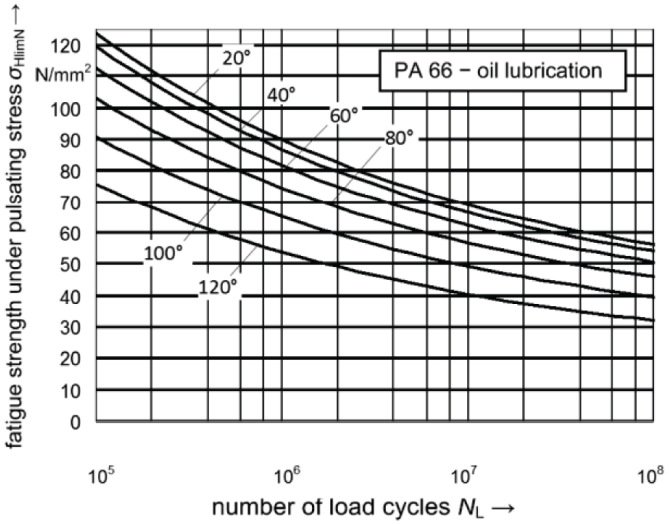

Figure A.7: Suggested values of σ_{HlimN} for PA 66 for different tooth flank operating temperatures and number of cycles, under oil lubrication [13].

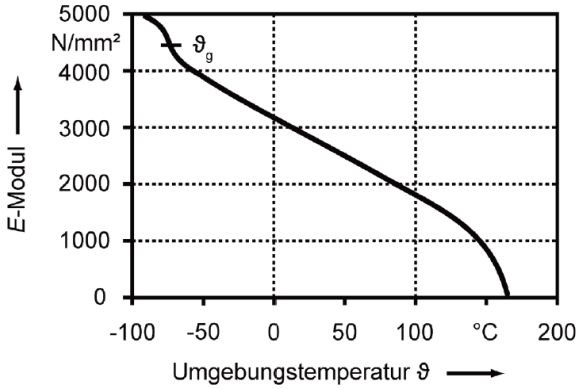

Figure A.8: Elasticity modulus for POM in function of tooth root temperature [13].

- Z_ε, the contact ratio factor, takes into account the influence of the effective length of the contact lines. It depends on the radial contact ratio $varepsilon_\alpha$, overlap contact ratio ε_β and the helix angle β. For a pressure angle $\alpha_n = 20°$, Figure A.5 is a possible way to assume a value for the contact ratio factor. For a rigorous calculation, once again, numerical values where obtained through Equation (A.14);

$$Z_\varepsilon = \begin{cases} \sqrt{\frac{4-\varepsilon_\alpha}{3} \cdot (1-\varepsilon_\beta) + \frac{\varepsilon_\beta}{\varepsilon_\alpha}}, & ; \quad \varepsilon_\beta < 1 \\ \sqrt{\frac{1}{\varepsilon_\alpha}}, & ; \quad \varepsilon_\beta \geq 1 \end{cases} \tag{A.14}$$

- Z_β, the spiral angle factor, takes into account the influence of the helix angle that is not covered by Z_ε. The values for this factor are close to one, so $Z_\beta = 1$ was the value used during this work;

- K_H is the factor for tooth flank loading and it is obtained in an analogous way to K_F in Section A.

σ_H and S_H tooth flank pressure and tooth flank safety factor

Once that we have a value for σ_H calculated with Equation (A.12), the tooth flank pressure safety factor may be obtained dividing the obtained stress value by σ_{HlimN}, which is the permissible value for the flank pressure under pulsating stress. Just as σ_{FlimN}, also σ_{HlimN} decreases with the increasing of flank temperature ϑ_{Fla} and number of loading cycles N_L. VDI 2736 does not give information about σ_{HlimN} for POM, since it is said that normally, there is no need for an analysis of the flank load-carrying capacity for POM. In the present work, an approach was made according to what is done in *Kisssoft 4.1* ® when using the calculation method VDI 2545. The database used in this software considers that $\sigma_{HlimN}[POM] = 0,9 \cdot \sigma_{HlimN}[PA66]$ and σ_{HlimN} for PA 66 (oil lubricated) present in [13] was taken as reference. Figure A.7 shows the influence of temperature and cycles number on permissible flank stress. Once again, for better and more rigorous calculations, a numerical value was obtained for permissible stress of PA 66, and then multiplied by a $0,9$ factor (check Equation (**??**).

Table A.6: Wear coefficients for different cases in $10^{-6}mm^3/(N \cdot m)$ [13].

Material	k_w
POM/Steel (where Rz=0,45μm)	1,0
POM/Steel (where Rz=1,5μm)	3,4
PBT/Steel (where Rz=0,45μm)	3,7
PBT/Steel (where Rz=1,5μm)	7,8

$$\sigma_{HlimN} = 0,9 \cdot [36 - 0,0012 \cdot \vartheta_{Fla}^2 + (1000 - 0,025 \cdot \vartheta_{Fla}^2) \cdot N_L^{(} - 0,21)] \tag{A.15}$$

$$N_L \in [10^5; 10^8]$$

The safety factor for flank load capacity results as:

$$S_H = \frac{\sigma_H}{\sigma_{HlimN}} \tag{A.16}$$

Frictional wear load capacity

Although wear calculation is more important for dry running, it was taken into consideration for study reasons. The calculation was made in terms of averaged linear wear W_m.

$$W_m = \frac{T_d \cdot 2 \cdot \pi \cdot N_L \cdot H_V \cdot k_w}{b_w \cdot z \cdot l_{Fl}} \tag{A.17}$$

Where k_w is the wear coefficient (check Table A.6) and l_{Fl} is the profile line length of the active tooth flank (check Equation (A.18)). A value of 3,4 was assumed for k_w during this calculations.

$$l_{Fl} = \frac{1}{d_b} \cdot \left(\left(\frac{d_{Na}}{2} \right)^2 - \left(\frac{d_{Nf}}{2} \right)^2 \right) \tag{A.18}$$

Where:

- d_b is the base circle diameter;
- d_{Na} is the usable addendum circle diameter;
- d_{Nf} is the usable root circle diameter.

All the used diameters are explained in anex X).

W_m should be lower than permissible linear wear W_{zul}. The value used for W_{zul} was:

$$W_{zul} = 0,1 \cdot m_n \tag{A.19}$$

Resulting for the wear safety factor:

$$S_{W_m} = \frac{W_m}{W_{zul}} \tag{A.20}$$

Deformation

We have seen already in Section **??** that deformation might be a critical parameter for a plastic gear. Especially for plastic gears with a narrow face width which is our case. The deformation of the tooth tip in the circumferential direction (in mm) λ is calculated according to Equation (A.21)

$$\lambda = \frac{7,5 \cdot F_t}{b \cdot \cos\beta}\left(\frac{1}{E_1} + \frac{1}{E_2}\right) \quad [1] \tag{A.21}$$

Permissible deformation λ_{zul} was defined as:

$$\lambda_{zul} \leq 0,07 \cdot m_n \tag{A.22}$$

Finally, the safety factor for deformation was defined as S_λ and was defined as:

$$S_\lambda = \frac{\lambda}{\lambda_{zul}} \tag{A.23}$$

Summary of the coefficients calculated

For easier comparison with other calculations, values of some calculated/used coefficients/parameters are listed on Table A.7

[1] The values considered for steel were $E = 206GPa$. For POM, E can be found on figure A.8.

Table A.7: Coefficients/parameters used or calculated.

Parameter	**C14**	**501**	**951**	**Units**
ϑ_0	20,00	20,00	20,00	°C
μ	0,055	0,055	0,055	-
H_V	0,1951	0,1639	0,1048	-
$k_{\vartheta,Fu\beta}$	$0,9 \cdot 10^3$	$0,9 \cdot 10^3$	$0,9 \cdot 10^3$	$\frac{K \cdot (m/s)^{0,75} \cdot mm^{2,15}}{W}$
$k_{\vartheta,Fla}$	$6,3 \cdot 10^3$	$6,3 \cdot 10^3$	$6,3 \cdot 10^3$	$\frac{K \cdot (m/s)^{0,75} \cdot mm^{2,15}}{W}$
$R_{\lambda,G}$	0,060	0,060	0,0600	$\frac{K \cdot m^2}{W}$
A_G	1,40	1,40	1,4000	m^2
ED	1,00	1,00	1,00	-
K_A	1,00	1,00	1,00	-
K_v	1,00	1,00	1,0000	
Y_{Fa1}	2,53	2,50	1,800	-
Y_{Fa2}	2,45	2,45	1,70	-
Y_{Sa1}	1,62	1,73	2,2500	-
Y_{Sa2}	1,75	1,77	2,4500	-
Y_ϵ	0,7710	0,7637	1,0509	-
K_F	1,0000	1,0000	1,0000	-
Y_β	1,00	0,9323	0,8750	-
E_1	206E3	206E3	206E6	Mpa
E_2	2,8E3	2,8E3	2,8E3	Mpa
ν_1	0,30	0,30	0,3000	-
ν_2	0,35	0,35	0,3500	-
Z_E	31,6476	31,6476	31,6476	$(N/mm^2)^{0,5}$
Z_H	2,3400	2,3400	2,3400	-
Z_ϵ	0,9241	0,8713	1,0334	-
Z_β	1,00	1,00	1,0000	-
K_H	1,00	1,00	1,00	-
k_w	3,4E-6	3,4E-6	3,4E-6	$\frac{mm^3}{N \cdot m}$

Appendix B

Standard calculation methods for plastic gears

Plastic gears use is getting more and more importance. Differently from this fact, the plastic gears scientific research is still very low if compared with steel gears [28]. The standards creation became a necessity, and an attempt to fight this situation was made in 1981: VDI 2545, a German guide-line. Unfortunately it was still very poor when compared to informations present on standards like AGMA 2001 or ISO 6336 for metal gears and now, VDI 2545 is currently invalid. This fact leaded to the necessity of some improvements.

A method called "VDI 2545 - modified" was purposed by Kisssoft ® team as an alternative for tooth flank and tooth root strength analysis in order to make VDI 2545 applicable and implementable on commercial software. Only on 2013, a new VDI guideline was published with some improvements: "VDI 2736". Also in 2013, a new Japanese Standard was published: JIS B 1759 "Estimation of tooth bending strength of cylindrical plastic gears" which is based on ISO 6336-3. In this chapter the major differences between some calculation methods are pointed, with a special focus on root and flank stress correction factors. [1].

Temperature prediction

Temperature is a critical parameter on plastics for all the reasons explained on Section 2.2.1. The equations used for temperature calculations on VDI 2545 and VDI 2736 are compared on this section.

VDI 2545

The assumption that the heat produced by the power loss in the tooth meshing is equal to the dissipated heat in the inner space of the gearbox housing, which, in its turn, is

[1] In some cases the nomenclature was changed to keep the same nomenclature in all the standards analysed so that the comparison can be done easier.

equal to the heat dissipated by the housing to the environment, leads to the formula suggested for the body temperature of plastic gears on VDI 2545:

$$\vartheta_{1,2} = \vartheta_0 + P \cdot \mu \cdot \frac{u+1}{z_2+5} \cdot \left(\frac{2325.6}{b \cdot z_{1,2}} \cdot \frac{k_2}{(v \cdot m_n)^{\kappa}} + 0.8568 \cdot \frac{k_3}{A_G} \right) \tag{B.1}$$

Where:

- P [W] is the transmitted power;
- k_2 [-] and κ [-] are factors that take the material combinations and lubrication type into account;
- k_3 [-] takes the influence of the housing conditions into account (it could be open, closed partially open etc.)
- A_G [m^2] is the surface area of the gearbox housing that can dissipate heat;

VDI 2736

The temperature calculation on VDI 2736 distinguishes two different temperatures:$\vartheta_{Fu\beta}$ the tooth root temperature, and ϑ_{Fla} the flank temperature (both in °C). The tooth root temperature is given by equation (B.2):

$$\vartheta_{Fu\beta_{1,2}} = \vartheta_0 + P \cdot \mu \cdot H_V \cdot \left(\frac{k_{\vartheta,Fu\beta}}{b \cdot z_{1,2} \cdot (v_t \cdot m_n)^{0,75}} + \frac{R_{\lambda,G}}{A_G} \right) \cdot ED^{0,64} \tag{B.2}$$

Where :

- $\vartheta_{Fu\beta_{1,2}}$ is the tooth root temperature on the pinion (1) or on the wheel (2);
- P [W] is the transmitted power;
- H_v is the degree of tooth loss and is calculated according to equation (B.3);

$$H_V = \frac{\pi \cdot (u+1)}{z_2 \cdot \cos(\beta_b)} \cdot \left(1 - \varepsilon_1 - \varepsilon_2 + \varepsilon_1^2 + \varepsilon_2^2\right) \tag{B.3}$$

  For the H_V calculation, ε_1 and ε_2 are necessary. They respect to the partial radial contact ratios for the wheel and the pinion.

- $k_{\vartheta,Fu\beta}$ (check Appendix A, Table A.3) is the heat transfer coefficient of the plastic gear for the tooth flank temperature calculation.
- $R_{\lambda,G}$ is the heat transfer resistance of the mechanism housing.

The calculation of the flank temperature may be done just by substituting the heat transfer coefficient $k_{\vartheta,Fu\beta}$ by $k_{\vartheta,Fla}$, which is the heat transfer coefficient for the tooth flank resulting:

$$\vartheta_{Fla_{1,2}} = \vartheta_0 + P \cdot \mu \cdot H_V \cdot \left(\frac{k_{\vartheta,Fla}}{b \cdot z_{1,2} \cdot (v_t \cdot m_n)^{0,75}} + \frac{R_{\lambda,G}}{A_G} \right) \cdot ED^{0,64} \tag{B.4}$$

Tooth root stress

Tooth root stress is originated due to the applied load. Tooth root stress is calculated dividing the tangential force at the reference diameter F_t by the under-load tooth section ($b \cdot m_n$). Affecting this values are correction factors that may be considered or not depending on the situation and on the calculation method (check Appendix A, Section A). The limit stress for the tooth root is given as function of the tooth root temperature and of the number of cycles which depends on the material. Correction factors will be analysed and compared, as well as the limit stresses suggested in different standards.

VDI 2545

VDI 2545 tooth root stress calculations are based on DIN 3990. The basic formula is given by [28]:

$$\sigma_F = K_A \cdot Y_{Fa} \cdot Y_\varepsilon \cdot Y_\beta \cdot \frac{F_t}{b \cdot m_n} \leq \frac{\sigma_{FlimN}}{S_F} \tag{B.5}$$

Where:

- K_A the application factor (DIN 3990);
- Y_{Fa} is the form factor (DIN 3990);
- Y_ε is the contact ratio factor ($1/\varepsilon_\alpha$ only applicable on method C);
- Y_β is the helix angle factor (DIN 3990);

σ_{FlimN} - Tooth root stress limit

Table B.1: σ_{FlimN} for POM given by VDI 2545 (MPa) [3].

N_L	Temperatures [°C]				
	20	60	80	100	120
10^5	66	56	50	42	28
10^6	50	44	35	28	19
10^7	42	34	25	19	13
10^8	35	28	20	14	9

VDI 2736

With a similar formula, VDI 2736 shows some differences including new correction factors [13].

$$\sigma_F = K_F \cdot Y_{Fa} \cdot Y_{Sa} \cdot Y_\varepsilon \cdot Y_\beta \cdot \frac{F_t}{b \cdot m_n} \leq \frac{\sigma_{FlimN}}{S_F} \tag{B.6}$$

$$K_F = K_A \cdot K_v \cdot K_{F\beta} \cdot K_{F\alpha} \tag{B.7}$$

The factors are:

- K_F, the tooth root load factor which is composed by:
  - K_A, the application factor (DIN 3990);
  - K_v, the dynamic factor;
  - $K_{F\beta}$ the width factor;
  - $K_{F\alpha}$ the face factor;
- Y_{Sa} the stress correction factor;

σ_{FlimN} - Tooth root stress limit

Table B.2: σ_{FlimN} for POM given by VDI 2736 (MPa) [13].

Cycles	Temperatures				
	20	40	60	80	100
10^5	65	65	57	50	41
10^6	50	47	42	35	26
10^7	41	38	33	26	17
10^8	35	32	27	20	11

Comparison of VDI 2736 and VDI 2545

The correction factors found on equations (B.5) and (B.6) are not the same. The application factor was substituted by the tooth root load factor, which combines the effect of the application factor with three more factors.

The appearance of the stress correction factor (Y_{Sa}) is important, because the values of this factor are in the range of 1,3 to 2,3 [13], which dramatically changes the safety factors obtained. This factor takes into consideration the stress concentration due to the notch effect (Figure B.1) during the load application at the tooth tip.

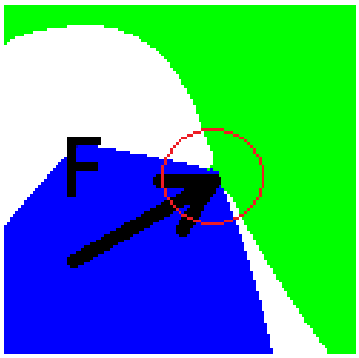

Figure B.1: Notch effect meshing moment (high stress concentrations).

Tooth flank pressure

The tooth flank pressure is one of the main failure causes on plastic gears. The temperature increase on the tooth flank makes it susceptible to failure due to critical flank pressures.

VDI 2545

VDI 2545 tooth flank pressure calculations basic formula is given by [28]:

$$\sigma_H = Z_E \cdot Z_H \cdot Z_\varepsilon \cdot \sqrt{\frac{F_t \cdot K_A}{b_w \cdot d_1} \cdot \frac{u+1}{u}} \leq \frac{\sigma_{HlimN}}{S_H} \tag{B.8}$$

Where:

- Z_E, is the material factor;
- Z_H, is the zone factor which transfer some tangential force from the reference circle to the operational pitch diameter;
- Z_ε is the overlap factor.

σ_{HlimN} - Tooth flank pressure limit

As VDI 2545 has no data available for the values of σ_{HlimN} for POM, the data for PA-66 with oil lubrication was chosen and analysed.

VDI 2736

VDI 2736 tooth flank pressure calculations basic formula is given by [13]:

$$\sigma_H = Z_E \cdot Z_H \cdot Z_\varepsilon \cdot Z_\beta \cdot \sqrt{\frac{F_t \cdot K_H}{b_w \cdot d_1} \cdot \frac{u+1}{u}} \tag{B.9}$$

Table B.3: σ_{HlimN} for PA-66 oil lubricated given by VDI 2545 (MPa) [3].

Cycles	Temperatures				
	20	60	80	100	120
10^5	120	115	108	99	91
10^6	95	90	85	78	68
10^7	70	67	63	58	50
10^8	52	50	47	44	37

The factors are:

- Z_β, the spiral angle factor which takes into account the effects of the spiral angle β that are not taken into account by the use of Z_ε. This factor Z_β is approximately equal to one.

- K_H, tooth flank loading factor, which is equal to to K_F and is obtained by the same way.

σ_{HlimN} - Tooth flank pressure limit

Table B.4: σ_{HlimN} for PA-66 oil lubricated given by VDI 2736 (MPa) [13].

Cycles	Temperatures				
	20	60	80	100	120
10^5	124	113	103	91	76
10^6	90	82	74	65	54
10^7	69	63	57	49	40
10^8	56	51	46	40	32

Comparison of VDI 2736 and VDI 2545

Once again it is seen that when comparing equations (B.8) and (B.9) new correction factors are found. Spiral angle factor Z_β is not a big influence since some of the effect of the spiral angle is already present on Z_ε. The application factor K_A is again substituted by the tooth flank loading factor K_H in the same way it happened in the tooth root equations.

Table B.5: Correction factors for different standard calculation methods [13, 28, 33].

Coefficient	VDI 2545	VDI 2545-mod.	VDI 2736
Tooth root calculation			
K_A	DIN 3990	DIN 3990	DIN 3990
K_v	-	-	ISO 6336
$K_{F\beta}$	-	-	ISO 6336
$K_{F\alpha}$	-	-	ISO 6336
Y_{Fa}	DIN 3990	DIN 3990	DIN 3990
Y_{Sa}	1.0 (fixed)	DIN 3990	DIN 3990
Y_β	DIN 3990	DIN 3990	DIN 3990
Y_ε	$\sqrt{1/\varepsilon_\alpha}$	$\sqrt{1/\varepsilon_\alpha}$	$0,25 + 0,75/\varepsilon_\alpha$
Tooth flank calculation			
Z_E	Henriot	Henriot	Henriot
Z_H	DIN 3990	DIN 3990	DIN 3990
Z_β	-	-	DIN 3990

JIS B 1759 - A new Japanese standard on load capacity

A new standard based on ISO 6336-3 "Calculation of load capacity of spur and helical gears - Part 3: Calculation of tooth bending strength" was established in Japan in 2013 [[27]]. It calculates tooth bending strength in a similar way as VDI standards, but with some differences.

The equation proposed is:

$$\sigma_F = \frac{F_{wt}}{b \cdot m_n} \cdot Y_{Fa} \cdot Y_{Sa} \cdot Y_\beta \cdot Y_f \cdot Y_B \tag{B.10}$$

Differently from VDI standards, the tangential force used F_{wt} is calculated on the working pitch circle and not on the reference circle. The fillet factor Y_f and the rim thickness factor Y_B are new factors that do not exist on VDI standards. Y_β and Y_{Sa} are calculated according to ISO 6336.

The tooth form factor Y_{Fa} is not calculated according to ISO 6336, since the change of the tangential force to the working pitch circle implies also the change of the pressure angle to α_{wt}, the working transverse pressure angle. With their own calculation method, for helical gears, if $\beta < 35$ °a difference of 2,1 % can be found when comparing JIS B 1759 with ISO 6336.

The tooth fillet factor Y_f considers the change on the tooth root stress if the tooth fillet is not based on the basic rack profile (following JIS B 1701-1). It is equal or bigger than 1.

The rim thickness factor Y_B considers the effect of the rim thickness on stress distribution on the tooth root. It may have influence if the rim thickness is small.

This standard will be proposed to ISO, however it only estimates the root bending stress and the need of the estimation of safety factors for other failure causes such as pitting and wear is being discussed [27].

Appendix C

Oil Datasheet - BP Energol GR-XP 150

Product Data

BP Energol GR-XP 150

Industrial Extreme Pressure Gear Oil

Description

The BP Energol™ GR-XP gear oil range of high quality lubricants are based upon highly refined mineral oil, enhanced with sulphur/phosphorus extreme pressure additive technology providing outstanding thermal stability and high load carrying capacity.

The advanced extreme pressure additive system not only provides high load carrying capacity, but was designed to provide microscopic wear protection. Microscopic wear protection, also known as micropitting protection, is critical in preventing destructive wear at the micro level therefore extending gear life and meeting the evolving demands of smaller and higher output gear boxes

Application

The Energol GR-XP range is recommended for the lubrication of industrial gearboxes using forced circulation or splash and oil bath lubrication. They may be used for the lubrication of spur and helical gears and in some lightly loaded worm type gear applications.

They have very good viscosity characteristics to ensure that starting torques are not excessively high in cold operating conditions. The additives are compatible with the ferrous and non-ferrous metals used in industrial gear units.

The Energol GR-XP range is fully compatible with nitrile, silicone and fluropolymer seal materials.

Energol GR-XP is classified as follows:
DIN Classification is CLP

Energol GR-XP grades meet the requirements of:
DIN 51517 Part 3
AGMA 9005 - D94
US Steel 224
David Brown Type E
Hansen Transmissions
Flender

Advantages

- ‘Clean gear’ additive technology ensures low deposit formation and enhanced filter life.
- Full Extreme Pressure (EP) performance* gives maximum protection of gears against wear and shock-loading.
- Good water separation and demulsification characteristics means reduced down time through prolonged lubricant life and increased equipment reliability.
- Excellent protection against corrosion and wear results in less maintenance.
- Suitable for Müller Weingarten equipment

* ISO 220 grade achieved FZG >14 rating under A16.6/90 (double speed) test conditions

Typical Characteristics

Test	Method	Units	68	100	150	220	320	460	680	1000
AGMA No.			2EP	3EP	4EP	5EP	6EP	7EP	8EP	-
Density @ 15°C	ISO 12185 / ASTM D4052	g/ml	0.88	0.89	0.89	0.89	0.9	0.9	0.92	0.93
K.V. @ 40°C	ISO 3104 / ASTM D445	mm2/s	68	100	150	220	320	460	680	1000
K.V. @ 100°C	ISO 3104 / ASTM D445	mm2/s	8.53	11.1	14.5	18.7	24	30.5	37.3	43.6
Viscosity Index	ISO 2909 / ASTM 2270	-	> 95	> 95	> 95	>95	> 95	> 95	85	80
Pour Point	ISO 3016 / ASTM D97	°C	-21	-21	-18	-18	-15	-12	-9	-3
Flash Point, PMC	ISO 2719 / ASTM D93	°C	220	220	220	226	226	226	230	230
Foam Seq I	ISO 6247 / ASTM D892	mls/mls	10/0	10/0	10/0	10/0	10/0	10/0	10/0	10/Nil
Copper Corrosion (3 hrs @ 100°C)	ISO 2160 / ASTM D130	-	1b	1b	1b	1b	1b	1b	1b	1b
Rust Test (24 hrs Synthetic sea water)	ISO / 7210 / ASTM D665B	-	Pass	Pass	Pass	Pass	Pass	Pass	Pass	Pass
Timken OK Load	ASTM D2782 / IP 240	lbs	-	-	-	70	70	70	70	70
FZG fail stage (A8.3/90)	ISO 14635-1 / DIN 51354	-	> 12	> 12	> 12	> 12	> 12	> 12	> 12	>12
FZG Micropitting										
Fail Stage	FVA Proj No. 54	-	-	-	-	>10	>10	>10	-	-	-
GFT Class	FVA Proj No. 54	-	-	-	-	High	High	High	-	-	-

Subject to usual manufacturing tolerances.

BP, Energol GR-XP, and the BP logo are trademarks of BP p.l.c, used under licence

This data sheet and the information it contains is believed to be accurate as of the date of printing. However, no warranty or representation, express or implied, is made as to its accuracy or completeness. Data provided is based on standard tests under laboratory conditions and is given as a guide only. Users are advised to ensure that they refer to the latest version of this data sheet.

It is the responsibility of the user to evaluate and use products safely, to assess suitability for the intended application and to comply with all applicable laws and regulations. Material Safety Data Sheets are available for all our products and should be consulted for appropriate information regarding storage, safe handling, and disposal of the product. No responsibility is taken by either BP plc or its subsidiaries for any damage or injury resulting from abnormal use of the material, from any failure to adhere to recommendations, or from hazards inherent in the nature of the material. All products, services and information supplied are provided under our standard conditions of sale. You should consult our local representative if you require any further information.

BP Limited, Pipers Way, Swindon, Wiltshire SN3 1RE, UK
www.castrol.com/industrial
www.castrol.com

Appendix D

POM (homopolymer) - Material Properties

POM (homopolymer)

General information

Designation

Polyoxymethylene, acetal (homopolymer)

Tradenames

Acetron; Alcom; Amcel; Amilus; Anjaform; BeetleAcetal; Bergaform; Celcon; Compocet; Dafnelan; Delrin; Deniform; Duracon; Durmax; Ecoform; Encore; Ensital; Ertacetal; Formax; Formosacan; Hostaform; Isotal; Iupital; Kematal; Kepital; Kocetal; Kopla; Latan; Lucel; Lucet; Lunex-T; Luvocom; Murytal; Nevipom; Niform; Nyloy; Palform; Paomalux; Pertal; Poliform; POLYform; Pomfor; Seratal; Sniatal; Talnex; Tarnoform; Taroform; Tecaform; Tekuform; Tenac; Tepcon; Terez; TismoPoticon; Ultraform; Whistatt

Typical uses

Bearings; Gears; Snap-fit components; Cams; Plumbing components; Carburetor bodies.

Composition overview

Composition (summary)

Homopolymer of (CH2-O)n (from formaldehyde or trioxane)

Base	Polymer
Polymer class	Thermoplastic : semi-crystalline
Polymer type	POM
Polymer type full name	Polyoxymethylene (acetal), homopolymer
Filler type	Unfilled

Composition detail (polymers and natural materials)

Polymer	100			%

Price

Price	* 2,37	-	2,61	EUR/kg

Physical properties

Density	1,41e3	-	1,43e3	kg/m^3

Mechanical properties

Young's modulus	2,76	-	3,59	GPa
Yield strength (elastic limit)	65,5	-	69	MPa
Tensile strength	66,9	-	69	MPa
Elongation	10	-	75	% strain
Compressive modulus	4,49	-	4,72	GPa
Compressive strength	* 108	-	124	MPa
Flexural modulus	2,61	-	3,37	GPa
Flexural strength (modulus of rupture)	93,8	-	110	MPa
Shear modulus	* 1,03	-	1,34	GPa
Bulk modulus	* 3,2	-	3,36	GPa
Poisson's ratio	0,33	-	0,35	
Shape factor	5,1			
Hardness - Vickers	* 19,7	-	24,8	HV
Hardness - Rockwell M	92	-	94	
Hardness - Rockwell R	114	-	126	
Fatigue strength at 10^7 cycles	* 23,8	-	31	MPa
Mechanical loss coefficient (tan delta)	* 0,0111	-	0,0145	

Impact & fracture properties

Fracture toughness	3,8	-	4,2	MPa.m^0.5
Impact strength, notched 23 ℃	7,24	-	12,4	kJ/m^2
Impact strength, notched -30 ℃	6,8	-	9,91	kJ/m^2
Impact strength, unnotched 23 ℃	590	-	600	kJ/m^2
Impact strength, unnotched -30 ℃	590	-	600	kJ/m^2

Thermal properties

Melting point	172	-	184	℃
Glass temperature	60	-	50	℃
Heat deflection temperature 0.45MPa	162	-	172	℃
Heat deflection temperature 1.8MPa	123	-	136	℃
Maximum service temperature	77	-	97	℃
Minimum service temperature	50	-	40	℃
Thermal conductivity	0,221	-	0,239	W/m.℃
Specific heat capacity	1,27e3	-	1,3e3	J/kg.℃
Thermal expansion coefficient	90	-	202	µstrain/℃

Electrical properties

Electrical resistivity	3,3e20	-	3e21	µohm.cm
Dielectric constant (relative permittivity)	3,6	-	3,8	
Dissipation factor (dielectric loss tangent)	0,0046	-	0,005	
Dielectric strength (dielectric breakdown)	15,7	-	19,7	MV/m
Comparative tracking index	300	-	600	V

Optical properties

Transparency	Opaque

Absorption & permeability

Water absorption @ 24 hrs	0,23	-	0,27	%
Permeability (O2)	4,37	-	7,21	$cm^3.mm/m^2.day.atm$

Processing properties

Polymer injection molding	Acceptable			
Polymer extrusion	Acceptable			
Polymer thermoforming	Unsuitable			
Linear mold shrinkage	1,8	-	2,5	%
Melt temperature	193	-	243	℃
Mold temperature	80	-	100	℃
Molding pressure range	68,8	-	138	MPa

Durability

Water (fresh)	Excellent
Water (salt)	Excellent
Weak acids	Acceptable
Strong acids	Unacceptable
Weak alkalis	Excellent
Strong alkalis	Excellent
Organic solvents	Acceptable
Oxidation at 500C	Unacceptable
UV radiation (sunlight)	Poor
Flammability	Highly flammable

Chemical resistance of polymers

Chemical resistance, data sources

Derived from Rapra ChemRes record for Acetal (homopolymer)

Acetaldehyde	Satisfactory
Acetic acid (10%)	Satisfactory
Acetic acid (glacial)	Unsatisfactory
Acetic anhydride	Unsatisfactory
Acetone	Limited
Acetonitrile	Unsatisfactory
Acetophenone	Unsatisfactory
Acetyl chloride	Unsatisfactory
Acrylic acid	Unsatisfactory

Aluminum chloride (10%)	Limited
Aluminum sulfate	Limited
Ammonium hydroxide (35%)	Satisfactory
Ammonium sulfate (50%)	Satisfactory
Amyl acetate	Satisfactory
Amyl alcohol	Satisfactory
Aniline	Satisfactory
Antimony trichloride (10%)	Unsatisfactory
Aqua regia	Unsatisfactory
Arsenic acid	Probably satisfactory
ASTM fuel A	Probably satisfactory
ASTM fuel B	Probably satisfactory
ASTM fuel C	Probably satisfactory
ASTM oil No. 1	Satisfactory
ASTM oil No. 2 or IRM902	Satisfactory
ASTM oil No. 3 or IRM903	Satisfactory
Barium chloride	Satisfactory
Benzaldehyde	Satisfactory
Benzene	Satisfactory
Benzyl alcohol	Satisfactory
Benzyl chloride	Satisfactory
Boric acid	Satisfactory
Bromine liquid	Unsatisfactory
Butyl acetate	Satisfactory
Butyl alcohol (butanol)	Satisfactory
Butyl chloride	Satisfactory
Butylamine	Satisfactory
Butyric acid	Limited
Calcium chloride	Satisfactory
Carbon disulfide	Satisfactory
Carbon tetrachloride	Satisfactory
Castor oil	Satisfactory
Cellosolve	Satisfactory
Cellosolve acetate	Probably satisfactory
Chloracetic acid	Unsatisfactory
Chlorine dioxide	Doubtful
Chlorine gas (dry)	Unsatisfactory
Chlorine water	Unsatisfactory
Chlorobenzene	Satisfactory
Chloroform	Limited
Chlorosulfonic acid	Unsatisfactory
Chrome plating solution	Unsatisfactory
Chromic acid	Limited
Citric acid (10%)	Satisfactory
Cod liver oil	Probably satisfactory
Copper sulfate	Satisfactory
Cotton seed oil	Satisfactory
Cresols	Unsatisfactory
Cyclohexane	Satisfactory
Cyclohexanol	Satisfactory
Cyclohexanone	Satisfactory
Decalin	Satisfactory
Diesel oil	Satisfactory
Diethyl ether	Satisfactory
Diethylamine	Unsatisfactory
Diethylene glycol	Satisfactory
Dimethyl formamide	Satisfactory
Dimethylamine	Probably satisfactory
Dimethylhydrazine	Probably satisfactory
Dioctyl phthalate	Limited
Dioxane	Satisfactory

Ethyl acetate	Satisfactory
Ethyl alcohol (ethanol)	Satisfactory
Ethyl chloride	Limited
Ethylamine	Probably satisfactory
Ethylene bromide	Probably satisfactory
Ethylene chloride (1,2 dichloroethane)	Limited
Ethylene glycol	Satisfactory
Ferric chloride	Limited
Fluoboric acid	Doubtful
Fluorine (gas)	Unsatisfactory
Fluosilicic acid	Doubtful
Formaldehyde (40%)	Satisfactory
Formic acid (90%)	Unsatisfactory
Freon - 11	Satisfactory
Freon - 113	Satisfactory
Freon - 115	Satisfactory
Freon - 12	Satisfactory
Freon - 13 B1	Satisfactory
Freon - 21	Satisfactory
Freon - 22	Satisfactory
Freon - 32	Satisfactory
Furfural	Satisfactory
Glycerol	Satisfactory
Hexane	Satisfactory
Hydrazine	Satisfactory
Hydrobromic acid (50%)	Unsatisfactory
Hydrochloric acid (10%)	Limited
Hydrochloric acid (36%)	Unsatisfactory
Hydrofluoric acid (40%)	Unsatisfactory
Hydrogen peroxide (35%)	Unsatisfactory
Hydrogen peroxide (87%)	Unsatisfactory
Hydrogen sulfide gas	Satisfactory
Iso-octane	Satisfactory
Iso-propyl alcohol (iso-propanol)	Limited
Lactic acid (90%)	Satisfactory
Lead acetate (10%)	Satisfactory
Linseed oil	Satisfactory
Lubricating oil	Satisfactory
Magnesium chloride	Satisfactory
Manganese sulfate	Satisfactory
Mercuric chloride	Doubtful
Methyl alcohol (methanol)	Satisfactory
Methyl bromide (gas)	Unsatisfactory
Methyl ethyl ketone	Satisfactory
Methylene chloride (dichloromethane)	Unsatisfactory
Molasses	Satisfactory
Monoethanolamine (2-aminoethanol)	Satisfactory
Nickel chloride	Satisfactory
Nitric acid (10%)	Limited
Nitric acid (70%)	Unsatisfactory
Nitrobenzene	Satisfactory
Nitromethane	Probably satisfactory
Nitropropane	Probably satisfactory
n-propanol	Limited
Oleic acid	Satisfactory
Olive oil	Satisfactory
Oxalic acid (solutions)	Limited
Ozone (gas)	Unsatisfactory
Paraffin oil (kerosene)	Satisfactory
Perchlorethylene	Satisfactory
Peroxymonosulfuric acid	Doubtful

Petrol (gasoline)	Satisfactory
Phenol	Unsatisfactory
Phosphoric acid (85%)	Unsatisfactory
Picric acid (solutions)	Doubtful
Plating solutions (non-chrome)	Doubtful
Potassium cyanide	Satisfactory
Potassium fluoride	Satisfactory
Potassium hydroxide (50%)	Satisfactory
Potassium permanganate (25%)	Satisfactory
Potassium sulfate	Satisfactory
Propionic acid	Unsatisfactory
Propylene oxide	Limited
Pyridine	Satisfactory
Rapeseed oil	Satisfactory
Silicone fluids	Limited
Silver nitrate	Satisfactory
Sodium borate	Satisfactory
Sodium carbonate (10%)	Satisfactory
Sodium chloride (25%)	Satisfactory
Sodium chlorite	Doubtful
Sodium cyanide	Satisfactory
Sodium hydroxide (10%)	Satisfactory
Sodium hydroxide (60%)	Satisfactory
Sodium hypochlorite (20%)	Unsatisfactory
Sodium nitrate	Satisfactory
Sour oil	Probably satisfactory
Stannic chloride	Satisfactory
Styrene	Satisfactory
Sulfamic acid (solutions)	Probably satisfactory
Sulfur dioxide (gas)	Unsatisfactory
Sulfuric acid (10%)	Doubtful
Sulfuric acid (70%)	Unsatisfactory
Sulfuric acid (96%)	Unsatisfactory
Sulfuric acid (fuming)	Unsatisfactory
Tetrachlorethane	Doubtful
Tetrahydrofuran	Satisfactory
Tetralin	Satisfactory
Thionyl chloride	Unsatisfactory
Titanium tetrachloride	Doubtful
Toluene	Satisfactory
Transformer oil	Satisfactory
Trichloracetic acid	Unsatisfactory
Trichlorethane	Satisfactory
Trichlorethylene	Limited
Tricresyl phosphate	Satisfactory
Triethanolamine	Satisfactory
Triethylamine	Satisfactory
Turpentine	Satisfactory
Vegetable oils (general)	Satisfactory
Vinyl acetate	Satisfactory
Vinyl chloride	Satisfactory
Water (distilled)	Satisfactory
Water (sea)	Satisfactory
White spirit	Satisfactory
Wine	Satisfactory
Xylene	Satisfactory
Zinc chloride (aq. sol.)	Limited

Primary production energy, CO2 and water

Embodied energy, primary production	* 85,4	-	94,4	MJ/kg
CO2 footprint, primary production	* 3,85	-	4,26	kg/kg

Water usage	138	-	413	l/kg

Processing energy & CO2 footprint

Polymer extrusion energy	* 5,76	-	6,36	MJ/kg
Polymer extrusion CO2	* 0,432	-	0,477	kg/kg
Polymer molding energy	* 16,9	-	18,7	MJ/kg
Polymer molding CO2	* 1,27	-	1,4	kg/kg
Coarse machining energy (per unit wt removed)	* 1,25	-	1,38	MJ/kg
Coarse machining CO2 (per unit wt removed)	* 0,0937	-	0,104	kg/kg
Fine machining energy (per unit wt removed)	* 8,22	-	9,08	MJ/kg
Fine machining CO2 (per unit wt removed)	* 0,616	-	0,681	kg/kg
Grinding energy (per unit wt removed)	* 16	-	17,6	MJ/kg
Grinding CO2 (per unit wt removed)	* 1,2	-	1,32	kg/kg

Recycling and end of life

Recycle	✓			
Embodied energy, recycling	* 29	-	32,1	MJ/kg
CO2 footprint, recycling	* 1,31	-	1,45	kg/kg
Recycle fraction in current supply	0,672	-	0,742	%
Downcycle	✓			
Combust for energy recovery	✓			
Heat of combustion (net)	* 15,5	-	16,3	MJ/kg
Combustion CO2	* 1,43	-	1,5	kg/kg
Landfill	✓			
Biodegrade	✗			

Notes

Warning

Compressive strength quoted at 10% strain. Not resistant to phenols. Degraded by contact with zinc ions. Very rapidly attacked by nitric acid. Decomposes explosively if processed with halogens.

Links

ProcessUniverse

Producers

Reference

Shape

IDES Plastics

CAMPUS Plastics

Appendix E

Test Datasheets - FZG and Roughness Tests

TEST DATASHEET - Plastic Gears

CETRIB
Unidade de Tribologia e Manutenção Industrial

Gear	*Pinion 1*
Ref.	C14_POM_01_P

ROUGHNESS [µm]

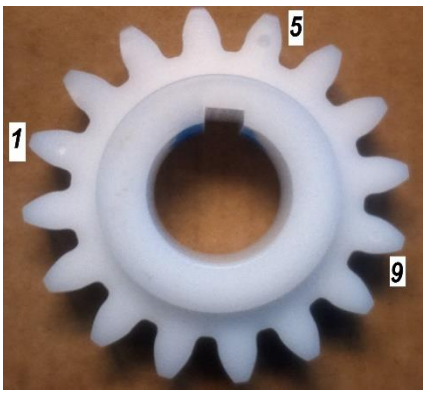

New	meas. n.	Ra	Rq	Rz	Rmax
Tooth 1	1	1.07	1.38	6.92	9.28
	2	1.05	1.40	7.67	12.04
	3	1.07	1.42	6.00	8.08
Tooth 5	4	1.31	1.63	7.38	8.17
	5	1.38	1.71	7.94	8.71
	6	1.36	1.70	7.65	8.89
Tooth 9	7	1.37	1.75	8.31	9.42
	8	1.37	1.75	7.90	8.70
	9	1.38	1.73	8.18	10.28

WEIGHING [g]

State	Ref Weight	Weight	Date
New	Broken		
Used			

Used	meas. n.	Ra	Rq	Rz	Rmax
Tooth 1	1	Broken Tooth			
	2				
	3				
Tooth 5	4	1.56	1.98	8.72	11.19
	5	1.69	2.12	8.76	12.90
	6	1.37	1.91	9.70	13.86
Tooth 9	7	1.78	2.23	9.56	13.22
	8	1.87	2.33	9.98	14.40
	9	1.90	2.34	9.78	13.74

FZG GEAR TESTS

K1 LOAD STAGE				
Speed(wheel) [rpm]	500	1000	2000	3000
Time [hours]	3	3	3	3
Total Cycles (POM)	1.35E+05	4.05E+05	9.45E+05	1.76E+06
Power Loss [W]	117.7	227.3	783.6	1865.4
Stabilization Temperatures [°C]				
Oil Temperature	34.0	43.1	47.0	68.1
Tooth Temperature	-	-	-	82.9
Ambient Temperature	25.0	26.7	-	28.1
FZG Base Temperature	37.2	40.2	-	39.6
Bearings Case (Test)	32.7	42.2	-	64.2
Top cover (Test)	32.0	33.2	-	65.7
Bearings Case (Slave)	71.5	73.1	-	63.6
Top cover (Slave)	67.5	69.5	-	63.6

Comments: Overwrited data during recording at 2000 rpm

CETRIB
Unidade de Tribologia e Manutenção Industrial

FZG GEAR TESTS

K2 LOAD STAGE				
Speed(wheel) [rpm]	500	1000	2000	3000
Time [hours]	4	2	1	0.67
Total Cycles (POM)	1.94E+06	2.12E+06	2.30E+06	2.48E+06
Power Loss [W]	97.6	232.1	790.3	1958.7
Stabilization Temperatures [°C]				
Oil Temperature	28.70	35.70	46.47	69.13
Tooth Temperature	-	44.20	-	81.90
Ambient Temperature	25.43	26.54	27.30	29.30
FZG Base Temperature	36.00	41.60	42.64	44.85
Bearings Case (Test)	30.11	39.07	52.23	73.86
Top cover (Test)	27.09	34.20	44.13	60.35
Bearings Case (Slave)	62.60	75.88	76.4	78.72
Top cover (Slave)	66.65	69.63	68.35	61.98
Comments:	Failure at K2@3000 rpm test end			

CETRIB
Unidade de Tribologia e Manutenção Industrial

TOPHOGRAFY

NEW

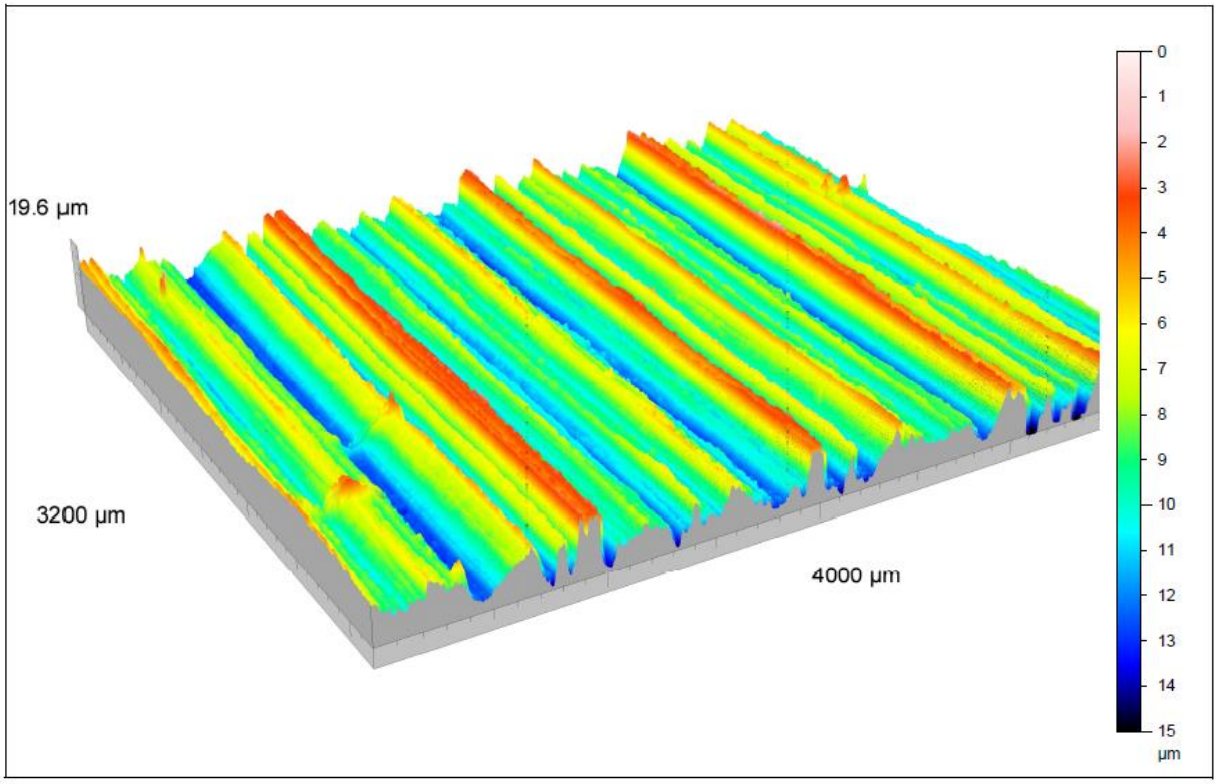

Identity card

Name: TOPO_C14_POM_01_A
Filename: D:\Perfis\André Lourenço\Pinion\01\f0\Topografia\TOPO_C14_POM_01_A.top

Axis: X
Length: 4800 µm
Size: 12084 points
Spacing: 0.397 µm

Axis: Y
Length: 4000 µm
Size: 401 lines
Spacing: 10 µm

Axis: Z
Length: 385 µm
Size: 3850 digits
Spacing: 0.1 µm

Parameters calculated on the surface TOPO_C14_POM_01_A > Roughness, Gaussian Filter, 800 µm

Sz, Sds and Ssc parameters are defined according to ISO standard.

Amplitude Parameters

Sa	= 2.25 µm
Sq	= 2.86 µm
Sp	= 9.47 µm
Sv	= 10.2 µm
St	= 19.6 µm
Ssk	= 1.16
Sku	= 2.99
Sz	= 19.6 µm

TEST DATASHEET - Plastic Gears

CETRIB
Unidade de Tribologia e Manutenção Industrial

Gear	*Pinion 2*
Ref.	C14_POM_02_P

ROUGHNESS [µm]

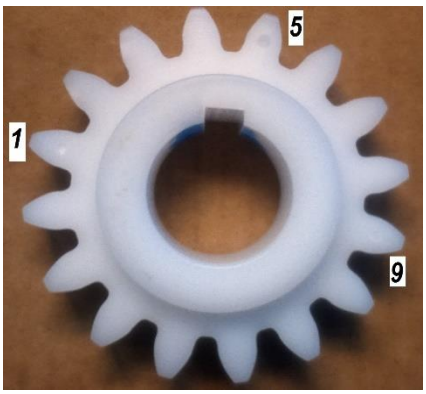

New	meas. n.	Ra	Rq	Rz	Rmax
Tooth 1	1	2.09	2.62	13.38	15.63
	2	2.08	2.63	13.01	16.06
	3	2.20	2.93	15.40	19.96
Tooth 5	4	2.25	2.85	13.63	18.30
	5	2.14	2.67	13.22	15.46
	6	2.30	2.91	13.95	17.92
Tooth 9	7	2.19	2.74	14.02	16.85
	8	2.13	2.70	13.89	16.03
	9	2.27	2.82	13.47	16.32

WEIGHING [g]

State	Ref Weight	Weight	Date
New Used	Broken		

Used	meas. n.	Ra	Rq	Rz	Rmax
Tooth 1	1	Broken Tooth			
	2				
	3				
Tooth 5	4	Broken Tooth			
	5				
	6				
Tooth 9	7	1.78	2.23	9.56	13.22
	8	1.87	2.33	9.98	14.40
	9	1.90	2.34	9.78	13.74

FZG GEAR TESTS

K2 LOAD STAGE				
Speed(wheel) [rpm]	500	1000	2000	3000
Time [hours]	4	2	1	0.67
Total Cycles (POM)	1.80E+05	3.60E+05	5.40E+05	7.20E+05
Power Loss [W]	92.4	220.2	774.2	2209.6
Stabilization Temperatures [°C]				
Oil Temperature	28.1	32.7	37.1	48.9
Tooth Temperature	32.2	-	44.2	62.9
Ambient Temperature	25.5	26.3	25.2	27.0
FZG Base Temperature	37.7	39.8	32.0	37.3
Bearings Case (Test)	29.1	35.4	41.3	52.4
Top cover (Test)	26.6	32.4	35.8	44.2
Bearings Case (Slave)	73.5	74.9	73.8	76.1
Top cover (Slave)	72.1	73.4	74.3	76.7

Comments: Pre heating at K1 (C14_POM_01_P) stabilization temperatures

CETRIB
Unidade de Tribologia e Manutenção Industrial

FZG GEAR TESTS

K3 LOAD STAGE				
Speed(wheel) [rpm]	500	1000	2000	3000
Time [hours]	4	2	1	0.67
Total Cycles (POM)	9.00E+05	1.08E+06	1.26E+06	1.44E+06
Power Loss [W]	110.1	266.9	826.0	2260.3
Stabilization Temperatures [°C]				
Oil Temperature	28.9	34.2	44.0	52.5
Tooth Temperature	32.4	42.3	56.6	66.3
Ambient Temperature	25.1	26.2	27.0	29.2
FZG Base Temperature	37.9	39.6	40.9	41.7
Bearings Case (Test)	30.1	37.8	49.3	58.4
Top cover (Test)	27.2	31.5	41.9	48.3
Bearings Case (Slave)	75.1	76.4	77.5	79.4
Top cover (Slave)	67.8	66.9	56.1	52.7

Comments: Pre heating at K2 (C14_POM_02_P) stabilization temperatures

CETRIB
Unidade de Tribologia e Manutenção Industrial

TOPHOGRAFY

NEW

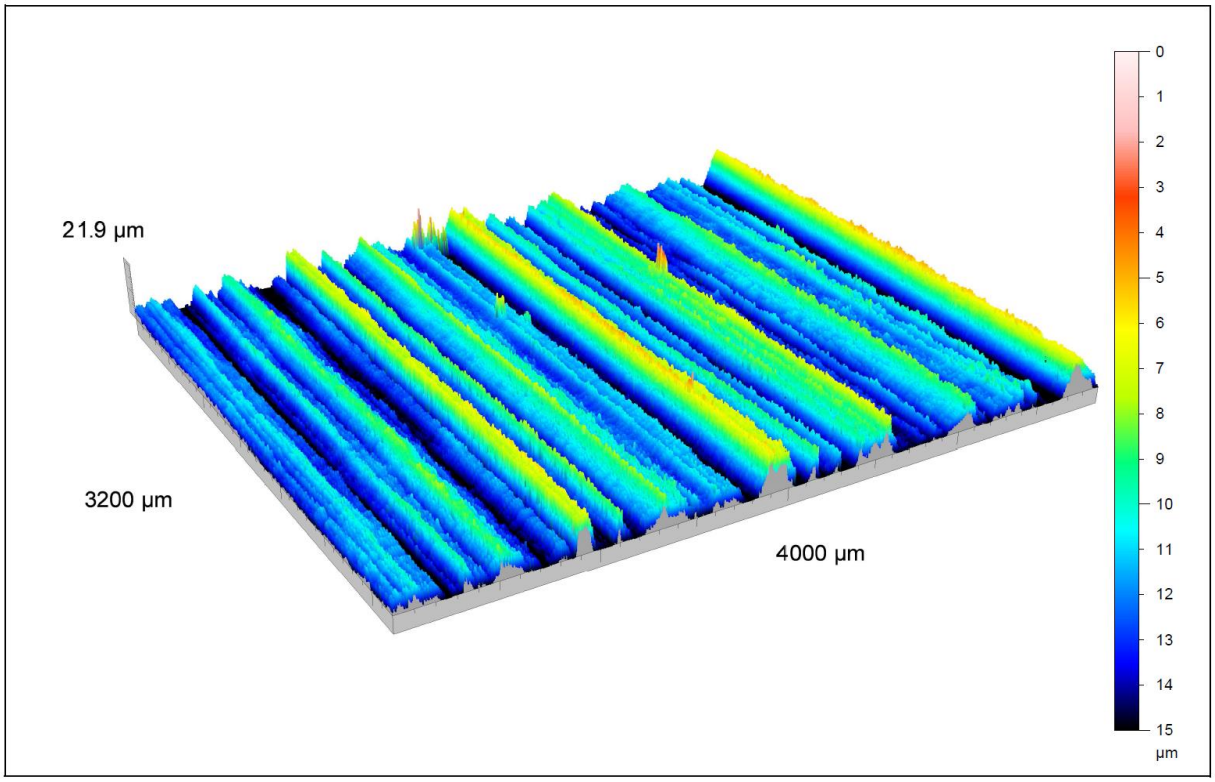

Identity card

Name: TOPO_C14_POM_02_A
Filename: D:\Perfis\André Lourenço\Pinion\02\f0\topografia\TOPO_C14_POM_02_A.top

Axis: X
Length: 4800 µm
Size: 12084 points
Spacing: 0.397 µm

Axis: Y
Length: 4000 µm
Size: 401 lines
Spacing: 10 µm

Axis: Z
Length: 331 µm
Size: 3305 digits
Spacing: 0.1 µm

Parameters calculated on the surface TOPO_C14_POM_02_A > Roughness, Gaussian Filter, 800 µm

Sz, Sds and Ssc parameters are defined according to ISO standard.

Amplitude Parameters

Sa = 2.1 µm
Sq = 2.68 µm
Sp = 13.2 µm
Sv = 8.75 µm
St = 21.9 µm
Ssk = 0.996
Sku = 3.22
Sz = 21.9 µm

TEST DATASHEET - Plastic Gears

CETRIB
Unidade de Tribologia e Manutenção Industrial

Gear	*Pinion 3*
Ref.	C14_POM_04_P

ROUGHNESS [µm]

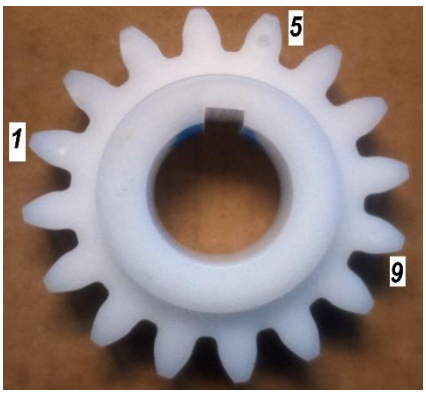

New	meas. n.	Ra	Rq	Rz	Rmax
Tooth 1	1	1.45	1.82	8.87	10.03
	2	1.42	1.79	8.48	9.50
	3	1.51	1.86	8.69	9.05
Tooth 5	4	1.57	1.97	9.72	10.76
	5	1.44	1.84	8.82	9.63
	6	1.44	1.82	8.56	9.13
Tooth 9	7	1.60	1.99	9.45	10.28
	8	1.62	2.01	9.40	9.55
	9	1.57	1.97	9.42	10.32

WEIGHING [g]

State	Ref Weight	Weight	Date
New Used	Broken		

Used	meas. n.	Ra	Rq	Rz	Rmax
Tooth 1	1	1.07	1.38	6.92	9.28
	2	1.05	1.40	7.67	12.04
	3	1.07	1.42	6.00	8.08
Tooth 5	4	1.31	1.63	7.38	8.17
	5	1.38	1.71	7.94	8.71
	6	1.36	1.70	7.65	8.89
Tooth 9	7	1.37	1.75	8.31	9.42
	8	1.37	1.75	7.90	8.70
	9	1.38	1.73	8.18	10.28

FZG GEAR TESTS

K2 LOAD STAGE				
Speed(wheel) [rpm]	500	1000	2000	3000
Time [hours]	4	2	2	-
Total Cycles (POM)	1.80E+05	3.60E+05	7.20E+05	-
Power Loss [W]	71.2	189.6	745.1	-
Stabilization Temperatures [°C]				
Oil Temperature	37.5	45.1	62.2	-
Tooth Temperature	40.5	48.5	69.5	-
Ambient Temperature	29.3	29.5	30.4	-
FZG Base Temperature	43.7	43.6	46.5	-
Bearings Case (Test)	36.8	45.0	61.8	-
Top cover (Test)	35.8	41.5	55.3	-
Bearings Case (Slave)	75.0	70.4	78.0	-
Top cover (Slave)	72.3	70.1	80.1	-

Comments: Pre heating at K2 (C14_POM_02_P) stabilization temperatures

CETRIB
Unidade de Tribologia e Manutenção Industrial

FZG GEAR TESTS

K3 LOAD STAGE				
Speed(wheel) [rpm]	500	1000	2000	3000
Time [hours]	4	2	0.68333	-
Total Cycles (POM)	9.00E+05	1.08E+06	1.20E+06	-
Power Loss [W]	110.1	-	826.0	-
Stabilization Temperatures [°C]				
Oil Temperature	37.8	46.3	58.1	-
Tooth Temperature	40.5	51.5	67.4	-
Ambient Temperature	28.3	28.8	29.7	-
FZG Base Temperature	41.7	42.8	37.0	-
Bearings Case (Test)	37.1	46.6	58.9	-
Top cover (Test)	34.4	36.3	50.8	-
Bearings Case (Slave)	66.1	67.7	71.4	-
Top cover (Slave)	66.5	69.1	75.6	-

Comments: Pre heating at K2 (C14_POM_02_P) stabilization temperatures
There was no time to stabilize temperature at 2000 rpm.

CETRIB
Unidade de Tribologia e Manutenção Industrial

TOPHOGRAFY

NEW

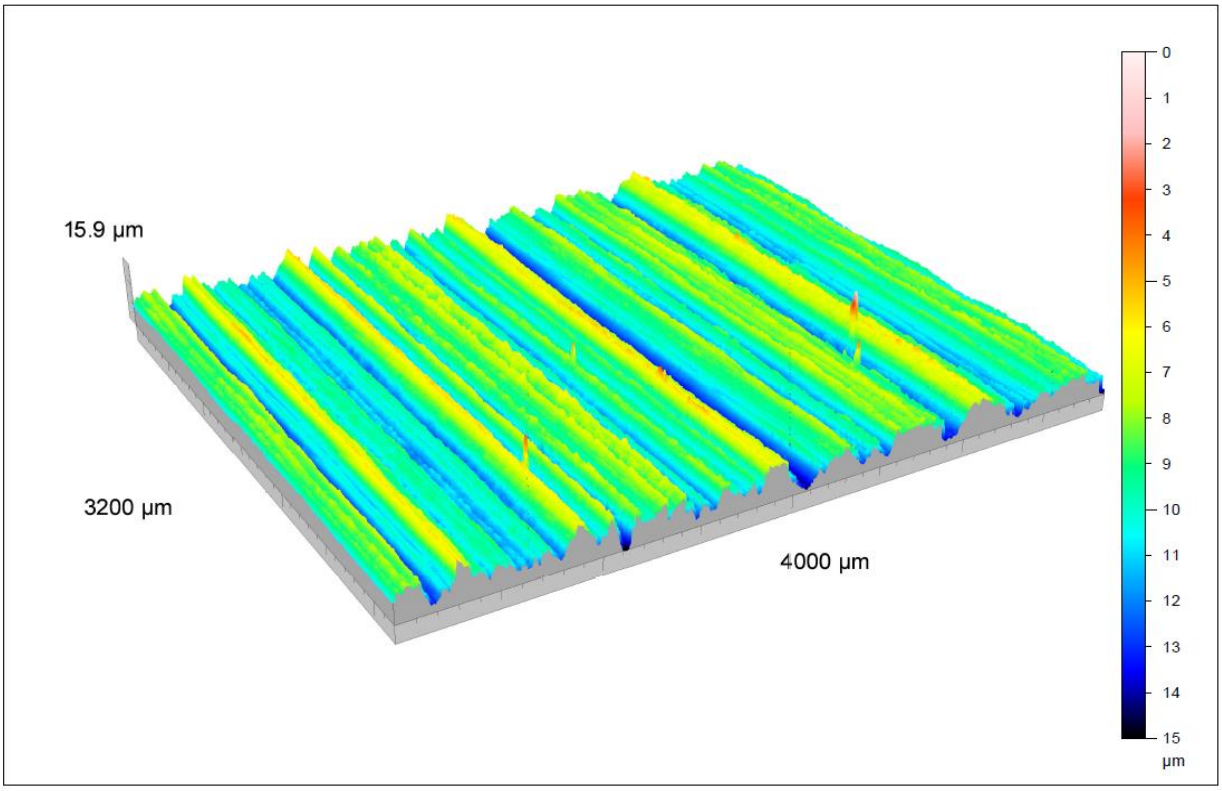

Identity card

Name: 163N3R
Filename: D:\Perfis\André Lourenço\Pinion\04\f0\Topografia\163N3R.top

Axis: X
Length: 4800 µm
Size: 12084 points
Spacing: 0.397 µm

Axis: Y
Length: 4000 µm
Size: 401 lines
Spacing: 10 µm

Axis: Z
Length: 318 µm
Size: 3182 digits
Spacing: 0.1 µm

Parameters calculated on the surface 163N3R > Roughness, Gaussian Filter, 800 µm

Sz, Sds and Ssc parameters are defined according to ISO standard.

Amplitude Parameters

Sa	= 1.62 µm
Sq	= 1.98 µm
Sp	= 10 µm
Sv	= 5.87 µm
St	= 15.9 µm
Ssk	= 0.817
Sku	= 2.57
Sz	= 15.9 µm

CETRIB
Unidade de Tribologia e Manutenção Industrial

TOPHOGRAFY

USED

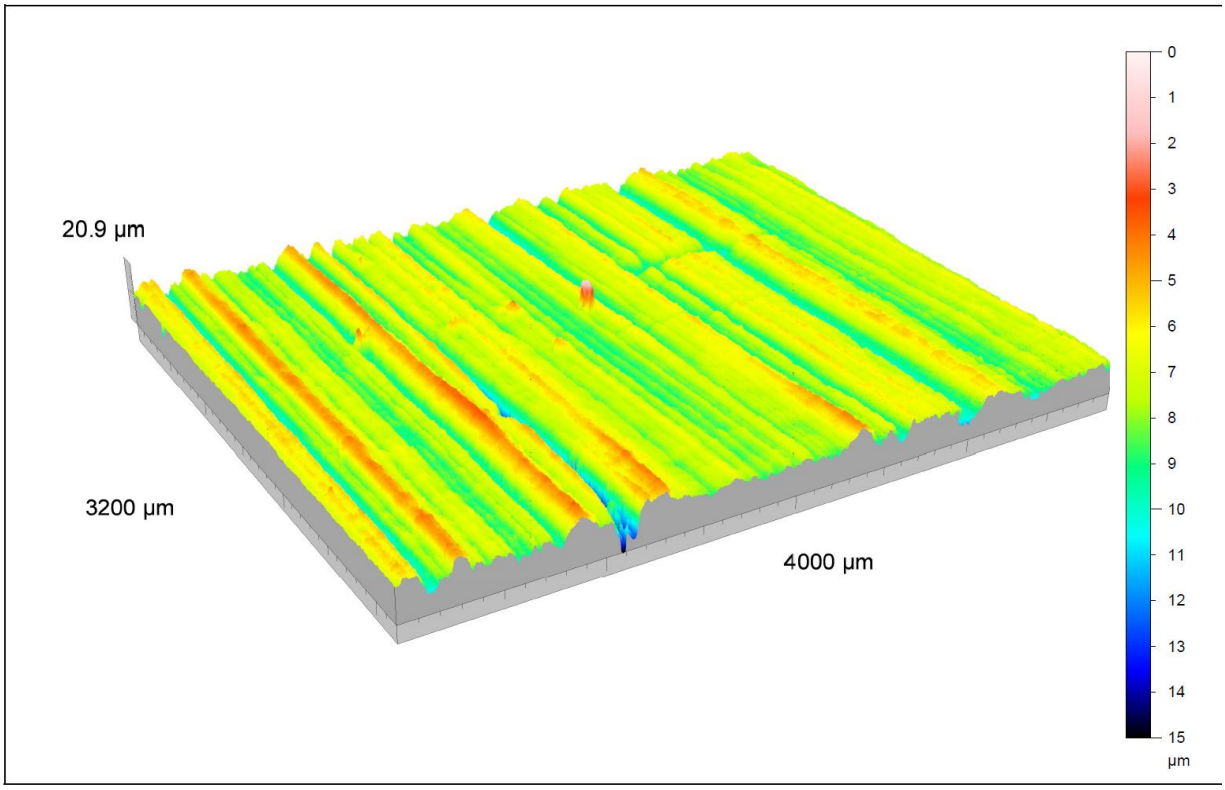

Identity card

Name: T_163U3R
Filename: D:\Perfis\André Lourenço\Pinion\04\f1_af @ 2000 rpm\Topografia\T_163U3R.top

Axis: X
Length: 4800 µm
Size: 12084 points
Spacing: 0.397 µm

Axis: Y
Length: 4000 µm
Size: 401 lines
Spacing: 10 µm

Axis: Z
Length: 230 µm
Size: 2302 digits
Spacing: 0.1 µm

Parameters calculated on the surface T_163U3R > Roughness, Gaussian Filter, 800 µm

Sz, Sds and Ssc parameters are defined according to ISO standard.

Amplitude Parameters

Sa	= 1.22 µm
Sq	= 1.52 µm
Sp	= 7.72 µm
Sv	= 13.2 µm
St	= 20.9 µm
Ssk	= 0.394
Sku	= 3.94
Sz	= 20.9 µm

TEST DATASHEET - Plastic Gears

CETRIB
Unidade de Tribologia e Manutenção Industrial

Gear	*Pinion 4*
Ref.	C14_POM_05_P

ROUGHNESS [µm]

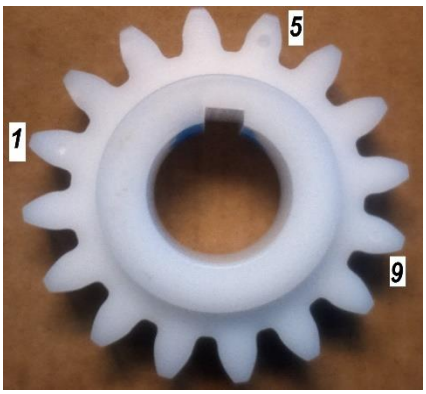

New	meas. n.	Ra	Rq	Rz	Rmax
Tooth 1	1	1.56	1.98	9.21	10.19
	2	1.56	1.92	8.76	10.18
	3	1.58	1.98	9.70	10.41
Tooth 5	4	1.55	1.95	8.76	9.52
	5	1.53	1.92	8.73	9.80
	6	1.53	1.92	9.02	10.55
Tooth 9	7	1.55	1.97	9.19	10.43
	8	1.51	1.87	8.68	10.92
	9	1.44	1.84	9.33	11.27

WEIGHING [g]

State	Ref Weight	Weight	Date
New	92.360	95.419	13/05/2015
Used	92.357	95.436	25/05/2015

Used	meas. n.	Ra	Rq	Rz	Rmax
Tooth 1	1	1.43	1.76	7.28	9.20
	2	1.37	1.67	7.13	8.56
	3	1.29	1.60	6.95	8.54
Tooth 5	4	1.34	1.65	7.29	7.88
	5	1.38	1.71	6.92	7.39
	6	1.27	1.57	6.86	8.54
Tooth 9	7	1.46	1.84	7.93	8.80
	8	1.53	1.87	7.63	8.34
	9	1.49	1.85	8.05	9.98

FZG GEAR TESTS

K2 LOAD STAGE				
Speed(wheel) [rpm]	500	1000	2000	3000
Time [hours]	-	111.11	-	-
Total Cycles (POM)	-	1.00E+07	-	-
Power Loss [W]	-	208.5	-	-
Stabilization Temperatures [°C]				
Oil Temperature	-	48.5/50.3	-	-
Tooth Temperature	-	60.8	-	-
Ambient Temperature	-	29.8	-	-
FZG Base Temperature	-	44.2	-	-
Bearings Case (Test)	-	54.3	-	-
Top cover (Test)	-	50.1	-	-
Bearings Case (Slave)	-	70.7	-	-
Top cover (Slave)	-	70.1	-	-

Comments: Controlled oil temperature: 50 °C

CETRIB
Unidade de Tribologia e Manutenção Industrial

TOPHOGRAFY

NEW

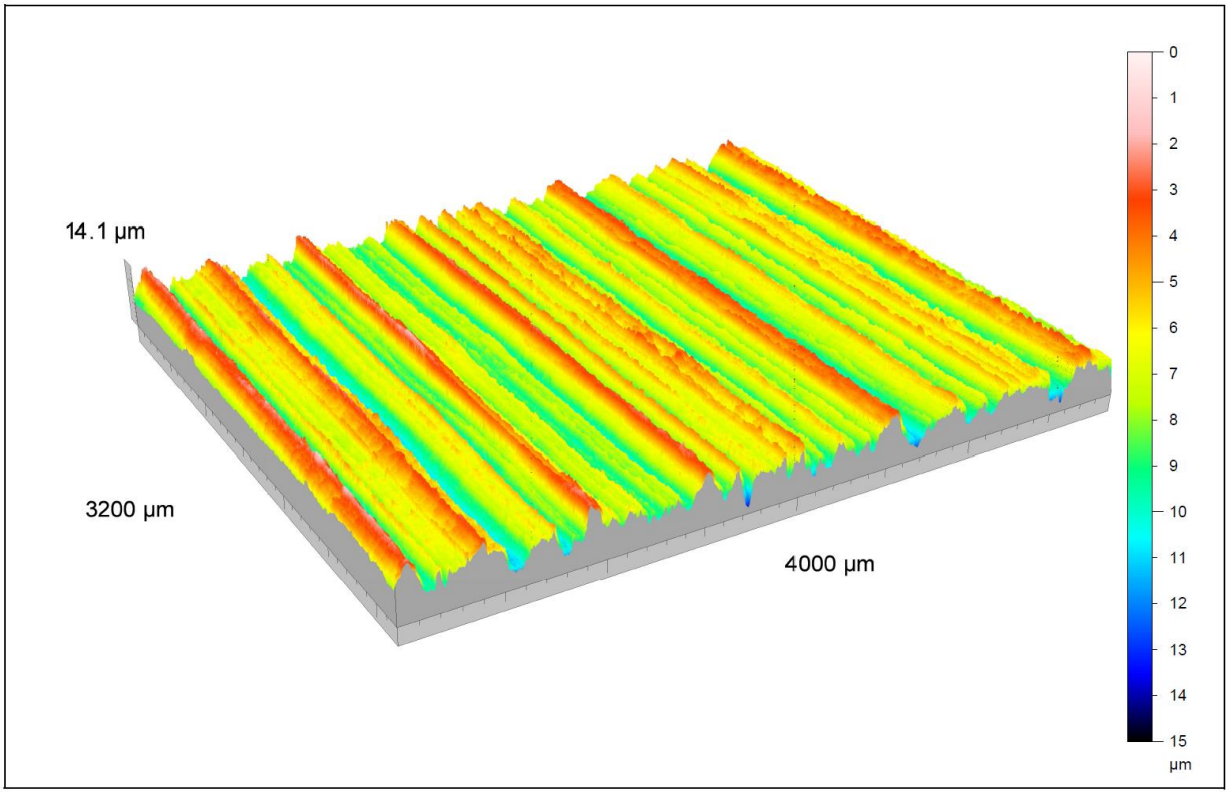

Identity card

```
Name:        T_164N3R
Filename:    D:\Perfis\André Lourenço\Pinion\05\f0
\Topografias\T_164N3R.top

Axis: X
  Length:   4800 µm
  Size:     12084 points
  Spacing:  0.397 µm

Axis: Y
  Length:   4000 µm
  Size:     401 lines
  Spacing:  10 µm

Axis: Z
  Length:   256 µm
  Size:     2558 digits
  Spacing:  0.1 µm
```

Parameters calculated on the surface T_164N3R > Roughness, Gaussian Filter, 800 µm

Sz, Sds and Ssc parameters are defined according to ISO standard.

Amplitude Parameters

Sa	= 1.78 µm
Sq	= 2.18 µm
Sp	= 7.48 µm
Sv	= 6.66 µm
St	= 14.1 µm
Ssk	= 1.11
Sku	= 2.65
Sz	= 14.1 µm

CETRIB
Unidade de Tribologia e Manutenção Industrial

TOPHOGRAFY

USED

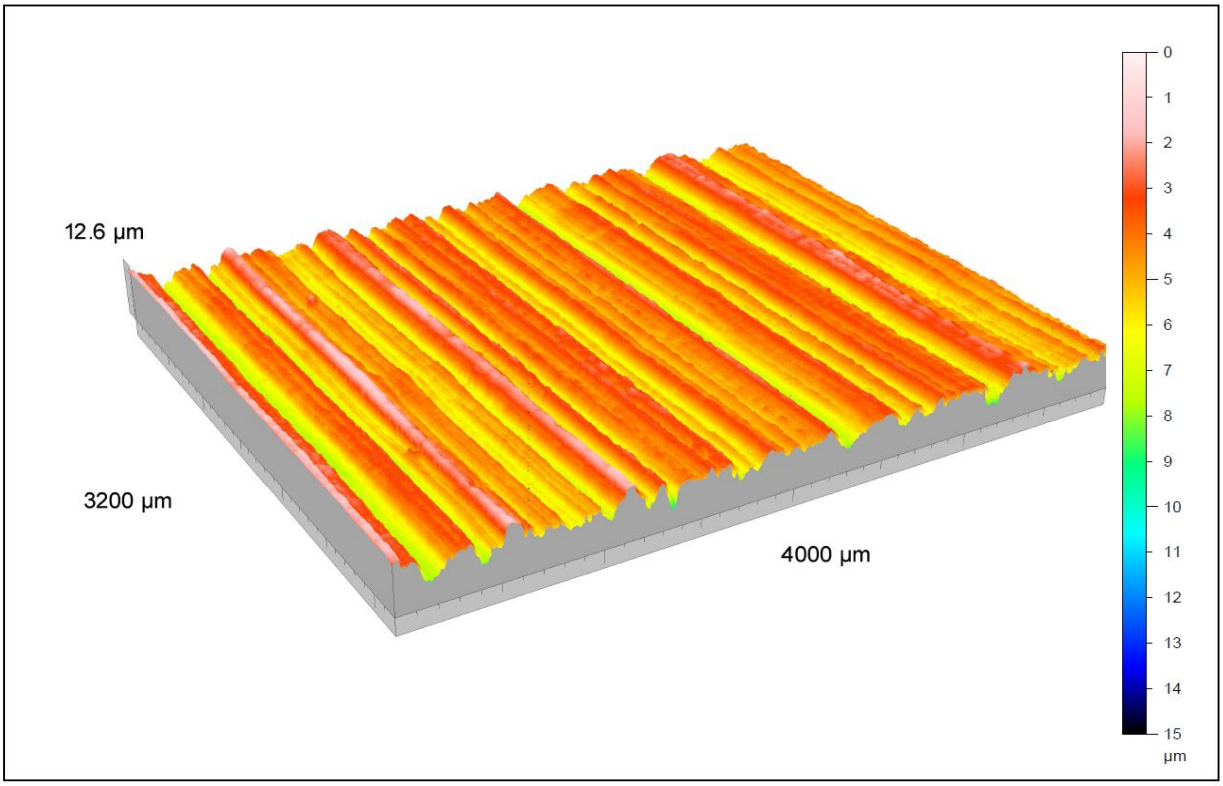

Identity card

Name: T_164U3R
Filename: D:\Perfis\André Lourenço\Pinion\05\f1_after 10milion k2\Topografia\T_164U3R.top

Axis: X
Length: 4800 µm
Size: 12084 points
Spacing: 0.397 µm

Axis: Y
Length: 4000 µm
Size: 401 lines
Spacing: 10 µm

Axis: Z
Length: 292 µm
Size: 2918 digits
Spacing: 0.1 µm

Parameters calculated on the surface T_164U3R > Roughness, Gaussian Filter, 800 µm

Sz, Sds and Ssc parameters are defined according to ISO standard.

Amplitude Parameters

Sa	= 1.38 µm
Sq	= 1.63 µm
Sp	= 4.91 µm
Sv	= 7.71 µm
St	= 12.6 µm
Ssk	= 0.899
Sku	= 2.33
Sz	= 12.6 µm

TEST DATASHEET - Plastic Gears

CETRIB
Unidade de Tribologia e Manutenção Industrial

Gear	*Pinion 5*
Ref.	C14_POM_06_P

ROUGHNESS [µm]

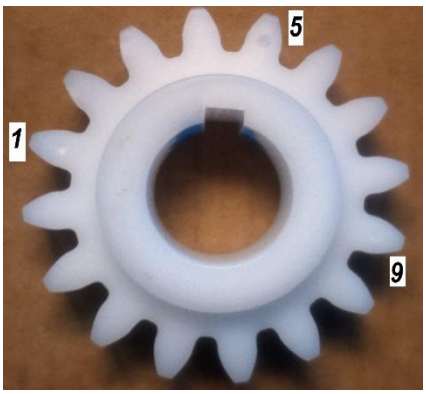

New	meas. n.	Ra	Rq	Rz	Rmax
Tooth 1	1	1.64	2.04	9.10	9.70
	2	1.62	2.03	9.56	10.80
	3	1.62	2.01	8.88	9.56
Tooth 5	4	1.57	1.98	9.14	10.43
	5	1.57	1.95	8.68	9.80
	6	1.61	2.03	8.80	9.56
Tooth 9	7	1.62	2.00	8.62	9.62
	8	1.53	1.92	8.40	9.61
	9	1.57	1.96	8.62	9.36

WEIGHING [g]

State	Ref Weight	Weight	Date
New	92.360	95.360	13/04/2015
Used	92.357	95.349	13/04/2015

Used	meas. n.	Ra	Rq	Rz	Rmax
Tooth 1	1	1.25	1.56	6.65	8.45
	2	1.16	1.47	6.21	8.33
	3	2.29	2.98	7.77	11.28
Tooth 5	4	1.12	1.39	5.80	7.57
	5	1.05	1.38	6.42	7.59
	6	1.17	1.49	6.81	7.62
Tooth 9	7	1.12	1.42	6.60	7.99
	8	1.44	1.77	7.64	8.71
	9	1.39	1.74	7.59	8.23

FZG GEAR TESTS

K3 LOAD STAGE				
Speed(wheel) [rpm]	500	1000	2000	3000
Time [hours]	-	61.19	-	-
Total Cycles (POM)	-	5.51E+06	-	-
Power Loss [W]	-	208.5	-	-
Stabilization Temperatures [°C]				
Oil Temperature	-	48.5/50.3	-	-
Tooth Temperature	-	58.8	-	-
Ambient Temperature	-	32.0	-	-
FZG Base Temperature	-	45.9	-	-
Bearings Case (Test)	-	53.6	-	-
Top cover (Test)	-	29.9	-	-
Bearings Case (Slave)	-	75.4	-	-
Top cover (Slave)	-	74.6	-	-

Comments: Controlled oil temperature: 50 °C

CETRIB
Unidade de Tribologia e Manutenção Industrial

TOPHOGRAFY

NEW

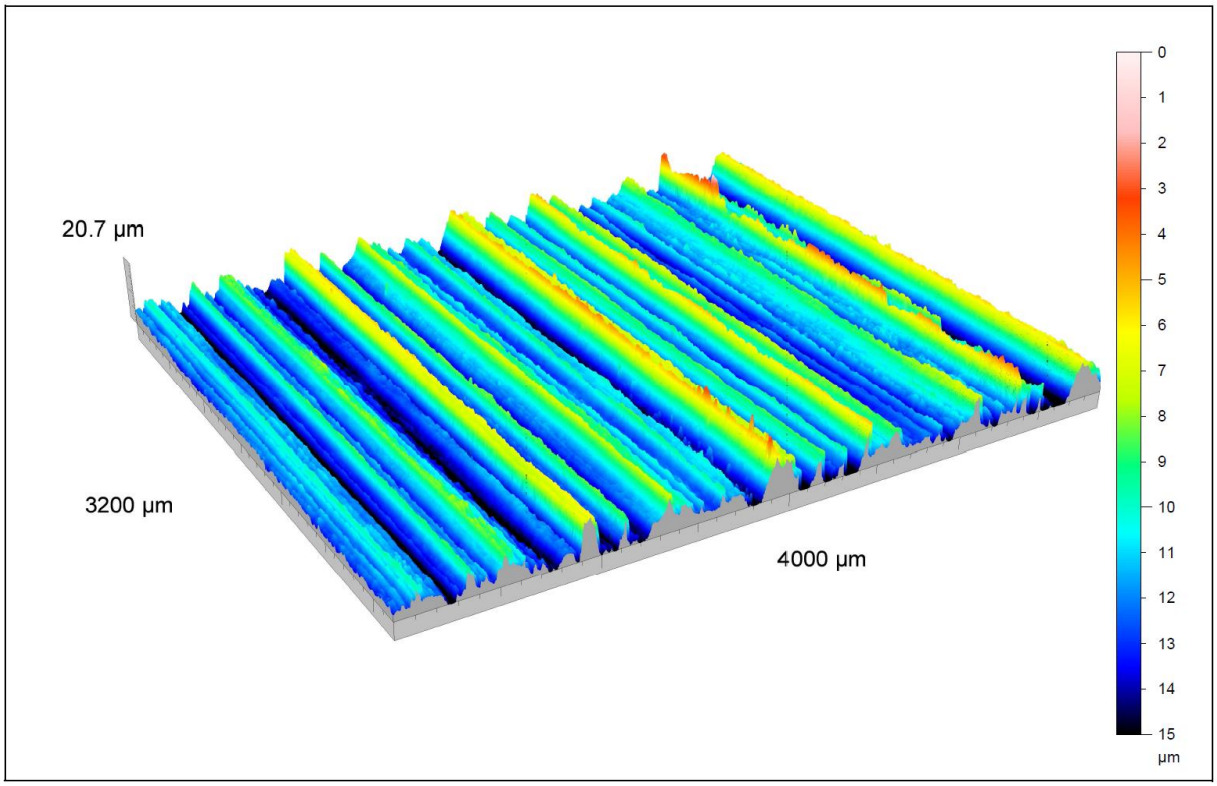

Identity card

Name: T_166N3R
Filename: D:\Perfis\André Lourenço\Pinion\07\f0\Topografia\T_166N3R.top

Axis: X
Length: 4800 µm
Size: 12084 points
Spacing: 0.397 µm

Axis: Y
Length: 4000 µm
Size: 401 lines
Spacing: 10 µm

Axis: Z
Length: 243 µm
Size: 2425 digits
Spacing: 0.1 µm

Parameters calculated on the surface T_166N3R > Roughness, Gaussian Filter, 800 µm

Sz, Sds and Ssc parameters are defined according to ISO standard.

Amplitude Parameters

Sa = 2.13 µm
Sq = 2.73 µm
Sp = 12.1 µm
Sv = 8.6 µm
St = 20.7 µm
Ssk = 0.912
Sku = 3.15
Sz = 20.7 µm

TEST DATASHEET - Plastic Gears

CETRIB
Unidade de Tribologia e Manutenção Industrial

Gear	*Pinion 6*
Ref.	C14_POM_07_P

ROUGHNESS [µm]

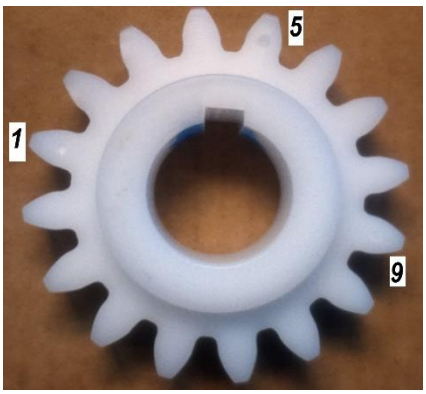

New	meas. n.	Ra	Rq	Rz	Rmax
Tooth 1	1	2.19	2.74	12.11	15.43
	2	2.04	2.61	11.85	15.72
	3	2.13	2.69	12.36	15.32
Tooth 5	4	2.03	2.57	11.35	14.79
	5	2.03	2.59	11.26	14.58
	6	2.05	2.60	11.75	14.75
Tooth 9	7	2.06	2.67	12.41	14.61
	8	2.14	2.74	13.53	17.29
	9	2.50	4.48	18.36	50.73

WEIGHING [g]

State	Ref Weight	Weight	Date
New	92.360	95.360	19/05/2015
Used	92.359	95.295	09/06/2015

Used	meas. n.	Ra	Rq	Rz	Rmax
Tooth 1	1	1.35	1.71	7.20	10.91
	2	1.38	1.72	8.10	10.43
	3	1.33	1.70	7.76	11.63
Tooth 5	4	1.30	1.67	7.82	9.31
	5	1.33	1.70	7.88	9.78
	6	1.34	1.79	8.37	11.31
Tooth 9	7	1.75	2.23	9.37	13.10
	8	1.81	2.24	10.07	14.02
	9	1.88	2.35	10.05	13.14

FZG GEAR TESTS

K4 LOAD STAGE				
Speed(wheel) [rpm]	500	1000	2000	3000
Time [hours]	-	19.44	-	-
Total Cycles (POM)	-	1.75E+06	-	-
Power Loss [W]	-	208.5	-	-
Stabilization Temperatures [°C]				
Oil Temperature	-	48.5/50.3	-	-
Tooth Temperature	-	59.2	-	-
Ambient Temperature	-	32.0	-	-
FZG Base Temperature	-	45.9	-	-
Bearings Case (Test)	-	53.6	-	-
Top cover (Test)	-	29.9	-	-
Beraings Case (Slave)	-	75.4	-	-
Top cover (Slave)	-	74.6	-	-

Comments: Controlled oil temperature: 50 °C

CETRIB
Unidade de Tribologia e Manutenção Industrial

TOPHOGRAFY

NEW

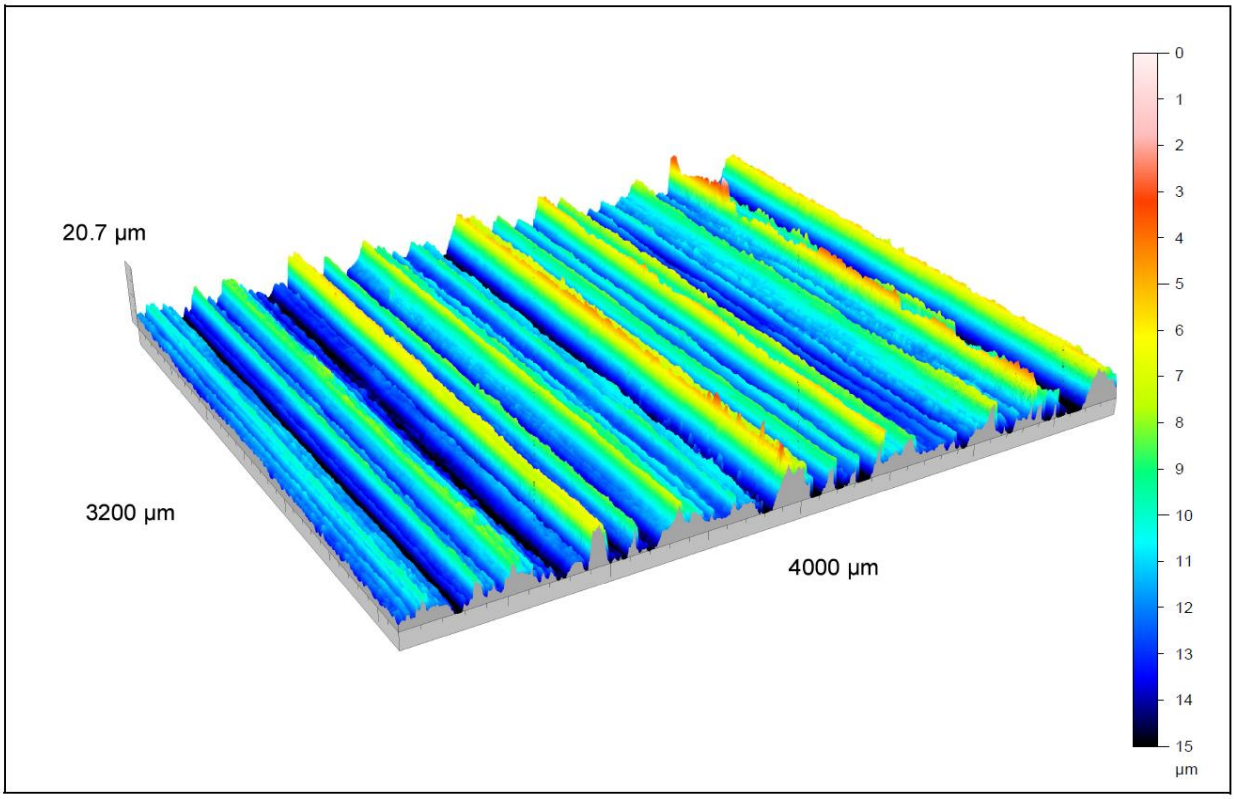

Identity card

Name: T_166N3R
Filename: D:\Perfis\André Lourenço\Pinion\07\f0\Topografia\T_166N3R.top

Axis: X
Length: 4800 µm
Size: 12084 points
Spacing: 0.397 µm

Axis: Y
Length: 4000 µm
Size: 401 lines
Spacing: 10 µm

Axis: Z
Length: 243 µm
Size: 2425 digits
Spacing: 0.1 µm

Parameters calculated on the surface T_166N3R > Roughness, Gaussian Filter, 800 µm

Sz, Sds and Ssc parameters are defined according to ISO standard.

Amplitude Parameters

Sa	= 2.13 µm
Sq	= 2.73 µm
Sp	= 12.1 µm
Sv	= 8.6 µm
St	= 20.7 µm
Ssk	= 0.912
Sku	= 3.15
Sz	= 20.7 µm

TEST DATASHEET - Plastic Gears

CETRIB
Unidade de Tribologia e Manutenção Industrial

Gear	*Pinion 7*
Ref.	H501_POM_01_P

ROUGHNESS [µm]

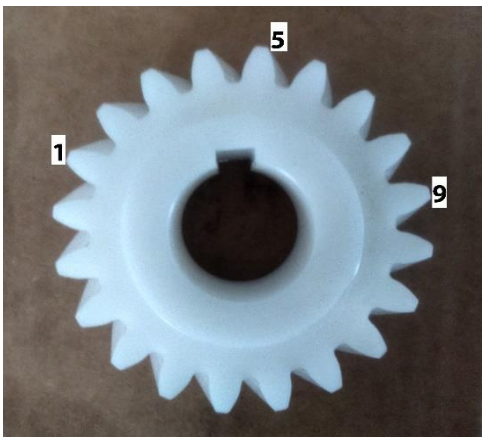

New	meas. n.	Ra	Rq	Rz	Rmax
Tooth 1	1	1.51	1.92	8.41	9.38
	2	1.45	1.83	7.99	9.55
	3	1.38	1.75	8.59	9.57
Tooth 5	4	1.53	2.05	8.85	15.81
	5	1.29	1.64	7.74	10.29
	6	1.38	1.79	8.26	13.49
Tooth 9	7	1.74	2.34	10.21	14.11
	8	1.60	2.33	11.40	18.96
	9	1.67	2.57	10.22	19.12

WEIGHING [g]

State	Ref Weight	Weight	Date
New Used	Broken		

Used	meas. n.	Ra	Rq	Rz	Rmax
Tooth 1	1	1.51	1.89	9.20	12.36
	2	1.37	1.73	7.88	11.24
	3	1.46	1.83	8.99	11.18
Tooth 5	4	2.00	3.10	12.78	29.63
	5	1.41	1.79	8.99	12.89
	6	1.44	1.83	8.01	9.08
Tooth 9	7	1.79	2.46	11.37	20.91
	8	0.77	0.99	4.21	6.17
	9	0.83	1.11	4.80	6.59

FZG GEAR TESTS

K4 LOAD STAGE				
Speed(wheel) [rpm]	500	1000	2000	3000
Time [hours]	-	111.11	-	-
Total Cycles (POM)	-	3.75E+06	-	-
Power Loss [W]	-	208.5	-	-
Stabilization Temperatures [°C]				
Oil Temperature	-	49.3/51.4	-	-
Tooth Temperature	-	60.1	-	-
Ambient Temperature	-	29.7	-	-
FZG Base Temperature	-	47.4	-	-
Bearings Case (Test)	-	54.2	-	-
Top cover (Test)	-	48.1	-	-
Bearings Case (Slave)	-	77.3	-	-
Top cover (Slave)	-	75.5	-	-

Comments: Controlled oil temperature: 50 °C

TEST DATASHEET - Plastic Gears

CETRIB
Unidade de Tribologia e Manutenção Industrial

Gear	*Pinion 8*
Ref.	H501_POM_02_P

ROUGHNESS [µm]

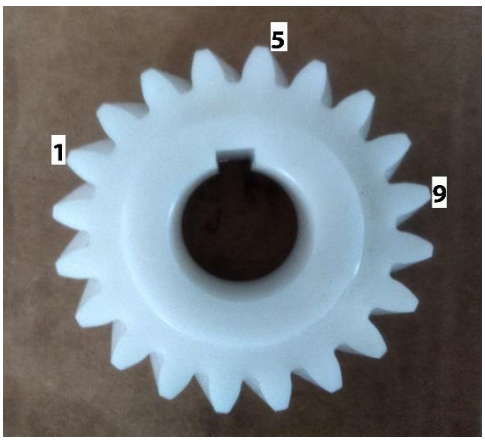

New	meas. n.	Ra	Rq	Rz	Rmax
Tooth 1	1	1.42	1.74	7.72	9.71
	2	1.65	2.10	9.85	13.48
	3	1.45	1.81	8.70	10.64
Tooth 5	4	1.46	1.84	8.78	10.60
	5	2.37	4.02	21.33	42.24
	6	2.39	3.98	20.76	40.10
Tooth 9	7	1.38	1.72	7.66	10.18
	8	1.45	1.82	8.53	9.74
	9	1.56	1.96	9.30	12.49

WEIGHING [g]

State	Ref Weight	Weight	Date
New Used	Broken		

Used	meas. n.	Ra	Rq	Rz	Rmax
Tooth 1	1				
	2				
	3				
Tooth 5	4				
	5	(Rugosimeter Unavailable)			
	6				
Tooth 9	7				
	8				
	9				

FZG GEAR TESTS

K4 LOAD STAGE				
Speed(wheel) [rpm]	500	1000	2000	3000
Time [hours]	-	41.67	-	-
Total Cycles (POM)	-	3.75E+06	-	-
Power Loss [W]	-	257.5	-	-
Stabilization Temperatures [°C]				
Oil Temperature	-	69.9/71.5	-	-
Tooth Temperature	-	82.5	-	-
Ambient Temperature	-	29.6	-	-
FZG Base Temperature	-	46.1	-	-
Bearings Case (Test)	-	73.4	-	-
Top cover (Test)	-	66.7	-	-
Bearings Case (Slave)	-	77.0	-	-
Top cover (Slave)	-	74.1	-	-

Comments: Controlled oil temperature: 70 °C